STATE OF CALIFORNIA • DEPARTMENT OF TRANSPORTATION

# TECHNICAL REPORT DOCUMENTATION PAGE

TR-0003 (REV 04/2024)

Lock Form

| 1. REPORT NUMBER | 2. GOVERNMENT ASSOCIATION NUMBER | 3. RECIPIENT'S CATALOG NUMBER |
|---|---|---|
| CA25-3945 | | |

| 4. TITLE AND SUBTITLE | 5. REPORT DATE |
|---|---|
| Hazard-Based Risk and Cost-Benefit Assessment of Temporary Bridges in California | June 02, 2025 |
| | 6. PERFORMING ORGANIZATION CODE |
| 7. AUTHOR | 8. PERFORMING ORGANIZATION REPORT NO. |
| Floriana Petrone, Sashi K. Kunnath, SeyyedMahdi Kashizadeh | |
| 9. PERFORMING ORGANIZATION NAME AND ADDRESS | 10. WORK UNIT NUMBER |
| University of Nevada, Reno<br>1664 N Virginia St.<br>Reno, NV 89557 | 11. CONTRACT OR GRANT NUMBER<br>Contract 65A0774 TO 006 |
| 12. SPONSORING AGENCY AND ADDRESS | 13. TYPE OF REPORT AND PERIOD COVERED |
| California Department of Transportation<br>1120 N St.<br>Sacramento, CA 95814 | Final Report<br>6/1/2022 to 5/31/2024 |
| | 14. SPONSORING AGENCY CODE |

15. SUPPLEMENTARY NOTES

16. ABSTRACT

Temporary bridges are systems designed for an expected service life of 5 years. In 2011, the California Department of Transportation issued a memo to designers advocating the use of design spectra corresponding to a return period of 100 years for temporary bridges. However, broad consensus on the most appropriate hazard level and design approach is yet to be achieved.

This study carries out fragility and risk analyses across a range of hazard levels, bridge life spans, and locations of different seismicity in California to provide recommendations to achieve a performance-based and hazard-consistent design for temporary bridges.

Bridges systems with lightweight superstructures are first designed for three hazard levels corresponding to 50, 100, and 200-year return periods at four sites in California based on the site-specific seismic demands obtained from the U.S. Geological Survey maps and the Caltrans Seismic Design Criteria without meeting the AASHTO minimum reinforcement requirements. The sites include San Francisco, Los Angeles, San Luis Obispo, and Sacramento. Fragility and risk calculations are carried out to assess the attainment of a set of damage states currently adopted by Caltrans. Results demonstrate that a hazard-based design can ensure satisfactory performance with damage limited to minor concrete cover spalling to large concrete cover spalling and extensive flexural cracks, even when the design minimum requirements for ordinary bridges are not met.

In addition, a baseline bridge model meeting the AASHTO (2020) and Caltrans (2019) minimum reinforcement requirements was used to identify the level of hazard resulting in Life Safety performance level, herein defined as the initiation of concrete core damage and longitudinal bar bucking. It was established that if a 200-year return period is targeted as the design return period for temporary bridges, the performance of the 'minimum design' bridge across the considered locations is satisfactory, with a probability of exceeding extensive flexural cracks and relatively large concrete cover spalling that substantially decreases for the locations with lower seismic hazard. Finally, an explicit comparison of the seismic risk for the bridges designed for 100 and 200-year return periods was carried out, showing that the risk is slightly affected by the change in the design return period from 100 to 200 years, thereby confirming the adequacy of the current recommendation of 100 years as the target return period when minimum design requirements are relaxed.

| 17. KEY WORDS | 18. DISTRIBUTION STATEMENT | |
|---|---|---|
| Temporary Bridges, Hazard-Consistent Seismic Design, Seismic Risk, Design Return Period, Lightweight Superstructure | | |
| 19. SECURITY CLASSIFICATION *(of this report)* | 20. NUMBER OF PAGES<br>90 | 21. COST OF REPORT CHARGED |

## DISCLAIMER STATEMENT

This document is disseminated in the interest of information exchange. The contents of this report reflect the views of the authors who are responsible for the facts and accuracy of the data presented herein. The contents do not necessarily reflect the official views or policies of the State of California or the Federal Highway Administration. This publication does not constitute a standard, specification or regulation. This report does not constitute an endorsement by the Department of any product described herein.

For individuals with sensory disabilities, this document is available in alternate formats. For information, call (916) 654-8899, TTY 711, or write to California Department of Transportation, Division of Research, Innovation and System Information, MS-83, P.O. Box 942873, Sacramento, CA 94273-0001.

# HAZARD-BASED RISK AND COST-BENEFIT ASSESSMENT OF TEMPORARY BRIDGES IN CALIFORNIA

## Final Report

Submitted to the California Department of Transportation
under Contract 65A0774

Floriana Petrone*, Principal Investigator
Sashi K. Kunnath+, Co-Principal Investigator
SeyyedMahdi Kashizadeh*, Ph.D. Student

---

* Department of Civil and Environmental Engineering, University of Nevada, Reno
+ Department of Civil and Environmental Engineering, University of California, Davis

# Contents

# List of Figures

# 1. Abstract

Temporary bridges are systems designed for an expected service life of 5 years. In 2011, the California Department of Transportation (Caltrans) issued a memo to designers advocating the use of design spectra corresponding to a return period of 100 years for temporary bridges. However, broad consensus on the most appropriate hazard level and design approach is yet to be achieved.

This study carries out fragility and risk analyses across a range of hazard levels, bridge life spans, and locations of different seismicity in California to provide recommendations to achieve a performance-based and hazard-consistent design for temporary bridges.

Bridges systems with light-weight superstructures are designed for three hazard levels corresponding to 50, 100 and 200-year return periods at four sites in California based on the site-specific seismic demands obtained from the U.S. Geological Survey (USGS) maps and the Caltrans Seismic Design Criteria (SDC), without meeting the AASHTO minimum reinforcement requirements.

Fragility and risk calculations are carried out to assess the attainment of a set of damage states currently adopted by Caltrans, including the initiation of concrete core damage and longitudinal bar bucking, which is herein associated with Life Safety performance.

Additionally, the performance of temporary bridges adopting standard bridge columns meeting the minimum AASHTO reinforcement requirements at each of the selected locations in California is evaluated. This facilitated the quantification of the return period at which the Life Safety performance criterion for temporary bridges is satisfied.

## 2. Notation & Acronyms

DS = Damage State

EDA = Elastic Dynamic Analysis

HCD = Hazard Consistent Design (column)

HL1 = Hazard Level 1, corresponding to 10% probability of exceedance in 5 years

HL2 = Hazard Level 2, corresponding to 5% probability of exceedance in 5 years

HL3 = Hazard Level 3, corresponding to 2.5% probability of exceedance in 5 years

HL4 = Hazard Level 4, corresponding to 1% probability of exceedance in 5 years

HL5 = Hazard Level 5, corresponding to 0.5% probability of exceedance in 5 years

LA = Los Angeles

MD = Minimum Design (column)

NLTH = Nonlinear Time-History (analysis)

SC = Sacramento

SF = San Francisco

SLO = San Luis Obispo

UHS = Uniform Hazard Spectra

# 3. Executive Summary

This study carries out fragility and risk analyses across a range of hazard levels, bridge life spans, and locations of different seismicity in California to provide recommendations to achieve a performance-based and hazard-consistent design for temporary bridges.

Bridges systems with lightweight superstructures are first designed for three hazard levels corresponding to 50, 100 and 200-year return periods at four sites in California based on the site-specific seismic demands obtained from the U.S. Geological Survey maps and the Caltrans Seismic Design Criteria, without meeting the AASHTO minimum reinforcement requirements. The sites include San Francisco, Los Angeles, San Luis Obispo, Sacramento. Fragility and risk calculations are carried out to assess the attainment of a set of damage states currently adopted by Caltrans. Results demonstrate that a hazard-based design can ensure satisfactory performance with damage limited to minor concrete cover spalling to large concrete cover spalling and extensive flexural cracks, even when the design minimum requirements for ordinary bridges are not met.

In addition, a baseline bridge model meeting the AASHTO (2020) and Caltrans (2019) minimum reinforcement requirements was used to identify the level of hazard resulting in Life Safety performance level, herein defined as the initiation of concrete core damage and longitudinal bar bucking. It was established that if a 200-year return period is targeted as the design return period for temporary bridges, the performance of the 'minimum design' bridge across the considered locations is satisfactory, with a probability of exceeding extensive flexural cracks and relatively large concrete cover spalling decreasing from 20% for San Francisco to zero percent for Sacramento.

Finally, an explicit comparison of the seismic risk for the hazard-consistent design bridges designed for 100 and 200-year return period was carried out by incorporating two additional return

periods into the set of analyses corresponding to 500 and 975 years. Results showed that the risk is slightly affected by the change in the design return period from 100 to 200 years thereby confirming the adequacy of the current recommendation of 100 years as the target return period when minimum design requirements are relaxed.

# 4. Introduction

Temporary bridges are structural systems built to ensure continuity of service during construction or maintenance of ordinary bridges, with an expected service life of 5 years. The main requirements for such structures include versatility, easiness of construction, and cost-effectiveness. For multi-span configurations, Caltrans' current practice relies on the use of cast-in-place reinforced concrete (RC) columns and prefabricated superstructures (e.g., steel decks, precast girders) connected to the columns through pin connections or bearing pads.

The history of prefabricated steel modular bridges dates to 1930, when the British military pioneered modular prefabricated steel bridge systems featuring trusses composed of bolted-together panels to facilitate and speed up construction in remote environments. The first prefabricated modular system was patented by A.M. Hamilton in 1935 providing identical members for the ease of use and installation on the site. In 1943, Donald Bailey patented a new system incorporating panel connections that enable the construction of longer spans. This system is still in use by the US military and State Departments of Transportation, such as Caltrans (SDR Engineering Consultants 2005).

However, while most of the prior research has focused on the optimization of the construction process and the superstructure performance, a unified performance-based approach for the seismic design of temporary bridges is yet to be achieved. The current practice for the design of ordinary bridges is based on a hazard level of 5% in 50 years, which corresponds to a 975-year return period. Extending this approach to the design of temporary bridges would be overly conservative and not economical. As a result, several simplified methods have been proposed to reduce the spectral accelerations for the design of temporary bridges. The AASHTO Guide Specifications for LRFD Seismic Bridge Design (2015) and AASHTO LRFD Bridge Design Specifications (2020)

recommend the use of reduction factors of 2.5 and 2, respectively, to apply to the design spectra for ordinary bridges for the calculation of elastic forces and displacements. However, the same codes advise conducting special studies when the sites of interest are close to an active fault. While this approach eliminates the need for employing probabilistic methods for the calculation of new spectra and only requires the application of reduction factors to design spectra for ordinary bridges, it does not explicitly incorporate the notion of return period and expected structural performance.

In 2011, Caltrans issued a memo to designers advocating the use of design spectra corresponding to a return period of 100 years, which entails the utilization of the USGS hazard maps and tools (USGS, 2018) to derive site-specific UHS for the targeted return period. Following the release of this memo, simplified methods have been proposed to reduce the spectral parameters for design. Stucki and Bruneau (2018) suggested adjusting the spectral response acceleration parameters (PGA, Ss, and S1) from a 1000-year to a 100-year return period based on the identification of three geographic groups. Following the analysis of 100 locations in the US, they identified two groups, one for western states and one for central and eastern states, proposing a reduction factor of 2.5 and 3.75 for the two groups, respectively.

While these efforts highlight the motivation to establish a rational, hazard-based approach for designing temporary bridges, a broad national consensus regarding the most appropriate hazard level – supported by robust fragility and risk analyses - has yet to be reached.

## 5. Objectives of Study

This research carries out a set of rigorous and systematic probabilistic analyses to assess the seismic performance of typical temporary bridges for different hazard levels in California and provide recommendations for performance-based seismic design of temporary bridges. Specifically, the following objectives were identified for the study:

- Establish column section designs consistent with the hazard at the site and conforming to the strength and ductility requirements specified in the Caltrans SDC.
- Assess the performance of each design through nonlinear time-history simulations and fragility analyses and verify if Life Safety performance criteria, herein associated with the initiation of concrete core damage and longitudinal rebars bucking, are satisfied.
- Evaluate the risk of temporary bridges with columns meeting minimum AASHTO reinforcement requirements at each of the selected locations of attaining selected damage states for different bridge life spans (i.e., 5, 10 and 15 years).

## 6. Assessment Methodology

This section provides a summary of the methodology employed in this study.

The original approach for this work was based on carrying out site-specific and hazard-consistent designs of temporary bridges for three hazard levels to eventually compare the bridge performance under suites of ground motions consistent with each design level. Hereafter, this will be called "Approach #1".

Subsequently, the performance of bridges with columns meeting the AASHTO (2020) minimum reinforcement requirements under the highest hazard level considered in Approach #1 as well as 2 additional hazard levels was assessed. Hereafter, this will be called "Approach #2".

## 6.1 Approach #1

Temporary bridges were designed at three locations in California and for three hazard levels. The locations are San Francisco, Los Angeles, San Luis Obispo, and Sacramento. The returned periods corresponding to the considered hazard levels are 50 years, 100 years, and 200 years. The design was based on the Uniform Hazard Spectra (UHS) from the 2018 USGS maps. This led to a total of twelve bridge designs (4 locations x 3 hazard levels).

For each location and hazard level, 30 ground motions were selected, rotated twice by 45 degrees, and scaled to the corresponding (design) UHS in the $0.5T_1$-$2T_1$ bandwidth (AASHTO, 2020), where $T_1$ represents the fundamental period of the structure. This led to a total of ninety pairs of ground motions that were used as input for the bridge model to perform nonlinear time-history analyses (NLTHA). For each bridge, ninety peak drift values were used to derive probabilistic demand models and fragility functions. The bridge column drifts were used as the reference engineering demand parameter (EDP), and the spectral acceleration at the fundamental period of the bridge was selected as the reference intensity measure, $Sa(T_1)$. The classical formulation $P[D \geq C|IM] = \Phi\left(\frac{\ln(EDP_D) - \ln(EDP_C)}{\beta_{EDP|IM}}\right)$ was used, where $EDP_D$ is the seismic demand median (i.e., obtained from the ninety runs), $EDP_C$ is the limit state median (i.e., the drift from each damage state - DS - obtained from the pushover analyses), and $\beta_{EDP|IM}$ is the dispersion of the seismic demand calculated from the actual population of ninety data points (that is, without making any prior assumption on the distribution). This process leads to fragility functions expressing the probability of exceeding each damage state as a function of $Sa(T_1)$.

## 6.2 Approach #2

A "minimum design" bridge (i.e., 1% longitudinal reinforcement ratio and 0.35% transverse reinforcement ratio) was subject to 90 x 3 = 270 pairs of ground motions selected and scaled following the method discussed above with UHS corresponding to the following return periods: 200 years (highest in Approach #1), 500 years, and 975 years. The data points obtained from these NLTHA were used to build fragility functions as done in Approach #1.

In addition, for Approach #2, a risk analysis was performed by integrating hazard and fragility. This was done using the total risk model proposed by Yoon et al. (2022) for three different life spans, namely 5, 10, and 15 years. The hazard curves at the latitude and longitude of the locations of interest (San Francisco, Los Angeles, San Luis Obispo, and Sacramento) were obtained from the U.S. Geological Survey web application. Linear interpolation between the hazard curves for 0.75 and 1 sec was used to derive the annual rate of exceedance for the spectral periods of the considered bridge, that is 0.83 sec for San Francisco and Los Angeles and 0.96 sec for San Luis Obispo and Sacramento. The probabilities of exceeding $DS_i$ at the design spectral acceleration (i.e., UHS acceleration at the fundamental period of the bridge) for the three return periods considered in Approach #2 (i.e., 200, 500, and 975 years) are used to derive a new fragility function representing the probability of exceeding the selected $DS_i$. Curve fitting across the three points is performed using the function scipy.stats in Python. The annual rate of occurrence is multiplied by the probability of exceeding $DS_i$ sampled at the same $S_a$, and all products across all spectral accelerations are summed up to obtain the annual rate of exceedance for $DS_i$. That is, $v(DS_i) = \sum_{S_a=1}^{n} \lambda(GM_{T\ year})\, P(DS_i|GM_{T\ year})$, where $v(DS_i)$ is the annual rate exceeding $DS_i$, $S_a$ is the spectral acceleration associated with the annual exceedance rate, $\lambda(GM_{T\ year})$ is the annual rate of occurrence of a given seismic intensity level, and $P(DS_i|GM_{T\ year})$ is the probability of exceeding

$DS_i$ at the given seismic intensity level. Finally, the probability of exceeding $DS_i$ within a desired life span is calculated with the classical formulation $P(DS_i) = 1 - exp^{-jv(DS_i)}$, where $j$ represents the life span of interest. For selected locations and DSs the fragility functions are not defined because the probabilities of exceeding a certain DS are either all 100% or 0% for the considered return periods and consequently the fragility function cannot be derived, and the risk cannot be calculated. This is one of the main limitations identified in this approach for risk calculation.

# 7. Research Tasks

To achieve the stated objectives of the research, the following tasks were carried out:

- Develop site-specific uniform hazard spectra for three return periods corresponding to exceedance probabilities of 10% in 5 years (hereafter HL1), 5% in 5 years (hereafter HL2, and 2.5% in 5 years (hereafter HL3), using the 2018 USGS maps for site class D (with shallow shear wave velocity, Vs30 = 259 m/sec), and for four selected locations in California, namely San Francisco (SF), Los Angeles (LA), San Louis Obispo (SLO), and Sacramento (SC).
- Complete the seismic design of column cross-sections for the four selected locations and three selected return periods (HL1, HL2, and HL3). These designs, which satisfy SDC strength and ductility requirements, are referred to as "Hazard Consistent Design" or "HCD". All temporary bridges are assumed to have cast-in-place RC columns and a lightweight continuous prefabricated steel superstructure (ACROW Corp. 2016).
- Select and scale suites of ground motions for each hazard level at each of the four sites.
- Carry out a systematic set of analyses on "HCD" temporary bridges designed for 50, 100, and 200-year return periods and four locations in California. To facilitate this, detailed

three-dimensional nonlinear models of the bridge are developed with the OpenSees software (McKenna, 2011).

- Repeat the simulations for the "Minimum Design" or "MD" bridges for all four different locations. In this case, the hazard levels are modified to assess the return period that will likely result in a damage state corresponding to Life Safety, herein defined as the initiation of concrete core damage and longitudinal rebars bucking. Additionally, the risk of exceeding certain damage states during the potential lifespan of the bridges is determined.

## 8. Seismicity and seismic hazard levels

The four sites selected to encompass a range of seismic hazard levels in California are SF, LA, SC, and SLO. Site-specific uniform hazard spectra were derived for return periods of 50 years (10.0% in 5 years - HL1), 100 years (5.0% in 5 years - HL2), and 200 years (2.5% in 5 years - HL3), using the 2018 USGS maps for site class D (shallow shear wave velocity, Vs30 = 259 m/sec).

Since the sites in SF and LA are located near active faults (<15 km), the UHS for these locations were modified to incorporate near-field effects through factors that linearly increase the spectral amplitudes from zero to 1.2 between 0.5 sec and 1 sec and keep the increase at 1.2 for periods longer than 1 sec, as per SDC. None of the selected sites are located on basins with features requiring consideration for spectral amplification. Figure 1 shows the final UHS for the selected locations, which were employed to carry out the bridge design using elastic dynamic analysis (EDA), and to scale the selected sets of ground motions to perform NLTH analyses.

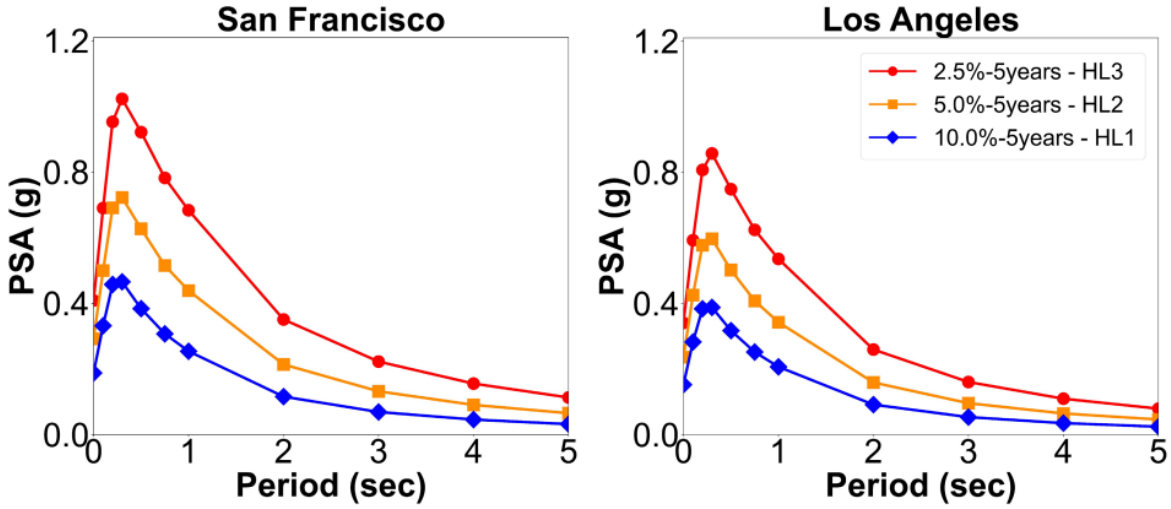

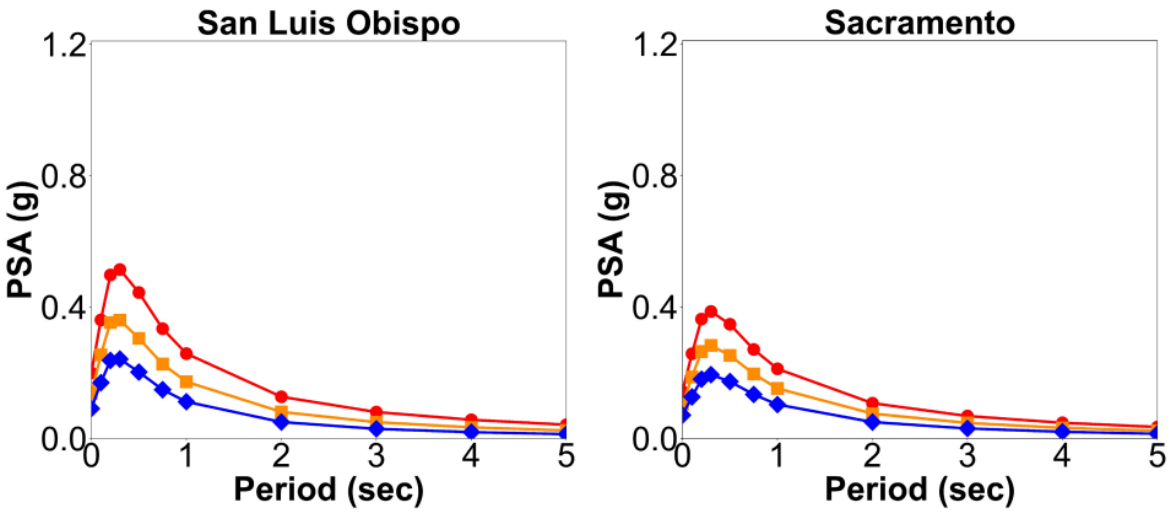


Figure 1. Uniform Hazard Spectra for the three selected hazard levels (HL1, HL2 and HL3) at the four locations (SF, LA, SLO, and SC).

# 9. Bridge modeling and design

Based on the documentation of existing temporary bridges in California, a two-span bridge, with a continuous straight steel deck (ACROW) pinned at the midspan to two cast-in-place circular reinforced concrete (RC) columns and simply supported at the two ends was selected as the prototype temporary bridge for all four locations (see detail in Figure 2). Each span is 150 feet long, the columns are 24 feet high with a diameter of 4 ft for SF and LA, and 18 ft high with a diameter of 3 ft for SLO and SC. In all cases, the distance between the columns is 30 ft. Based on an expected concrete strength of 5 ksi, the modulus of elasticity of concrete is assumed to be $E_c$ = 4,286 ksi. Grade 60 steel with an expected yield strength of 68 ksi and modulus $E_s$ = 29,000 ksi is used.

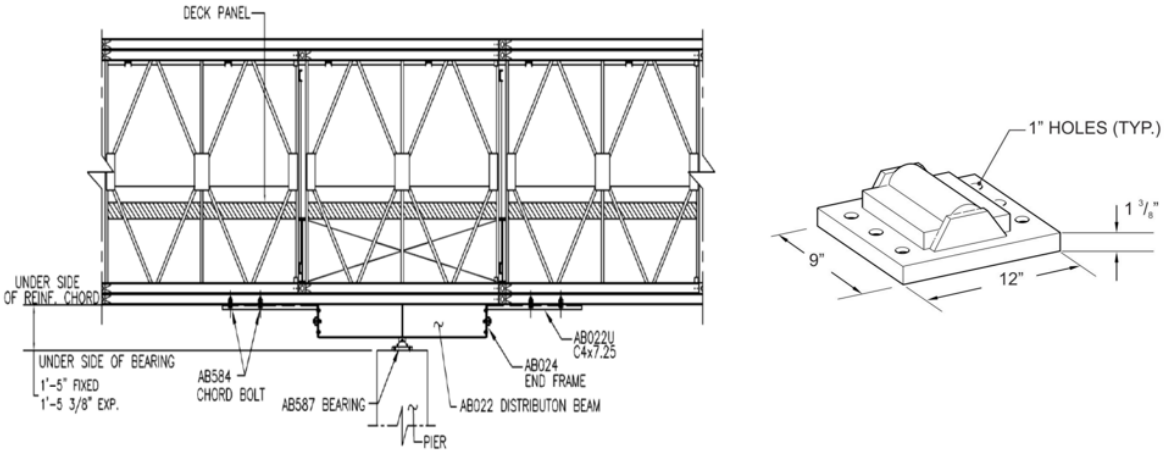


Figure 2. Pin connection detail according to Caltrans documentation

The HCD bridge design was carried out primarily based on the displacement ductility criteria set forth in the SDC 4.4.1 (2019). The displacement ductility is defined as $\mu_D = \Delta_D/\Delta_Y$, where $\Delta_D$ is the elastic demand obtained from EDA, and $\Delta_Y$ is the yielding demand obtained from nonlinear lateral analyses.

## 9.1 Linear model

A three-dimensional (3D) bridge elastic model was first developed with the CSiBridge software (Computers & Structures, 2022) to perform EDA and obtain $\Delta_D$. The superstructure was modeled using elastic linear elements with the inertial properties provided by the ACROW manufacturer for the deck type TDR3H (ACROW Corporation, 2016).

Each span was discretized into ten elements and the mass representing the self-weight of the deck (including the truss, handrail, 2L30 panel, and polyester overlay) was applied to the element nodes. The pinned connections between the columns and the deck were modeled as two-node links to allow rotations about the longitudinal and transverse axes (per manufacturer's communication). Both columns were fixed at the base. An offset between the top of the columns and the deck was imposed through rigid links to account for the physical distance of the deck cross-section centroid from the top of the columns and the actual location of the pins. A rigid link was also used to connect the two columns, as no relative displacement in the transverse direction between the columns was expected to occur. Expansion bearings at both ends of the deck were modeled with linear springs allowing rotation about the longitudinal, transverse, and vertical axes, and restraining the translation along vertical axes. The stiffness of the springs in each direction was determined as half of the stiffness provided by the two-column bent system in each direction and was determined based on the results of separate linear lateral load analyses performed on the standalone bent. The column elements were modeled using elastic elements with the properties of cracked cross-sections (3.4.2 in SDC, 2019). Figure 3 provides a schematic representation of the bridge model.

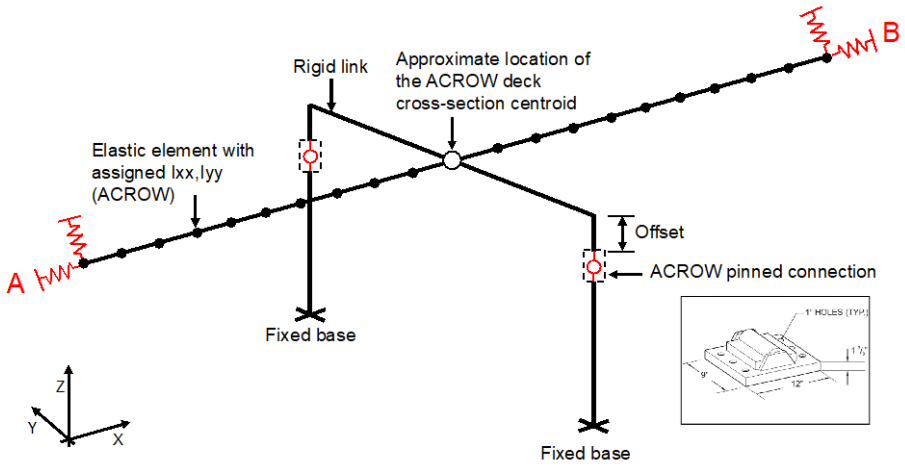


Figure 3. Bridge numerical model.

Following the provisions in SDC 4.2.2, the uniform hazard spectra for the considered hazard levels (10%, 5%, and 2.5% in 5 years, corresponding to 50, 100 and 200-year return period) were applied to the bridge in both transverse and longitudinal directions using the complete quadratic combination (CQC3). P-delta effects were incorporated into the analysis. Upon application of the load combinations in the AASHTO 2020 provisions, the load combination 'Extreme 1' (1D+1EQ) was found to control the design and used to calculate $\Delta_D$.

The dynamic properties of the bridge considering the inertial properties of the cracked section were determined through an eigenvalue analysis. The fundamental modal periods in the transverse and longitudinal directions are 0.83 sec and 0.81 sec for the bridges in SF and LA, and 0.96 sec and 0.95 sec for the bridges in SLO and SC.

For the bridge with a 4-ft diameter column, $P/f_c'A_g = 0.045$ and $L/P = 0.3$, where P is the axial force induced by the dead loads, $f_c'$ is the concrete compressive strength, $A_g$ is the gross cross-sectional area, and L is the axial force induced by the live loads. When using the 3-ft diameter columns in SLO and SC the axial load ratio increases to 0.07.

## 9.2. Nonlinear Model and Validation

A three-dimensional nonlinear model was developed using OpenSees (McKenna, 2011) to perform a lateral load analysis to obtain $\Delta_Y$, and subsequently perform NLTH analyses. The configuration for the nonlinear OpenSees model is generally similar to the linear model, with the main difference being that the columns are modeled as *nonlinearbeamcolumn* force-based elements with fiber sections and with a prescribed plastic hinge at the base ($L_{p_i}$). The length of the plastic hinge was calculated based on the recommendations in section 5.3.4 of SDC (2019). It is a function of the expected yield strength of rebars, nominal diameter of rebars and length of column maximum moment to the point of contraflexure.

The choice of using a distributed plasticity model was driven by the intent to capture any potential spread of plasticity beyond the predefined length of the plastic hinge. The beam-column element employs six integration points following the HingeRadau method (Scott and Fenves, 2006). The cross-section was discretized into ninety-six fibers (eight radially and twelve circumferentially). In addition to capturing the main features of the bridge's nonlinear global response, this modeling approach can provide measures of the stress and strain attained at locations in the concrete section (cover and concrete) and in the steel rebars, which was essential for assessing different damage states in the bridge under different earthquake intensities. The cyclic response of plain concrete was modeled using *Concrete02* material in OpenSees (McKenna, 2011), which is based on the model by Yassin (1994) and encompasses a nonlinear curve in compression up to the peak strength followed by linear softening, and linear elastic behavior in tension up to cracking followed by linear softening. The residual strength in compression for unconfined concrete was set to zero and the unloading stiffness in compression was set as 20% of the initial stiffness. The properties of the confined core were derived from the confinement model proposed

by Mander et al. (1984) incorporating the effects of transverse reinforcement to define how hoops confinement increases both the peak compressive strength and strain capacity of concrete. The response of the rebars was simulated using the *Hysteretic* material, which models inelastic behavior under cyclic loading, and captures energy dissipation and stiffness degradation in post-ultimate softening behavior in compression and tension. Specifically, it defines a post-yielding softening response beyond the peak stress through a three-point piecewise function. The three-point stress-strain behavior in tension is defined based on the recommendation of Table 3.3.3-1 of SDC (2019). The input parameters for capturing the buckling in compression were defined based on the model proposed by Zong et al. (2014), which utilizes a beam-on-springs model. On the compression side, the behavior is modeled using the following equations:

$$f_{n1} = -f_y \tag{3.2-1}$$

$$\varepsilon_{n1} = -\varepsilon_y = -\frac{f_y}{E_s} \tag{3.2-2}$$

Where $f_{n1}$ and $\varepsilon_{n1}$ are the stress and strain of the first point, $f_y$ and $\varepsilon_y$ are the yield strength and strain of the longitudinal bars, and $E_s$ is the steel Young's modulus.

The following expressions are then used to determine the stress and strain of the second point:

$$f_{n2} = -C_s((L_1 + 1)(\frac{\alpha}{100} - 1) f_y \tag{3.2-3}$$

$$\varepsilon_{n2} = C_s L_1 \varepsilon_y \tag{3.2-4}$$

Where $C_s$ is the stiffness reduction coefficient expressed as $C_s = \begin{cases} (1-\left(1-\frac{K}{K_0}\right)^2)^{1/\beta} & 0<\frac{K}{K_0}<1 \\ 1.0 & \frac{K}{K_0}\geq 1 \end{cases}$, with $K = \frac{F_y}{\Delta_y}$ being the spring's effective stiffness and $K_0 = 0.02\pi^4 E I_b s^3$ the critical stiffness defining the minimum buckling length. In the expression of $K$, $\Delta_y$ is solved iteratively using $\frac{R(tan\theta-\theta)}{\pi R} = \varepsilon_y \leftrightarrow \theta = \arccos(\frac{R}{R+\Delta})$ and $F_y = 2\frac{R(tan\theta-\theta)}{\pi R} \mathrm{E} A_h \sin(\arccos\left(\frac{R}{R+\Delta}\right))$ where $R$ is the radius of the column core (in mm), $L_1 = -800\left(\frac{\sqrt{\frac{f_y}{420}}s}{d_b}\right)^{-2.5} - 2.5$, with $s$ being the center-to-center spacing of the transverse reinforcement (in mm), $d_b$ the diameter of the longitudinal rebars (in mm), and $\alpha = 3.0 - 0.2\left(\frac{\sqrt{\frac{f_y}{420}}s}{d_b}\right)^2$

Finally, the third negative point is obtained as:

$$f_{n3} = 0.8 f_{n2} \tag{3.2-5}$$

$$\varepsilon_{n3} = (\min(C_s L_1 - 40; 1.5 C_s L_1) + C_s L_1)\varepsilon_y \tag{3.2-6}$$

Figure 4 provides a representation of the main features of the nonlinear column modeled in OpenSees (McKenna, 2011).

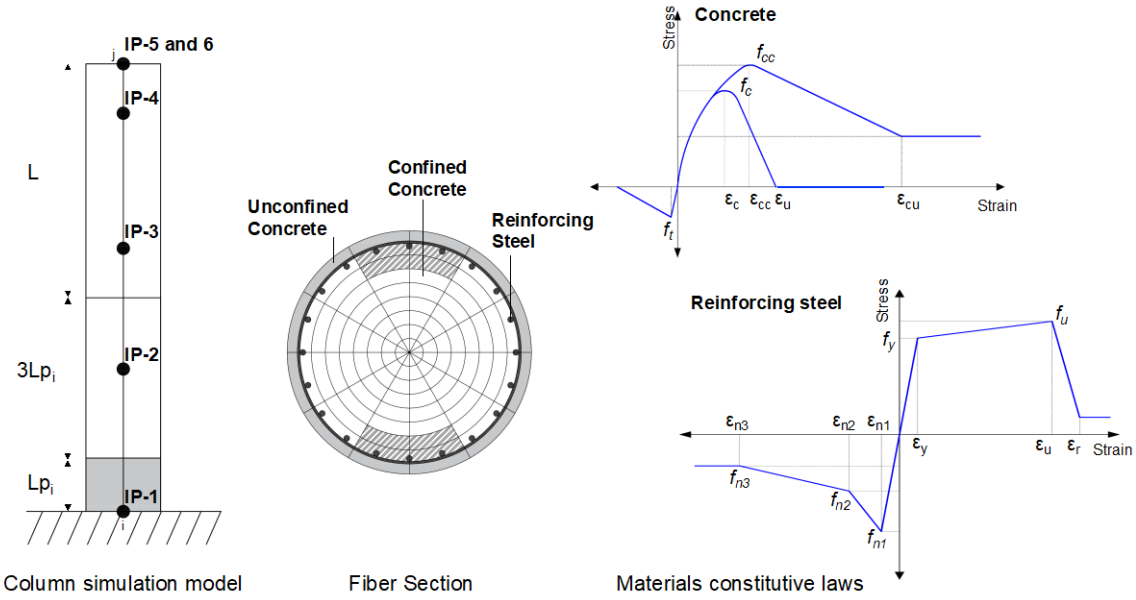


Figure 4. Column modeling approach: column simulation model, fiber section, and materials constitutive laws.

To ensure the reliability of the presented modeling methodology, numerical simulations were compared against experimentally tested columns documented in the literature. Specifically, the column model with the features described above (i.e., element and cross-section discretization, material parameters, etc.) was used to simulate the cyclic lateral response of two columns experimentally tested by Lehman and Moehle (2000) and Henry and Mahin (1999). These columns were selected given the similarities with columns utilized in this study. Table 1 summarizes the main features of the columns. The validation study demonstrated a high sensitivity of the column response to the steel parameters. Upon comparison and calibration against the experimental tests, the parameters controlling pinching (PinchX and PinchY) were both set to 1, and those controlling ductility and degradation (damage1 and damage2) were set to 0.01 and 0.0, respectively.

**Table 1.** Key features of the columns considered in the validation study.

| Feature | Lehman and Moehle (2000) | Henry and Mahin (1999) |
|---|---|---|
| Diameter (ft) | 2 | 2 |
| Height (ft) | 16 | 8 |
| Cover (in) | 0.75 | 0.75 |
| Trans. Reinforcement (%) | #2 @ 1.25" [0.7] | #2 @ 2.5" [0.35] |
| Long. Reinforcement (mm) | 22#5 [1.49] | 22#5 [1.49] |
| Concrete strength $f'_c$ (ksi) | 4.5 | 5.4 |
| Steel yield fy (ksi) | 66.9 | 66.9 |

Figure 5 provides the comparison of the simulation results and experimental data for the two selected columns. For the test by Lehman and Moehle (2000), the peak force of the numerical solution is approximately 31 kips, while it is 34 kips in the experimental test (9% difference); for the test by Henry and Mahin (1999), the simulated peak lateral force is 59 kips while the experimental one is 64 kips (8% difference), demonstrating a reasonable agreement in the prediction of the peak strength and cyclic behavior. Reasonable agreement is also observed in the pinching behavior and overall dissipated energy across the cycles.

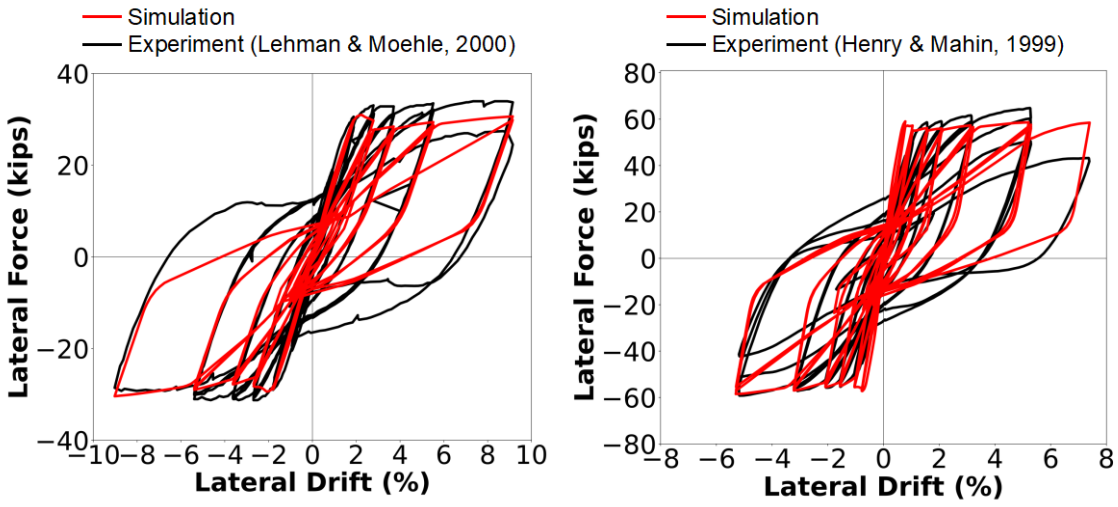


Figure 5. Numerical model validation. Comparison between simulated and experimental responses of selected columns from the literature (A) Lehman & Moehle (2000) and (B) Henry & Mahin (1999).

According to section 4.4 of the SDC v2 (2019), the elastic ($\Delta_D$) and yielding ($\Delta_Y$) displacements are used to calculate the displacement ductility demand $\mu_D$. The resulting values were compared against the limits in Table 4.4.1-1. In this study, the functional evaluation earthquake (FEE) in recovery standard bridges was considered as a reference, corresponding to $\mu_{D,max} = 2$. Table 2 reports the computed values across all locations and hazard levels.

**Table 2.** Displacement ductility demand values for all four locations and hazard levels.

| Location | Hazard Level | Type | Displacements | | | Displacement ductility demand |
|---|---|---|---|---|---|---|
| | | | $U_x$ (in) | $U_y$ (in) | $U_z$ (in) | |
| San Francisco | 100 years | Elastic | 3.21 | 3.4 | -0.012 | 1.3 < 2 |
| | | Yield | | 2.6 | | |
| | 200 years | Elastic | 4.93 | 5.22 | -0.012 | 1.8 < 2 |
| | | Yield | | 2.9 | | |
| Los Angeles | 100 years | Elastic | 2.53 | 2.68 | -0.014 | 1.0 < 2 |
| | | Yield | | 2.6 | | |
| | 200 years | Elastic | 3.91 | 4.14 | -0.014 | 1.6 < 2 |
| | | Yield | | 2.6 | | |
| San Louis Obispo | 100 years | Elastic | 1.42 | 1.53 | -0.018 | 0.8 < 2 |
| | | Yield | | 1.95 | | |
| | 200 years | Elastic | 2.12 | 2.28 | -0.018 | 1.2 < 2 |
| | | Yield | | 1.95 | | |
| Sacramento | 100 years | Elastic | 1.24 | 1.34 | -0.018 | 1.0 < 2 |
| | | Yield | | 1.35 | | |
| | 200 years | Elastic | 1.73 | 1.86 | -0.018 | 1.4 < 2 |
| | | Yield | | 1.35 | | |

In this study, $\Delta_Y$ was defined as the displacement corresponding to minor concrete cover spalling and the onset of rebar yielding. Details on the method used to identify the attainment of such conditions in the modeled columns is provided in the section 'Damage States'.

The columns' design for each hazard level was carried out without consideration of the minimum reinforcement requirements in AASHTO (2020). The final column sections and

corresponding reinforcement for all four locations and selected hazard levels are reported in Table 3.

**Table 3.** Summary of column geometry and reinforcement data for all locations and hazard levels.

| Location | Design Approach | H (ft) | D (ft) | Long. Reinforcement (%) | | | Trans. Reinforcement (%) | |
|---|---|---|---|---|---|---|---|---|
| | | | | 2.5%-5Years | 5.0%-5Years | 10.0%-5Years | 2.5%-5Years | 5.0%-5Years |
| San Francisco | HC | 24 | 4 | 26#9 (1.4%) | 20#9 (1.1%) | 15#9 (0.8%) | 1#4@6 in (0.3%) | |
| Los Angeles | | | | 20#9 (1.1%) | 12#9 (0.7%) | 8#9 (0.4%) | 1#4@6 in (0.3%) | |
| San Luis Obispo | | 18 | 3 | 14#7 (0.8%) | 10#7 (0.6%) | 8#7 (0.5%) | 1#3@4.5 in (0.3%) | |
| Sacramento | | | | 10#7 (0.6%) | 8#7 (0.5%) | 6#7 (0.4%) | 1#3@4.5 in (0.3%) | |

# 10. Ground-Motion Selection and Scaling

The Pacific Earthquake Engineering Research Center (PEER) NGA-W2 database was employed to select the suite of pairs of ground-motion records to perform NLTH analyses. Hazard disaggregation at the fundamental period of vibration of the bridge (approximated to 1 sec) was performed at each site of interest to center the range of variability of magnitude (M) and distance from the fault ($R_{rup}$) and inform ground-motion selection. Specifically, $M_{l,u} = M \mp 1$ and $R_{rup,l,u} = R_{rup} \mp 10\ km$ where $l$ and $u$ stand for lower and upper bound, respectively. The fault with the greatest contribution to the hazard was used to define these ranges, which are the Hayward fault for SF, the Elysian Park fault for LA, the San Andreas fault for SLO, and the Hunting Creek fault for SC. Finally, the $V_{S30}$ was made to vary within the upper and lower bounds of site class D (ASCE 7-22), that is $180 < V_{S30} < 360$ m/sec. The records selected following these criteria were scaled to approach the UHS in Figure 1. The records were ranked based on the minimum error observed in approaching the design spectrum in the spectral period bandwidth 0.5T to 2T, where T is the fundamental period of the bridge under consideration. This range is defined following the provisions in sections 3.10.2.2 and 4.7.4.3b of AASHTO (2020) and accounts for the effect of the higher modes on the dynamic response of the bridge and the possible elongation of the fundamental period due to post-peak softening and a reduction in effective stiffness induced by the material nonlinearities occurring under strong motions. The mean squared error (MSE) is used to assess how closely the ground-motion spectra approach the UHS. The first thirty pairs of ground motions (i.e., the geometric mean of the two horizontal components) with the least MSE and with $f < 3$ were selected. Considerations were also incorporated for the consideration of an adequate number of impulsive motions employing the model by Hayden et al (2014). Appendix A reports the details

of the hazard disaggregation results and ground-motion selection for San Francisco and Los Angeles at HL3. The same approach was extended to the other locations and hazard levels.

Moreover, in accordance with section 4.2.3 of the SDC v2 (2019), each pair of ground motions was rotated twice by 45 degrees to account for different possible orientations of the bridge with respect to the fault, resulting in a total of three sets of ground motions, rotated by 0 deg (original orientation of the pair), 45 deg, and 90 deg. The rotated ground motions applied in principal directions of the bridge are obtained as:

$$a_L(t) = a_{H1}(t)\, cos\, \theta + a_{H2}(t)\, sin\, \theta \quad (4\text{-}1)$$

$$a_T(t) = -\mathrm{a_{H1}(t)} \sin\theta + \mathrm{a_{H2}(t)} \cos\theta \quad (4\text{-}2)$$

where $a_L$ and $a_T$ are the accelerations in the longitudinal and transverse direction, respectively; $a_{H1}$ and $a_{H2}$ are accelerations in the original horizontal directions, H1 and H2, as obtained from the PEER NGA-W2 database; and $\theta$ is the rotation angle.

Therefore, for each location and hazard level, ninety sets of ground motions were obtained and used to perform NLTH analyses.

Figures 6 to 9 show the UHS (black thick line) for HL1, HL2 and HL3 at the four sites, the set of scaled motions (gray thin lines) and corresponding median $\pm$ one standard deviation (red lines), for each rotated pair of ground motions. Since the scaling is performed on the geometric mean of the ground-motion horizontal components, the scaling is performed once for the 0 and 90-degree orientations and once for the 45-degree orientation. The ground motions rotated by 0 and 90 degrees, although having the same geometric mean and scale factors, are applied along the longitudinal and transverse direction of the bridge separately, thus yielding 60 different responses.

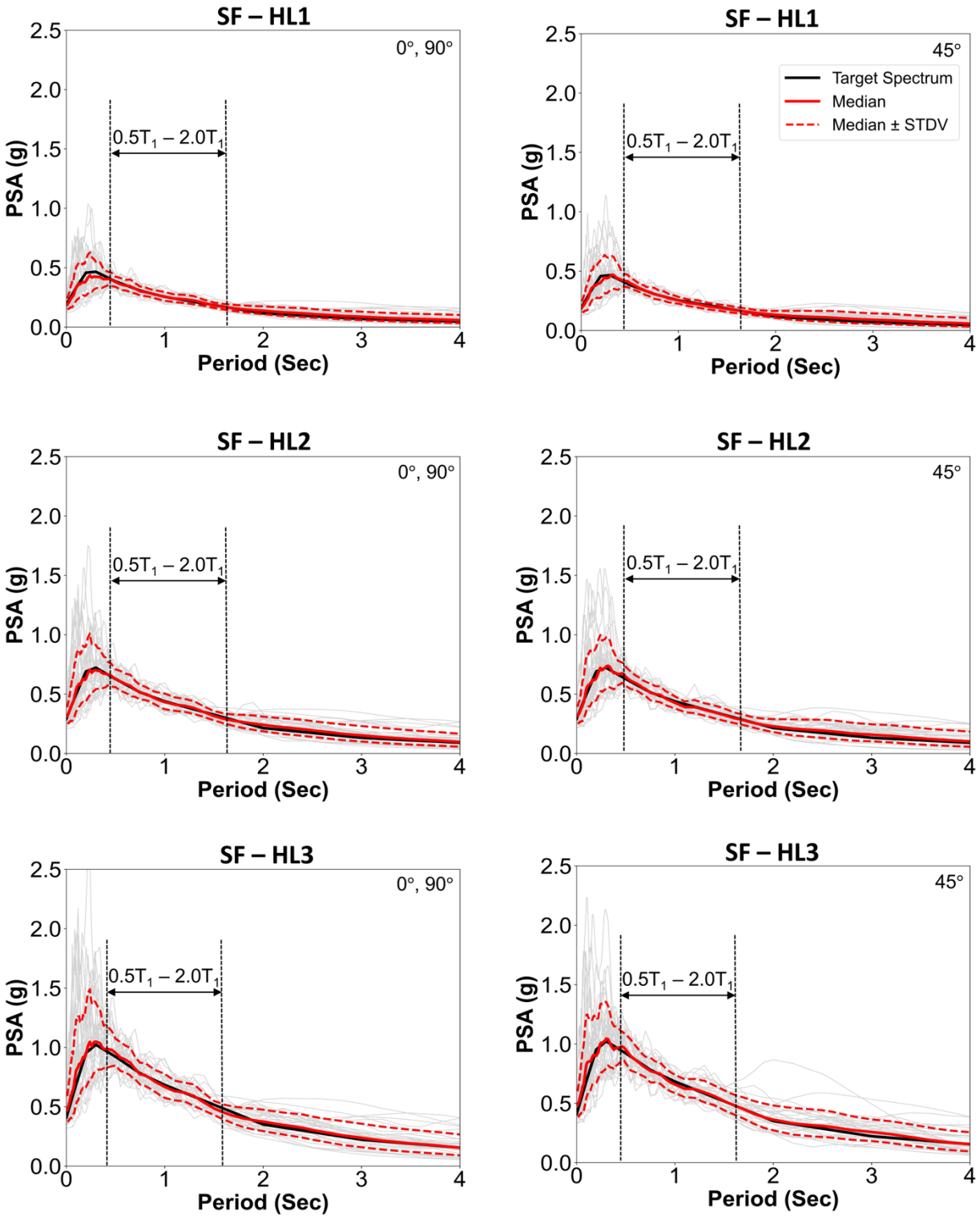


Figure 6. San Francisco: UHS for HL1, HL2, HL3, with the sets of scaled ground motions. HL1 with motions rotated by 0, 90, and 45 degrees (first row); HL2 with motions rotated by 0, 90, and 45 degrees (second row); HL3 with motions rotated by 0, 90, and 45 degrees (third row)

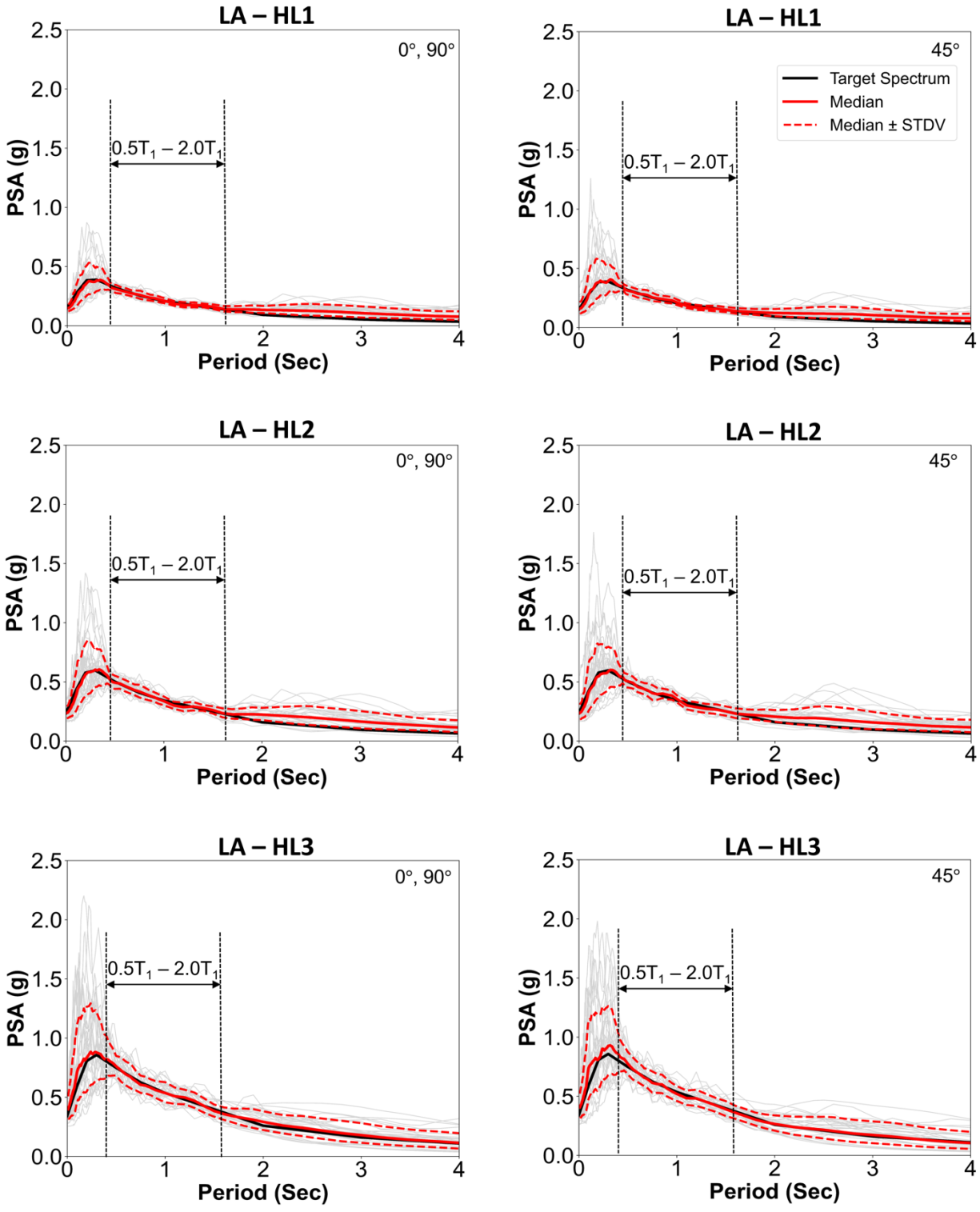


Figure 7. Los Angeles: UHS for HL1, HL2, and HL3 with the sets of scaled ground motions. HL1 with motions rotated by 0, 90, and 45 degrees (first row); HL2 with motions rotated by 0, 90, and 45 degrees (second row); HL3 with motions rotated by 0, 90, and 45 degrees (third row)

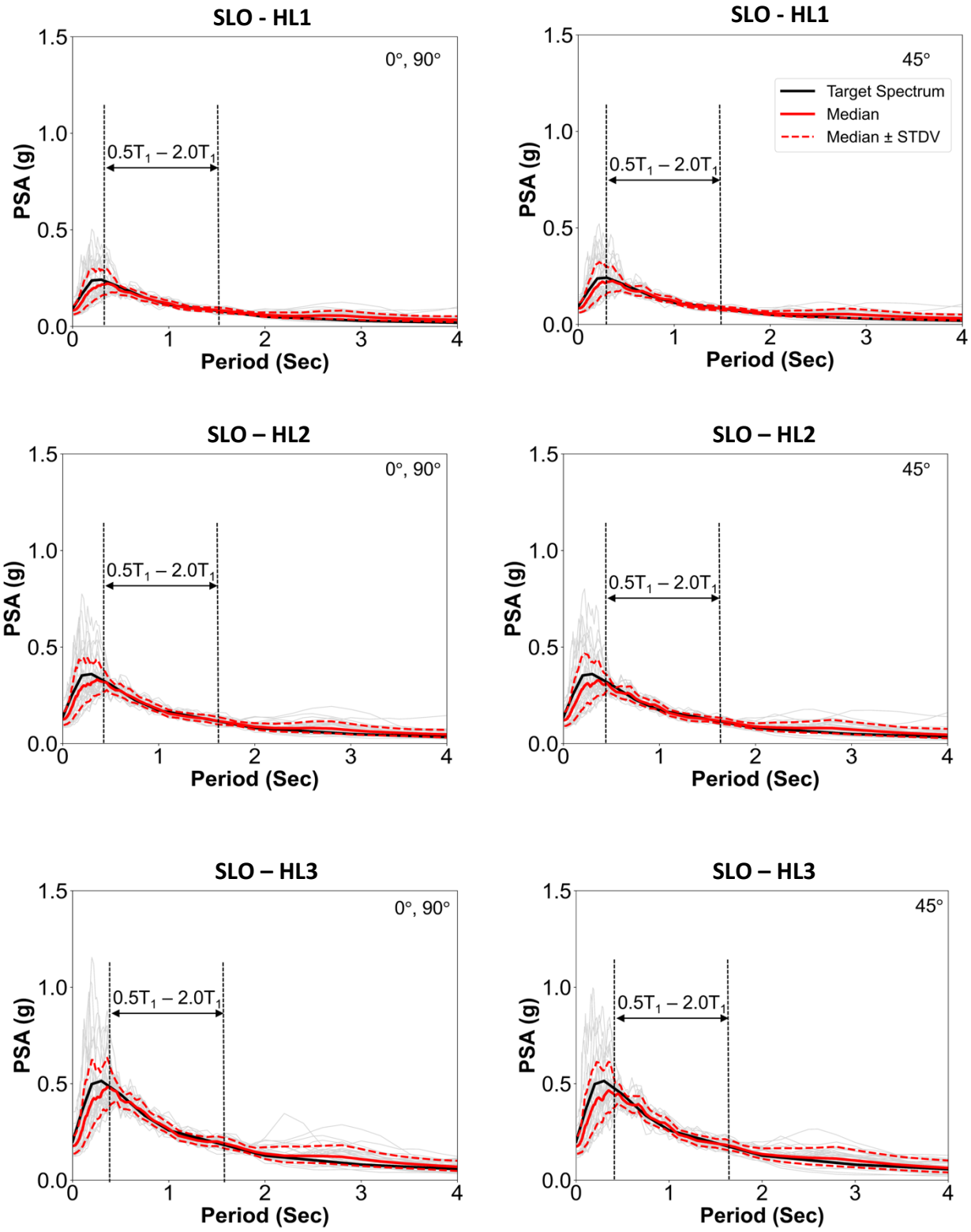


Figure 8. San Luis Obispo: UHS for HL1, HL2, and HL3 with the sets of scaled ground motions. HL1 with motions rotated by 0, 90, and 45 degrees (first row); HL2 with motions rotated by 0, 90, and 45 degrees (second row); HL3 with motions rotated by 0, 90, and 45 degrees (third row)

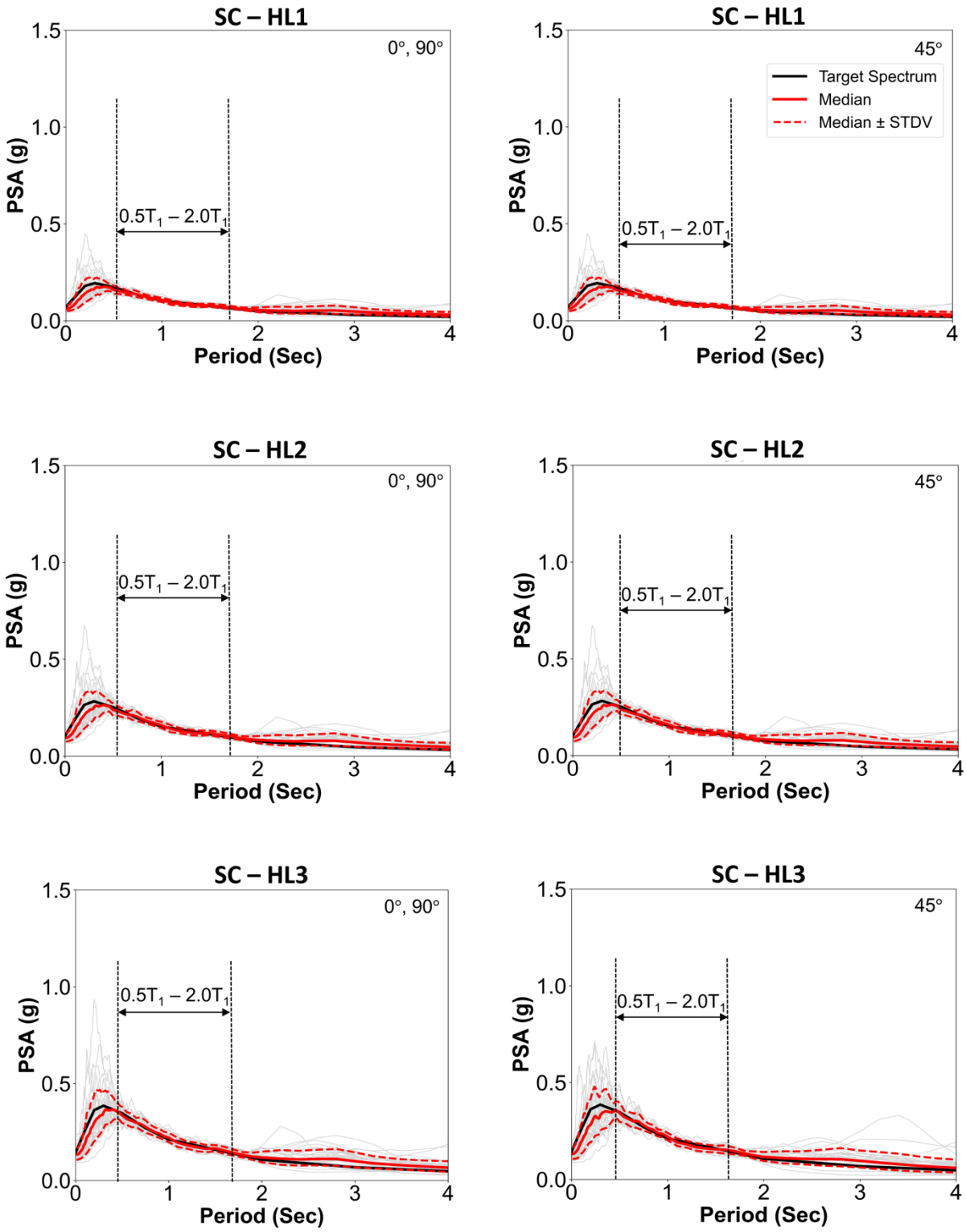


Figure 9. Sacramento: UHS for HL1, HL2, and HL3 with the sets of scaled ground motions. HL1 with motions rotated by 0, 90, and 45 degrees (first row); HL2 with motions rotated by 0, 90, and 45 degrees (second row); HL3 with motions rotated by 0, 90, and 45 degrees (third row)

# 11. Damage States

The DSs proposed by Vosooghi and Saiidi (2012) and used by Caltrans at the time of this research were selected to assess the response of the bridges. These DSs were defined based on shake-table tests performed on 32 bridge RC columns and comprise five levels of damage that can be visually identified on the columns (DS-1 through DS-5). In the current study, an additional damage state (DS-6) was added to represent collapse. The levels of progressive damage associated with each DS can be observed in Figure 10.


Damage State 1 Damage State 2 Damage State 3


Damage State 4 Damage State 5 Damage State 6

Figure 10. Damage states visualization (DS1 to DS6)

To identify the attainment of each DS in the numerical model, a set of strain and stress-based criteria were introduced based on cyclic pushover analysis. Table 4 defines each DS and the corresponding criteria utilized for their identification in the numerical model.

**Table 4.** Description of damage states.

| Column Damage State | Definition from Vosooghi and Saiidi (2010) | Criterion |
|---|---|---|
| DS-1 | Flexural cracking | Zero tensile stress is attained in the concrete cover. |
| DS-2 | Minor concrete cover spalling and shear cracks | The maximum compressive stress of unconfined concrete is attained in the concrete cover ($f_c = f'_c$) and at least one rebar has yielded |
| DS-3 | Extensive flexural cracks and relatively large concrete cover spalling | Zero stress – corresponding to crushing – is attained in the concrete cover. |
| DS-4 | Exposed lateral and longitudinal rebars | The maximum compressive stress is attained in the confined core concrete ($f_{cc}$), see shaded patches in Figure 5. |
| DS-5 | Initiation of concrete core damage and initiation of longitudinal rebars bucking. | 80% peak stress is attained in the confined core concrete ($0.80f_{cc}$) on the softening branch, outer shaded patches in Figure 5. |
| DS-6 | Loss of axial load bearing due to the extensive rebar buckling and core crushing | Buckling/rupture of at least two longitudinal rebars is attained. |

Figure 11 demonstrates the attainment of each DS on the monotonic (HL1, HL2 and HL3) and cyclic (HL3) pushover curves relevant to each column design, providing a measure of the column drift corresponding to each DS.

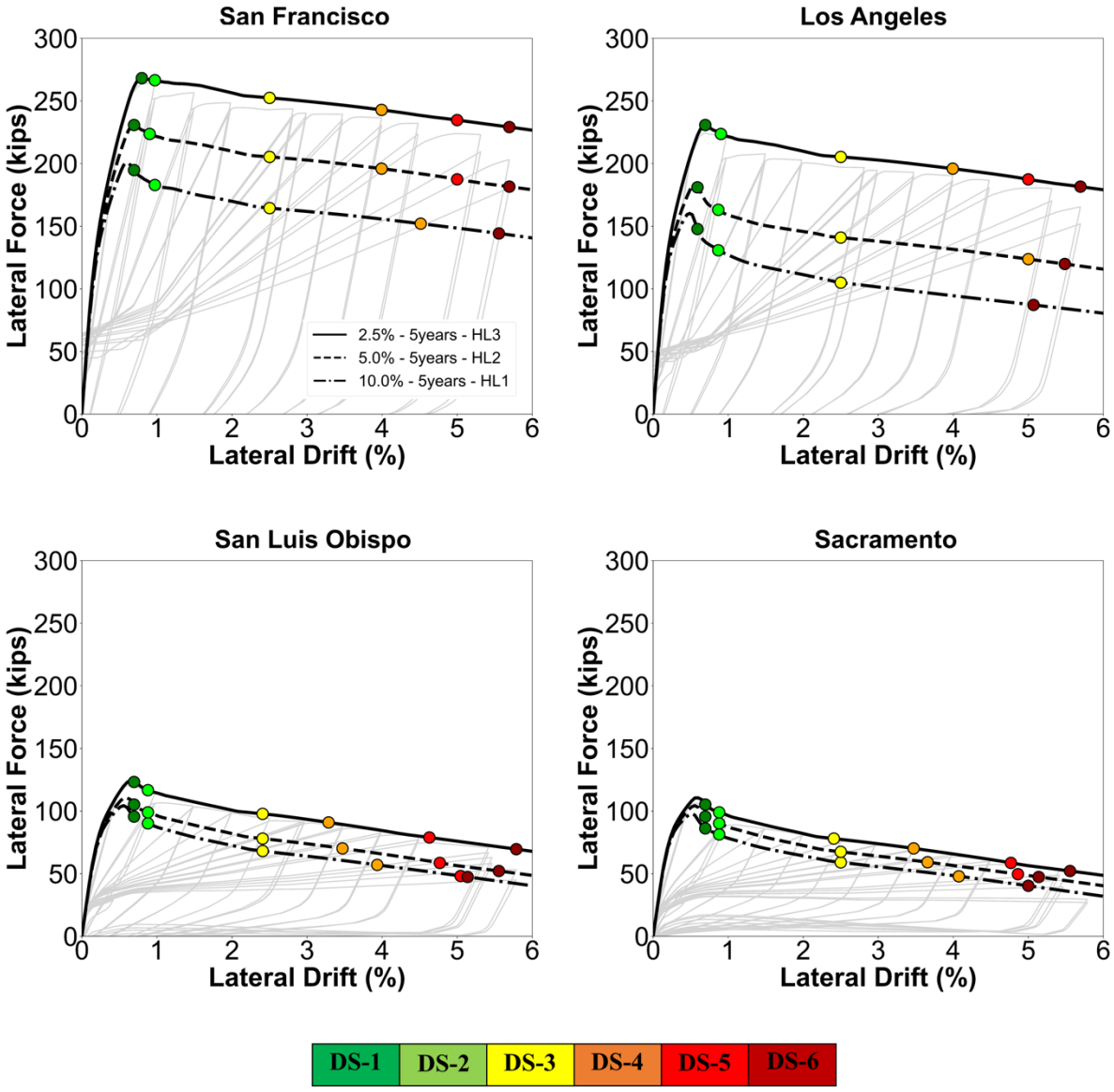


Figure 11. Pushover curves and damage states for all locations and designs.

# 12. Bridge Response Assessment

The three-dimensional nonlinear bridge model was subjected to bidirectional motions with a UniformExcitation load pattern in OpenSees (McKenna, 2011). Specifically, the ninety pairs of ground motions selected and scaled as described in the previous section, were applied along the two principal directions of the bridge (transverse, T, and longitudinal, L), for each location and hazard level. Therefore, a total of 3 x 2 x 90 = 540 analyses were executed. The structural response was assessed in terms of maximum drift recorded at the top of the columns in the bridge's principal directions.

Figures 12 to 14 show the statistics of the drift (median, $16^{th,}$ and $84^{th}$ percentiles, minimum and maximum) for the two separate components of the bridge across all locations and for HL1 and HL2. As a reminder, the subscript 'HCD' next to each location acronym stands for 'hazard consistent design' to distinguish it from the 'minimum design' (MD) that will be discussed in the next section. Note that the color bar indicates the attainment of each damage state for each column design consistently with the color code adopted in Figure 11.

For HL1, the median and dispersion of the drifts fall within and below DS-1. For HL2, the median and dispersion of the drifts are seen to fall within DS-1 and DS-2 across all four locations. A similar trend is observed for HL3, for which the median and dispersion of the drifts are seen to fall within DS-2, pointing to a performance consistent with the hazard-based design. Appendix B reports the distribution of the ductility demands.

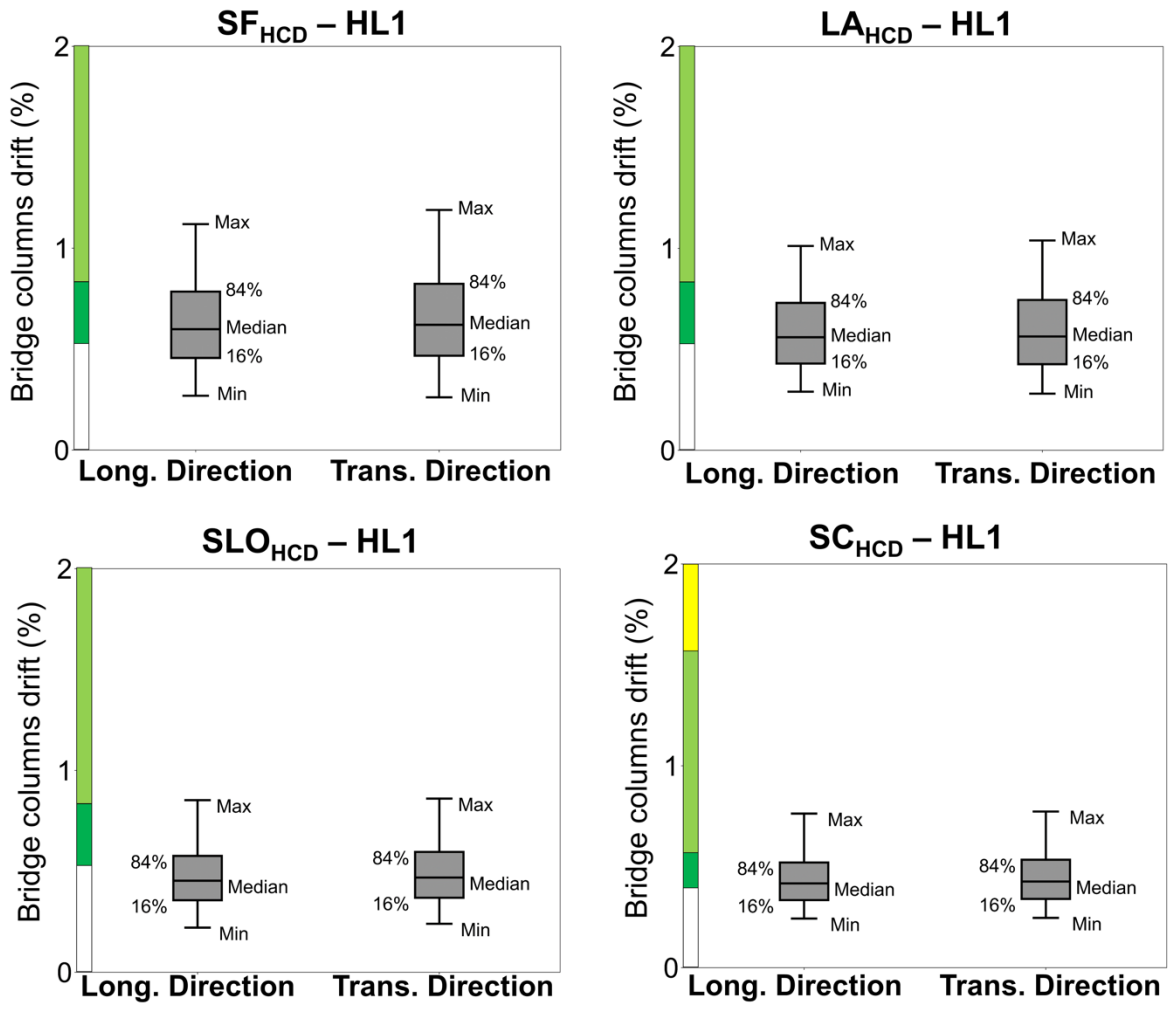


Figure 12. Bridge response statistics for the hazard-consistent bridges in San Francisco, Los Angeles, San Louis Obispo, and Sacramento for HL1.

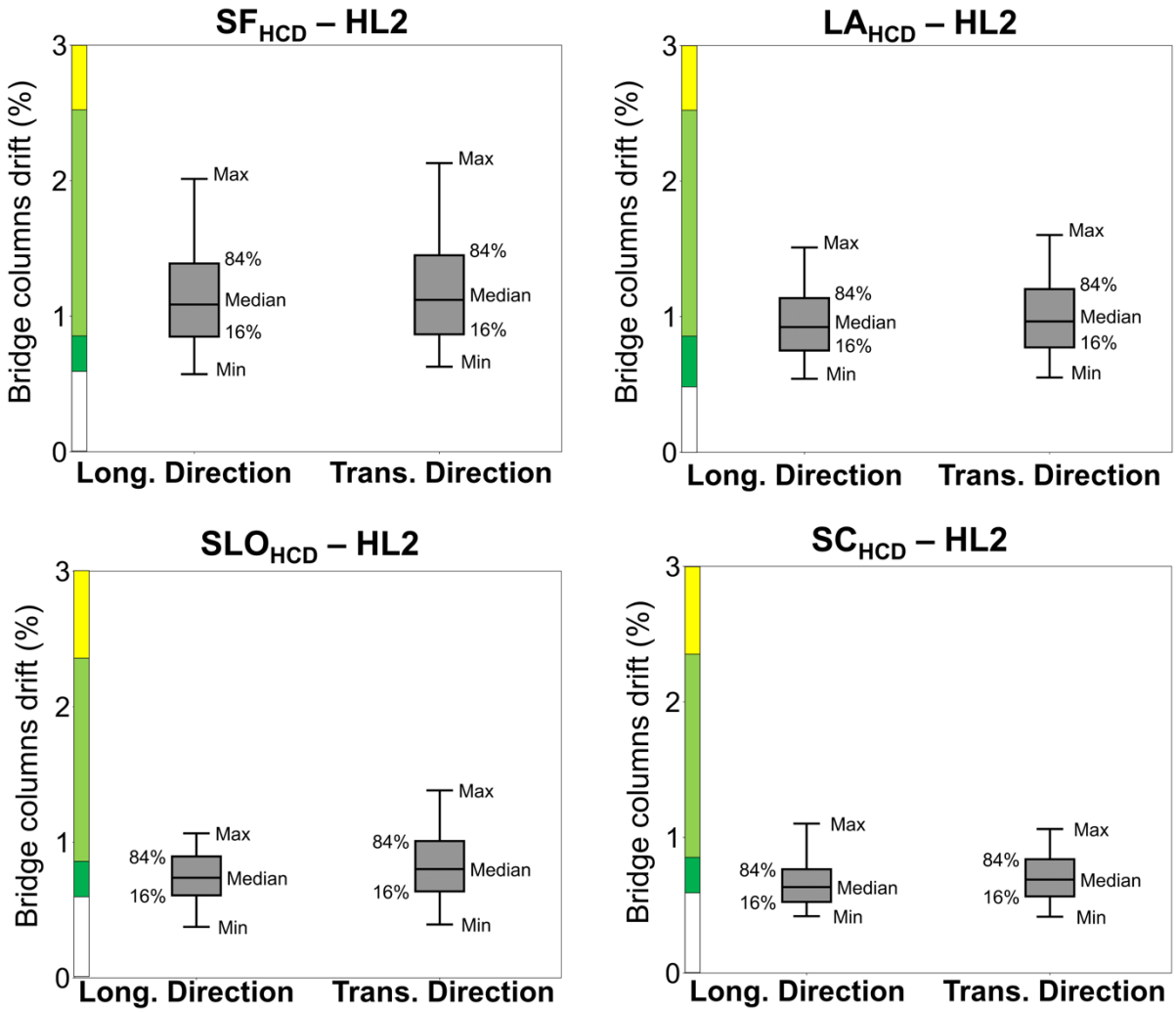


Figure 13. Bridge response statistics for the hazard-consistent bridges in San Francisco, Los Angeles, San Louis Obispo, and Sacramento for HL2.

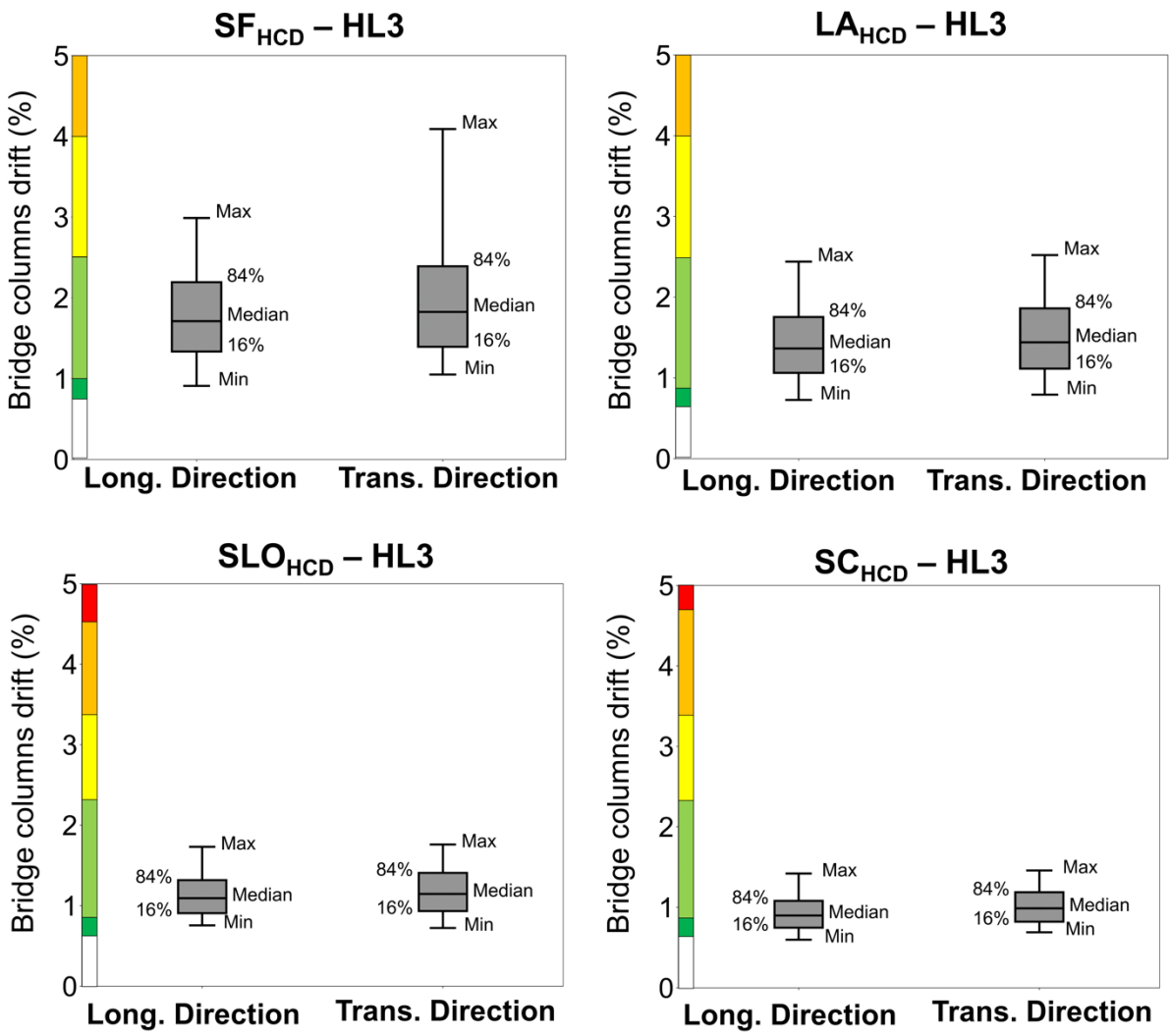


Figure 14. Bridge response statistics for the hazard-consistent bridges in San Francisco, Los Angeles, San Louis Obispo, and Sacramento for HL3.

The bridge responses for HL2 and HL3 were used to develop fragility functions, by which the probability of exceeding each damage state is assessed across all hazard levels. Probabilistic seismic demand models (PSDMs) were developed considering the drifts in each principal direction of the bridge as the reference engineering demand parameter ($EDP_{T,L}$) and the pseudo-spectral acceleration at the fundamental period of the bridge in each principal direction as the reference

intensity measure ($IM_{T,L}$). Therefore, separate PSDMs were generated for the two directions and used to develop the fragility functions, as shown below:

$$\mathrm{P}\left[D_{T,L} \geq C_{T,L} \middle| \mathrm{IM}_{T,L}\right] = \Phi\left(\frac{\ln\left(EDP_{d(T,L)}\right) - \ln\left(EDP_{c(T,L)}\right)}{\beta_{EDP_{(T,L)}|IM_{(T,L)}}}\right) \quad (6\text{-}1)$$

where $EDP_{d,(T,L)}$ = the seismic demand median (i.e., the median of the drift for each, location, HL, and direction, see Figure 12-14), $EDP_{c(T,L)}$= the limit state median (i.e., the values of the drift from each DS obtained from the pushover analyses, see Figure 11), and $\beta_{EDP_{(T,L)}|IM_{(T,L)}} =$ the dispersion of the seismic demand (i.e., the standard deviation in lognormal units in Figures 12-14).

Fragility functions were developed for each DS and shown in Figure 15. Also included in the plots are the design spectral accelerations at the fundamental period of the bridge, indicated with a black dotted line. Based on the fragility plots shown, it is found that temporary bridges designed for earthquakes with return periods of 100 or 200 years will exhibit repairable damage even when the AASHTO minimum reinforcement requirements are not met.

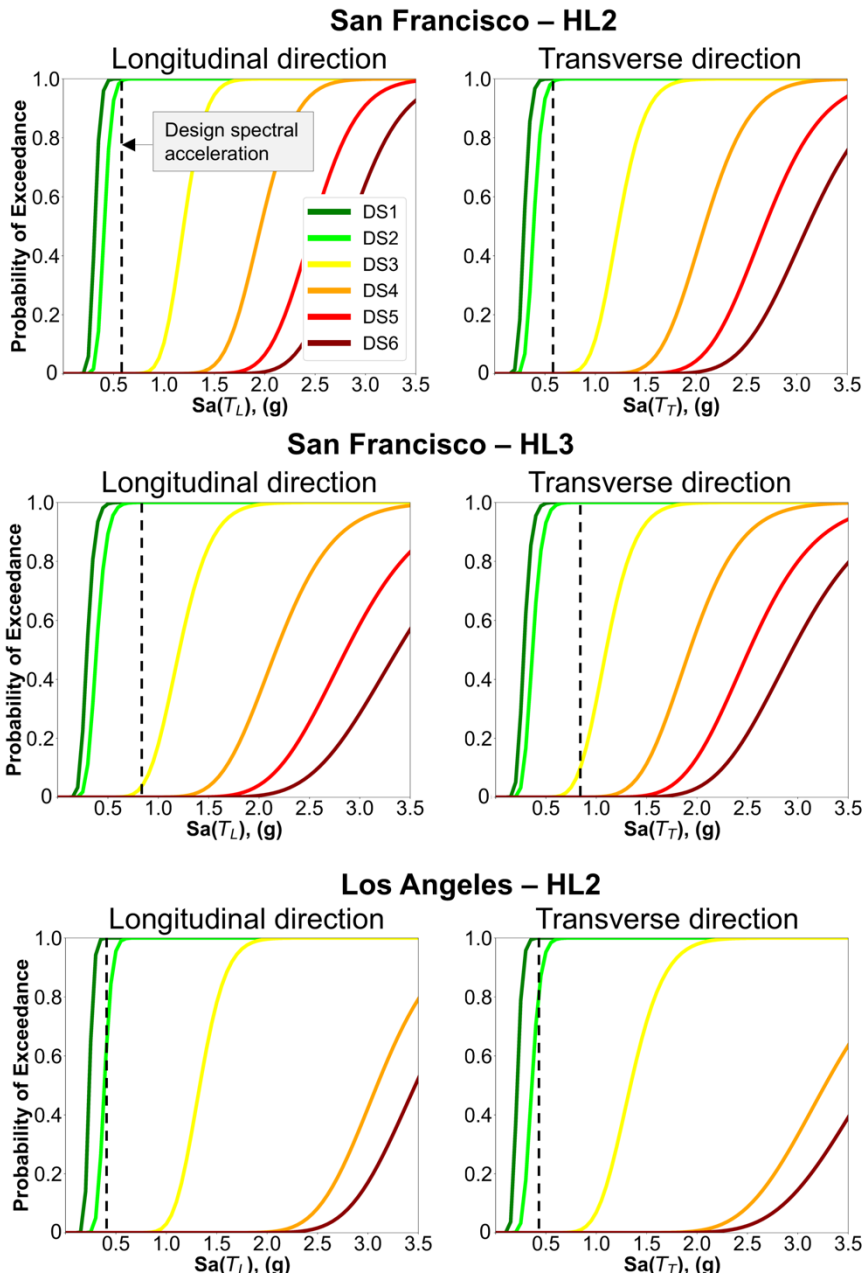
San Francisco – HL2
Longitudinal direction
Transverse direction
Probability of Exceedance
Design spectral acceleration
DS1
DS2
DS3
DS4
DS5
DS6
Sa($T_L$), (g)
Sa($T_T$), (g)
San Francisco – HL3
Longitudinal direction
Transverse direction
Probability of Exceedance
Sa($T_L$), (g)
Sa($T_T$), (g)
Los Angeles – HL2
Longitudinal direction
Transverse direction
Probability of Exceedance
Sa($T_L$), (g)
Sa($T_T$), (g)

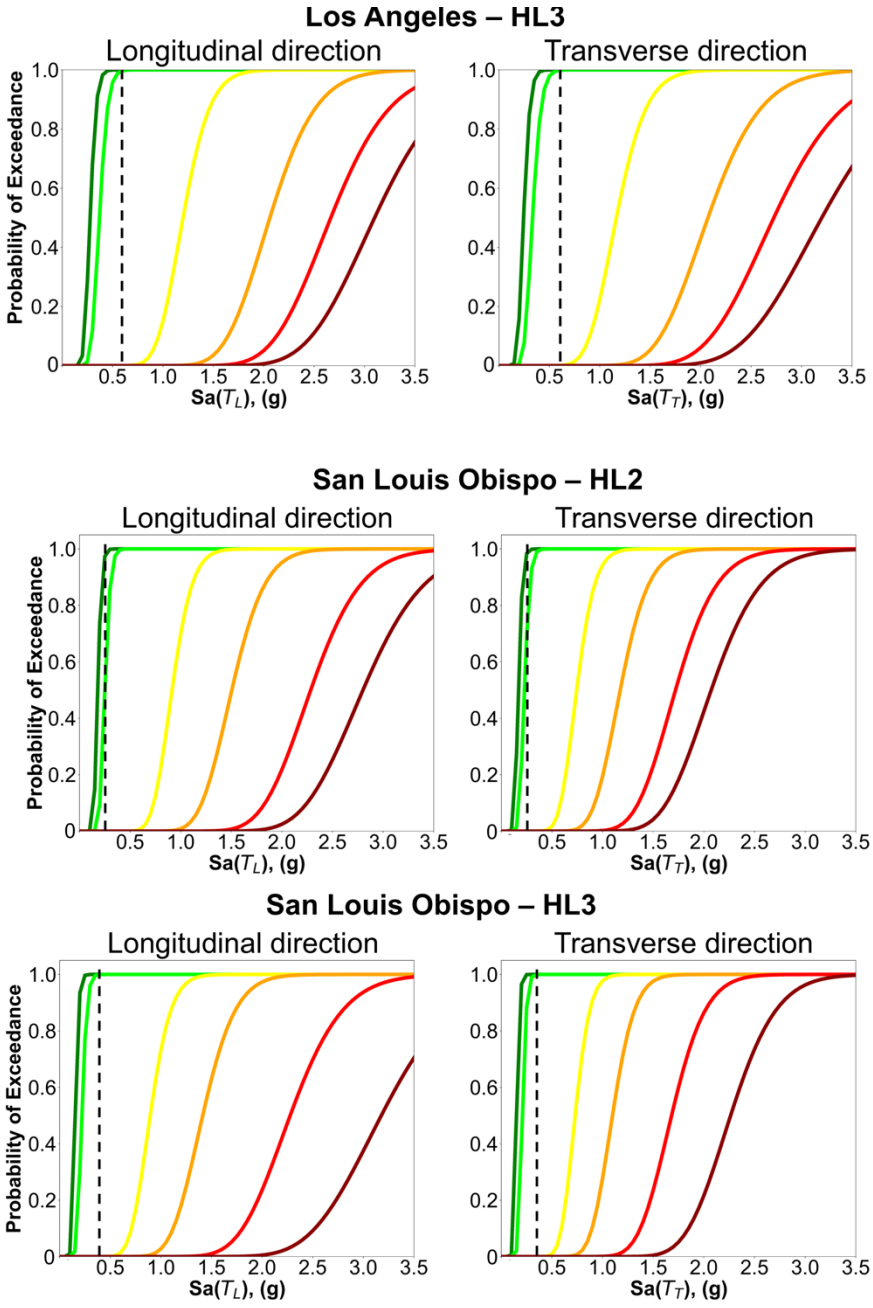
Los Angeles – HL3
Longitudinal direction
Transverse direction
Probability of Exceedance
Sa($T_L$), (g)
Sa($T_T$), (g)
San Louis Obispo – HL2
Longitudinal direction
Transverse direction
Probability of Exceedance
Sa($T_L$), (g)
Sa($T_T$), (g)
San Louis Obispo – HL3
Longitudinal direction
Transverse direction
Probability of Exceedance
Sa($T_L$), (g)
Sa($T_T$), (g)

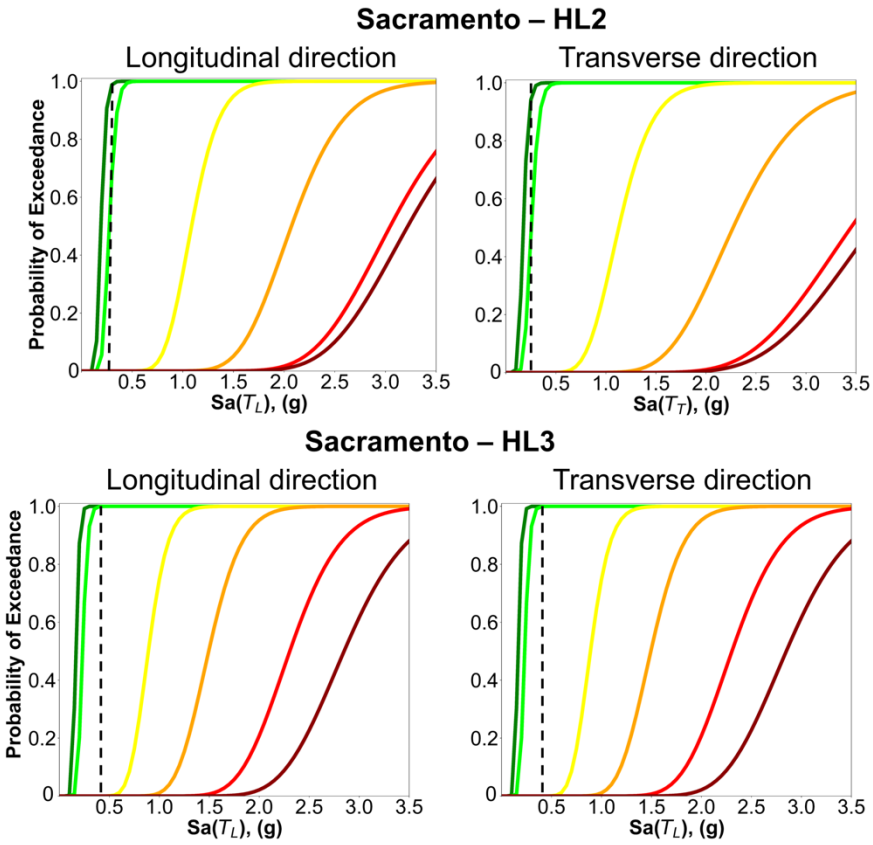


Figure 15. Fragility functions across all considered locations (San Francisco, Los Angeles, San Louis Obispo and Sacramento), and hazard levels (HL2 = 100-year return period, HL3 = 200-year return period).

Based on the evidence from this first phase of the work, defined as Approach #1, this study takes a step forward and attempts to identify the HL for which a 'baseline' temporary bridge designed to strictly meet the AASHTO minimum reinforcement requirements can ensure life safety, thus relieving from the need to perform a site-specific analysis. This second phase is referred to as Approach #2.

# 13. Performance of Bridges Satisfying Minimum Reinforcement Requirements

Based on the AASHTO provisions, the column with minimum reinforcement requirements, hereafter referred to as MD column, is assumed to have the following properties: circular cross-section with a diameter = 4 ft, height = 24 ft, 1% longitudinal reinforcement ratio, and 0.35% transverse reinforcement ratio. This column is employed for the bridge models across all considered locations (SF, LA, SLO and SC) and hazard levels considered in Approach #2, that is 200 years (2.5% probability of exceedance in 5 years, which corresponds to the same HL3 discussed earlier), 500 years (1% probability of exceedance in 5 years) referred to as HL4 hereafter, and 975 years (0.5% probability of exceedance in 5 years) referred to as HL5 hereafter and corresponding to the return period for ordinary bridges.

Figure 16 shows the monotonic (in black) and cyclic (in gray) pushover curves for the MD column with the colored dots representing the attainment of the damage states defined in Table 4. Figure 17 reports the UHS corresponding to the two additional return periods (500 and 975 years) considered in this portion of the study. The same selection and scaling methods illustrated earlier were employed to obtain a set of thirty ground motions for HL4 and HL5, at each location. The motions were again rotated twice by 45 deg, thus leading to a total of 180 new pairs of motions and corresponding nonlinear time-history analyses performed in OpenSees (McKenna, 2011).

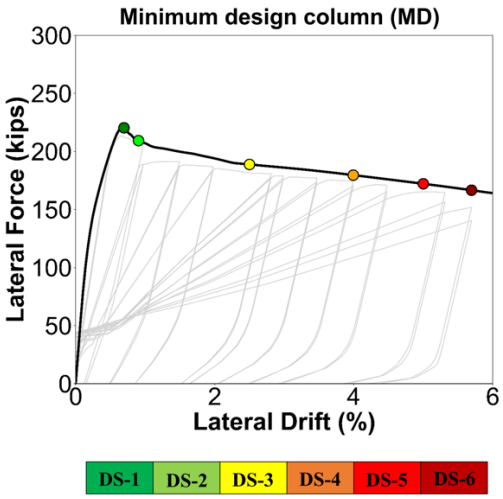


Figure 16. Monotonic and cyclic pushover curves and damage states for the 'minimum design' column.

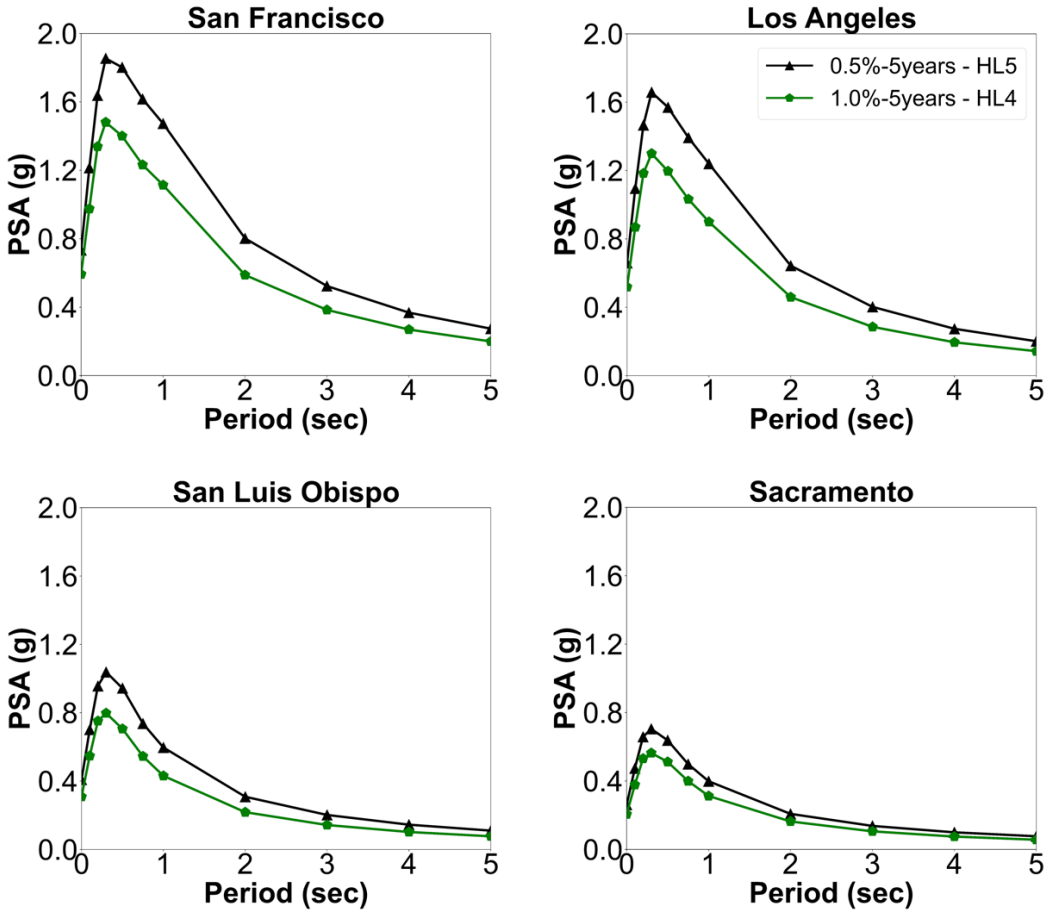


Figure 17. Uniform Hazard Spectra (UHS) for the four selected levels (HL4, and HL5) of hazard at the four locations (SF, LA, SLO, and SC)

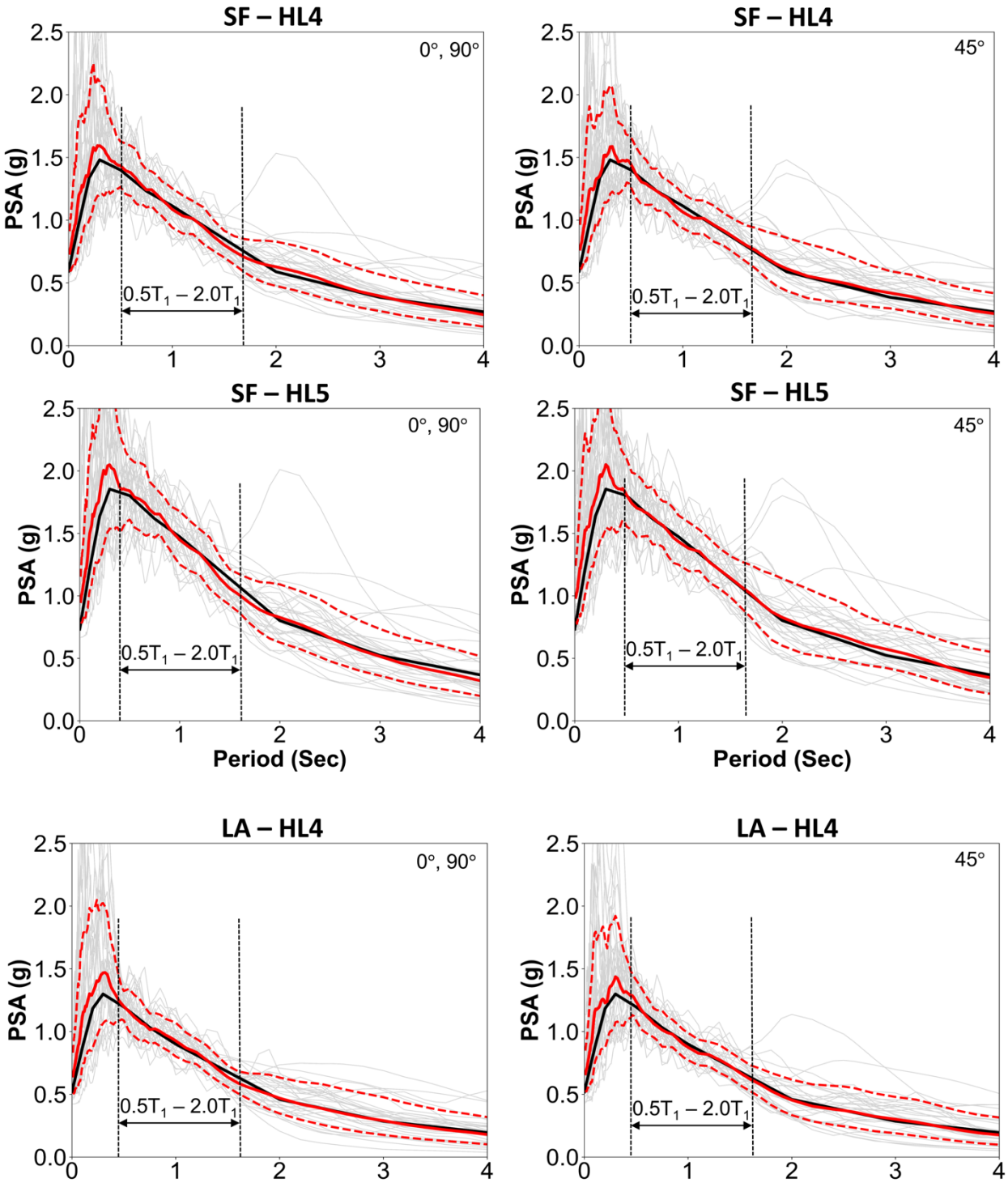
SF – HL4
0°, 90°
SF – HL4
45°
SF – HL5
0°, 90°
SF – HL5
45°
LA – HL4
0°, 90°
LA – HL4
45°
PSA (g)
Period (Sec)
0.5T1 – 2.0T1

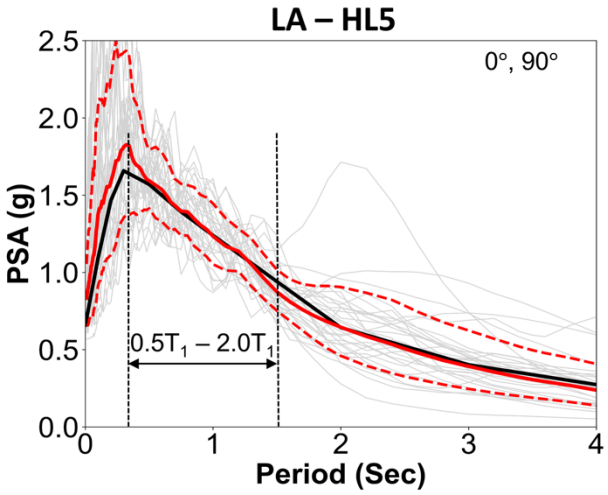
LA – HL5
0°, 90°
PSA (g)
0.5T1 – 2.0T1
Period (Sec)

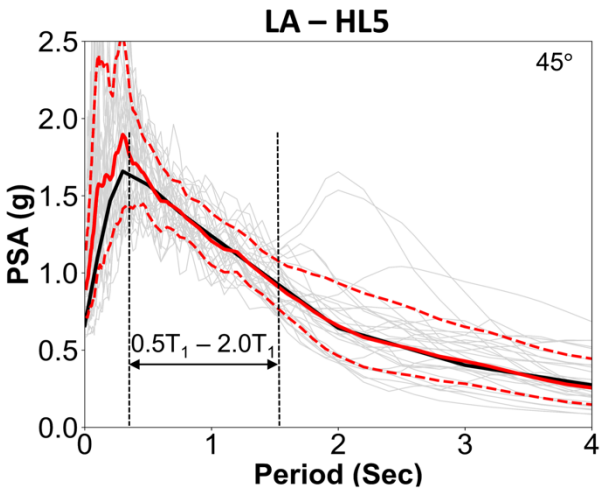
LA – HL5
45°
PSA (g)
0.5T1 – 2.0T1
Period (Sec)

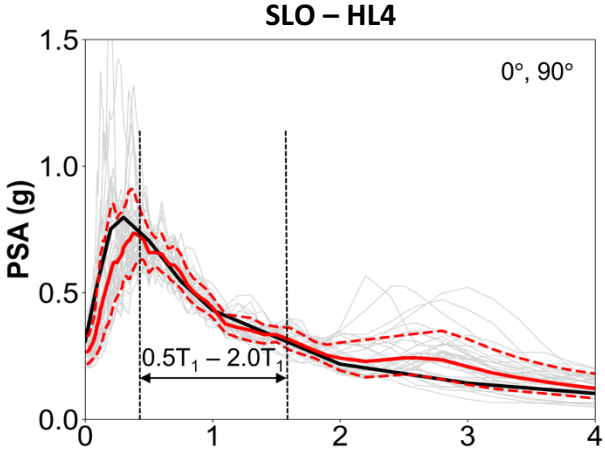
SLO – HL4
0°, 90°
PSA (g)
0.5T1 – 2.0T1

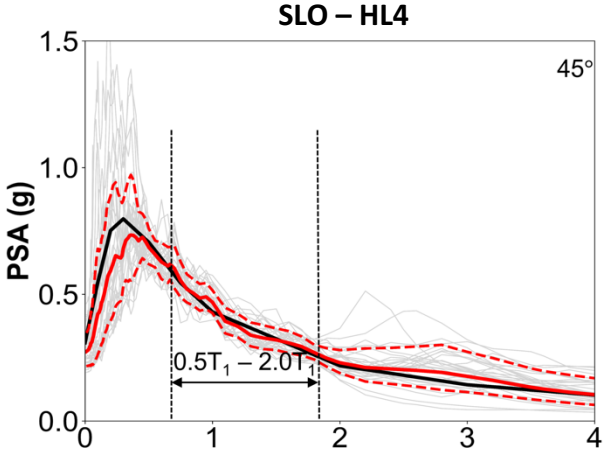
SLO – HL4
45°
PSA (g)
0.5T1 – 2.0T1

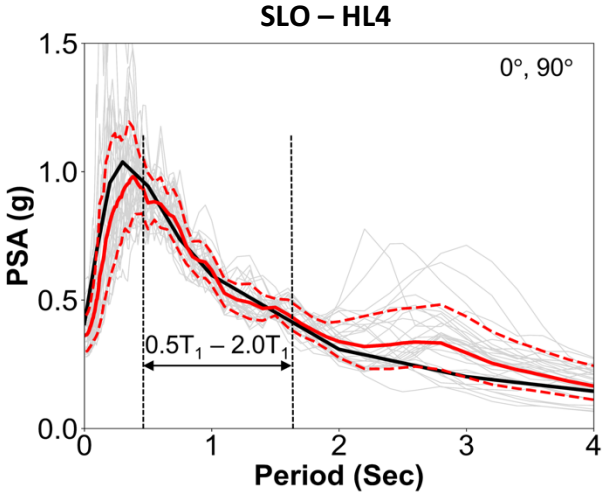
SLO – HL4
0°, 90°
PSA (g)
0.5T1 – 2.0T1
Period (Sec)

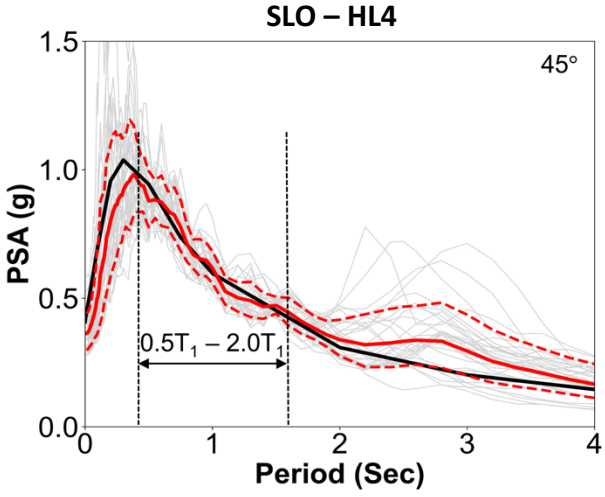
SLO – HL4
45°
PSA (g)
0.5T1 – 2.0T1
Period (Sec)

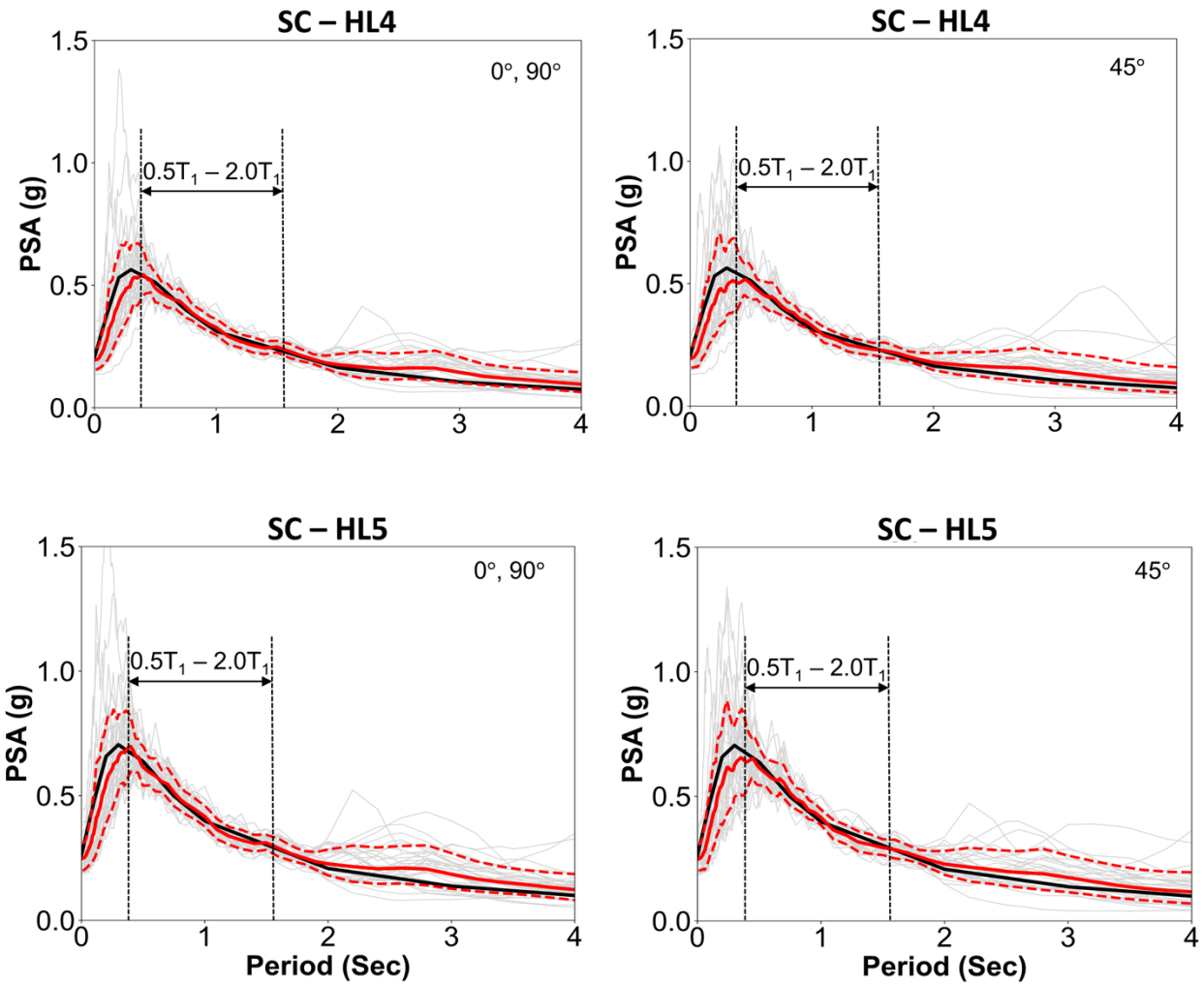


Figure 18. UHS for HL4, and HL5, with the sets of scaled ground motions rotated by 0, 90, and 45 degrees for all four locations.

The statistics of the bridge drifts obtained from this set of analyses are summarized in Table 5 and Figures 19 and 20. As in the case of the HCD column, demand median and dispersion substantially fall within DS-2 across all four locations for HL3 (200-year return period). Noteworthy, the increase in cross-section size and reinforcement ratio for the bridge in SLO and SC did not reflect substantial differences in the structural response, which are seen again to fall at the onset of DS-2. This is due to the competing effect of increased structural stiffness (4-ft vs. 3-ft column diameter) and strength (1% longitudinal reinforcement and 0.35% transverse reinforcement affecting

confinement) and the larger spectral accelerations at shorter spectral periods. The fundamental periods of the bridge at the SLO and SC location are seen to change from $T_T = 0.96$ sec, $T_L = 0.95$ sec for the HC column, to $T_T = 0.83$ sec, $T_L = 0.82$ for the MD column, with a consequent increase of spectral accelerations from 0.26 g to 0.31 g. Considering that the bridge remains substantially linear for drifts around 1%, an increase of about 29% in the structural stiffness and an increase in the spectral acceleration at the fundamental period of the structure of about 20% leads to slightly larger responses in the HCD column compared to the MD column.

As expected, the analyses for HL4 demonstrate that with the MD bridge the median drifts reach DS-3 in SF, with the 84$^{th}$ percentile attaining DS-4 in the transverse direction. Maximum values of the drifts in the transverse direction are also seen to attain values as high as 7.7%, corresponding to DS-6. This is obtained with the 2007 Chuetsu-oki earthquake at the Kashiwazaki City Center EW station, when the ground-motion components are rotated by 45 deg. Upon a closer analysis, this ground motion shows a high polarization, with the ratio of the spectral acceleration of the two components at the fundamental period of the bridge of about 2.5. Specifically, the spectral acceleration of the rotated component H2, which is applied in the transverse direction of the bridge, attains a value of 1.9 g, which is about 1.36 times larger than the design spectral acceleration at the fundamental period of the bridge. Similarly to SF, the median demands at the LA location for HL4 reach DS-3 in both longitudinal and transverse directions. Once again, the maximum drift of 5.6% corresponding to DS-5, is seen for the 2007 Chuetsu-oki earthquake at the NIG018 EW station. The response statistics at SLO and SC show an expected increase compared to HL2 due to the higher spectral accelerations corresponding to shorter periods, but still with both the median and 84$^{th}$ percentile falling within DS-2.

For HL5, at the SF location, the median values reach DS-4 in the longitudinal direction and DS-5 in the transverse direction, herein associated with Life Safety, with the 84$^{th}$ percentile attaining DS-6 for both directions. The maximum demand in the transverse direction has a value of 11.1%, which is caused by the observed ground-motion polarization. At the LA location, the median demands fall within DS-3 for the longitudinal direction and within the DS-4 for the transverse direction. The response statistics for the SLO show an expected increase placing the median response within the upper bound of DS-2 for the longitudinal direction and DS-3 for the transverse direction. At the SC location, both the median and 84$^{th}$ percentile are within DS-2. The drift distributions are reported in Figures 19 and 20 and summarized in Table 5. Appendix B reports the distribution of the ductility demands.

**Table 5.** Drift distribution table for MD approach.

| | | HL3 (200 years) | | | | | | HL4 (500 years) | | | | | | HL5 (975 years) | | | | | |
|---|---|---|---|---|---|---|---|---|---|---|---|---|---|---|---|---|---|---|---|
| | | Longitudinal | | | Transverse | | | Longitudinal | | | Transverse | | | Longitudinal | | | Transverse | | |
| | | θ=0° | θ=45° | θ=90° | θ=0° | θ=45° | θ=90° | θ=0° | θ=45° | θ=90° | θ=0° | θ=45° | θ=90° | θ=0° | θ=45° | θ=90° | θ=0° | θ=45° | θ=90° |
| San Francisco | Min | 1.05 | 0.91 | 1.24 | 1.36 | 1.25 | 1.21 | 2.14 | 1.76 | 2.61 | 2.64 | 2.35 | 2.26 | 3.20 | 2.38 | 3.42 | 3.20 | 3.33 | 3.22 |
| | 16% | 1.46 | 1.41 | 1.49 | 1.62 | 1.47 | 1.61 | 2.76 | 2.46 | 2.83 | 3.07 | 2.86 | 3.08 | 3.96 | 3.42 | 3.96 | 4.37 | 4.37 | 4.34 |
| | Median | 1.92 | 1.88 | 1.87 | 2.02 | 2.00 | 2.09 | 3.52 | 3.34 | 3.47 | 3.84 | 4.03 | 3.92 | 5.08 | 4.63 | 4.85 | 5.50 | 5.99 | 5.56 |
| | 84% | 2.51 | 2.51 | 2.34 | 2.53 | 2.72 | 2.71 | 4.49 | 4.53 | 4.26 | 4.81 | 5.68 | 5.00 | 6.52 | 6.27 | 5.94 | 6.93 | 8.20 | 7.13 |
| | Max | 3.26 | 3.16 | 3.24 | 3.49 | 3.98 | 3.53 | 5.65 | 5.77 | 5.65 | 6.52 | 7.74 | 6.26 | 8.44 | 8.00 | 8.02 | 9.40 | 11.10 | 9.14 |
| Los Angeles | Min | 0.80 | 0.77 | 0.83 | 1.00 | 0.86 | 0.84 | 1.70 | 1.33 | 2.03 | 2.23 | 1.73 | 1.78 | 2.16 | 2.00 | 2.98 | 2.83 | 2.41 | 2.39 |
| | 16% | 1.02 | 1.10 | 1.15 | 1.26 | 1.13 | 1.10 | 2.14 | 1.90 | 2.28 | 2.46 | 2.19 | 2.29 | 3.06 | 2.79 | 3.26 | 3.56 | 3.35 | 3.38 |
| | Median | 1.34 | 1.41 | 1.47 | 1.60 | 1.47 | 1.44 | 2.73 | 2.60 | 2.85 | 3.11 | 2.99 | 2.95 | 3.95 | 3.75 | 4.01 | 4.49 | 4.75 | 4.37 |
| | 84% | 1.74 | 1.80 | 1.88 | 2.02 | 1.90 | 1.88 | 3.49 | 3.55 | 3.56 | 3.93 | 4.09 | 3.80 | 5.11 | 5.05 | 4.94 | 5.66 | 6.73 | 5.64 |
| | Max | 2.45 | 2.25 | 2.50 | 2.64 | 2.40 | 2.50 | 4.53 | 4.55 | 4.44 | 5.04 | 5.56 | 4.92 | 6.41 | 6.61 | 6.54 | 7.58 | 8.98 | 7.29 |
| San Louis Obispo | Min | 0.58 | 0.58 | 0.59 | 0.57 | 0.62 | 0.63 | 1.29 | 1.06 | 1.13 | 1.13 | 1.00 | 1.31 | 1.68 | 1.51 | 1.91 | 1.95 | 1.76 | 1.71 |
| | 16% | 0.78 | 0.78 | 0.81 | 0.82 | 0.79 | 0.80 | 1.43 | 1.33 | 1.34 | 1.37 | 1.46 | 1.47 | 2.04 | 1.82 | 2.07 | 2.17 | 2.20 | 2.10 |
| | Median | 0.96 | 0.93 | 1.01 | 1.03 | 1.01 | 0.97 | 1.65 | 1.65 | 1.58 | 1.63 | 1.82 | 1.71 | 2.39 | 2.33 | 2.41 | 2.54 | 2.65 | 2.47 |
| | 84% | 1.17 | 1.12 | 1.28 | 1.30 | 1.29 | 1.18 | 1.91 | 2.05 | 1.87 | 1.94 | 2.26 | 1.98 | 2.81 | 2.99 | 2.82 | 2.99 | 3.19 | 2.89 |
| | Max | 1.54 | 1.24 | 1.67 | 1.67 | 1.73 | 1.51 | 2.12 | 2.53 | 2.20 | 2.28 | 2.40 | 2.19 | 3.23 | 3.68 | 3.33 | 3.37 | 3.61 | 3.48 |
| Sacramento | Min | 0.45 | 0.49 | 0.49 | 0.50 | 0.47 | 0.46 | 0.90 | 0.75 | 0.70 | 0.82 | 0.89 | 0.90 | 1.10 | 0.93 | 0.96 | 0.96 | 0.98 | 1.21 |
| | 16% | 0.62 | 0.61 | 0.67 | 0.67 | 0.65 | 0.62 | 1.01 | 0.90 | 0.95 | 1.01 | 1.08 | 1.02 | 1.26 | 1.16 | 1.23 | 1.24 | 1.41 | 1.32 |
| | Median | 0.76 | 0.74 | 0.85 | 0.85 | 0.81 | 0.76 | 1.13 | 1.10 | 1.17 | 1.22 | 1.31 | 1.15 | 1.47 | 1.41 | 1.50 | 1.53 | 1.69 | 1.53 |
| | 84% | 0.94 | 0.89 | 1.07 | 1.08 | 1.02 | 0.93 | 1.26 | 1.34 | 1.45 | 1.47 | 1.60 | 1.30 | 1.72 | 1.70 | 1.82 | 1.87 | 2.02 | 1.77 |
| | Max | 1.02 | 1.06 | 1.30 | 1.35 | 1.35 | 1.00 | 1.38 | 1.55 | 1.89 | 1.91 | 1.76 | 1.49 | 1.97 | 2.15 | 2.38 | 2.48 | 2.22 | 2.00 |

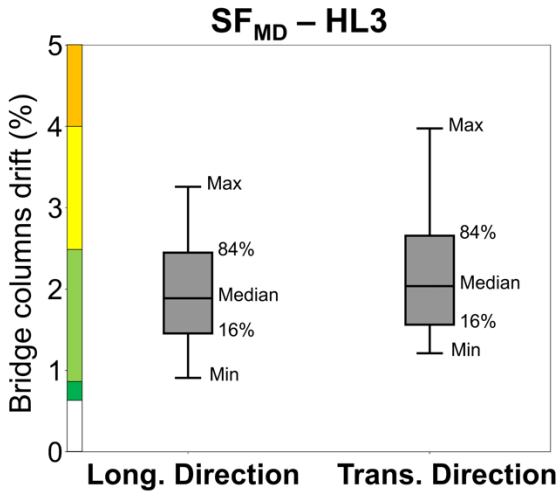
SF$_{MD}$ – HL3
Bridge columns drift (%)
0
1
2
3
4
5
Max
84%
Median
16%
Min
Max
84%
Median
16%
Min
Long. Direction
Trans. Direction

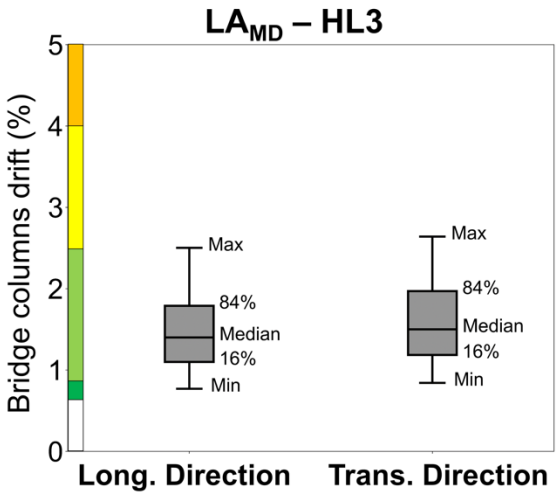
LA$_{MD}$ – HL3
Bridge columns drift (%)
0
1
2
3
4
5
Max
84%
Median
16%
Min
Max
84%
Median
16%
Min
Long. Direction
Trans. Direction

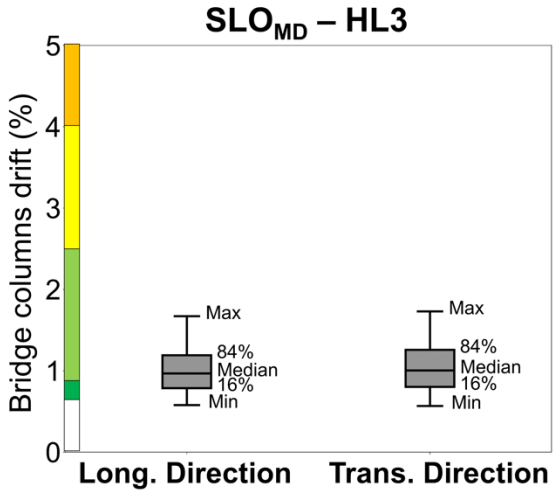
SLO$_{MD}$ – HL3
Bridge columns drift (%)
0
1
2
3
4
5
Max
84%
Median
16%
Min
Max
84%
Median
16%
Min
Long. Direction
Trans. Direction

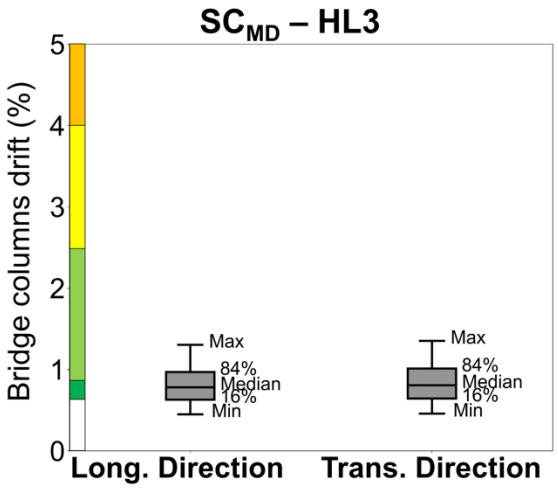
SC$_{MD}$ – HL3
Bridge columns drift (%)
0
1
2
3
4
5
Max
84%
Median
16%
Min
Max
84%
Median
16%
Min
Long. Direction
Trans. Direction

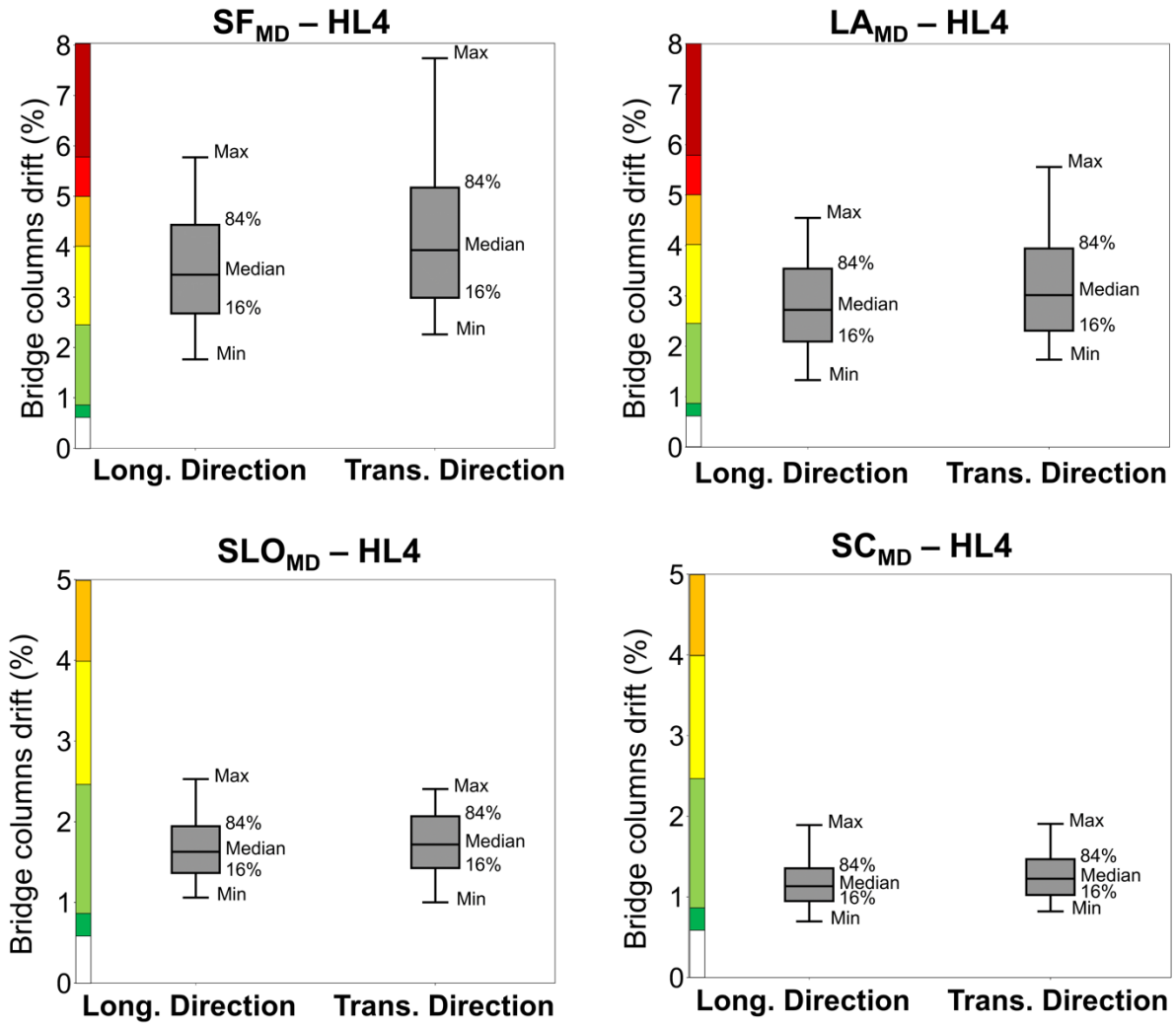


Figure 19. Bridge response statistics for the minimum design bridges in San Francisco, Los Angeles, San Louis Obispo, and Sacramento for HL3 and HL4.

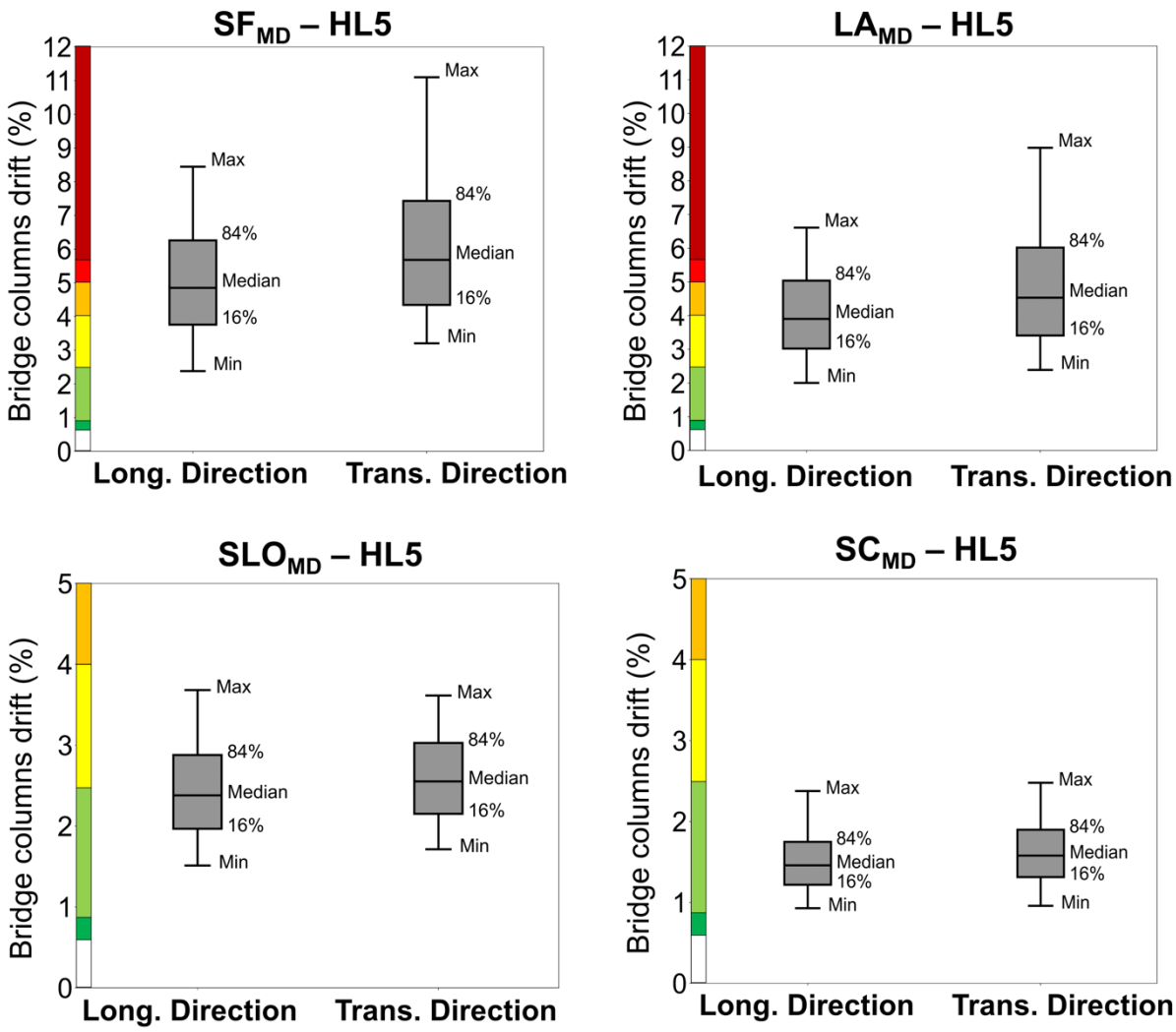


Figure 20. Bridge response statistics for the minimum design bridges in San Francisco, Los Angeles, San Louis Obispo, and Sacramento for HL5 (same return period of ordinary bridges).

PSDMs were generated to establish the relationship between the spectral acceleration at the fundamental period of the bridges and the seismic demands and finally generate the fragility functions. PSDMs, in fact, allow to transition from deterministic, mechanics-based models to probabilistic, statistic-based models representing the probabilistic distribution of demand parameters at a given intensity measure. Figures 21 to 24 report the PSDMs across all locations and HLs.

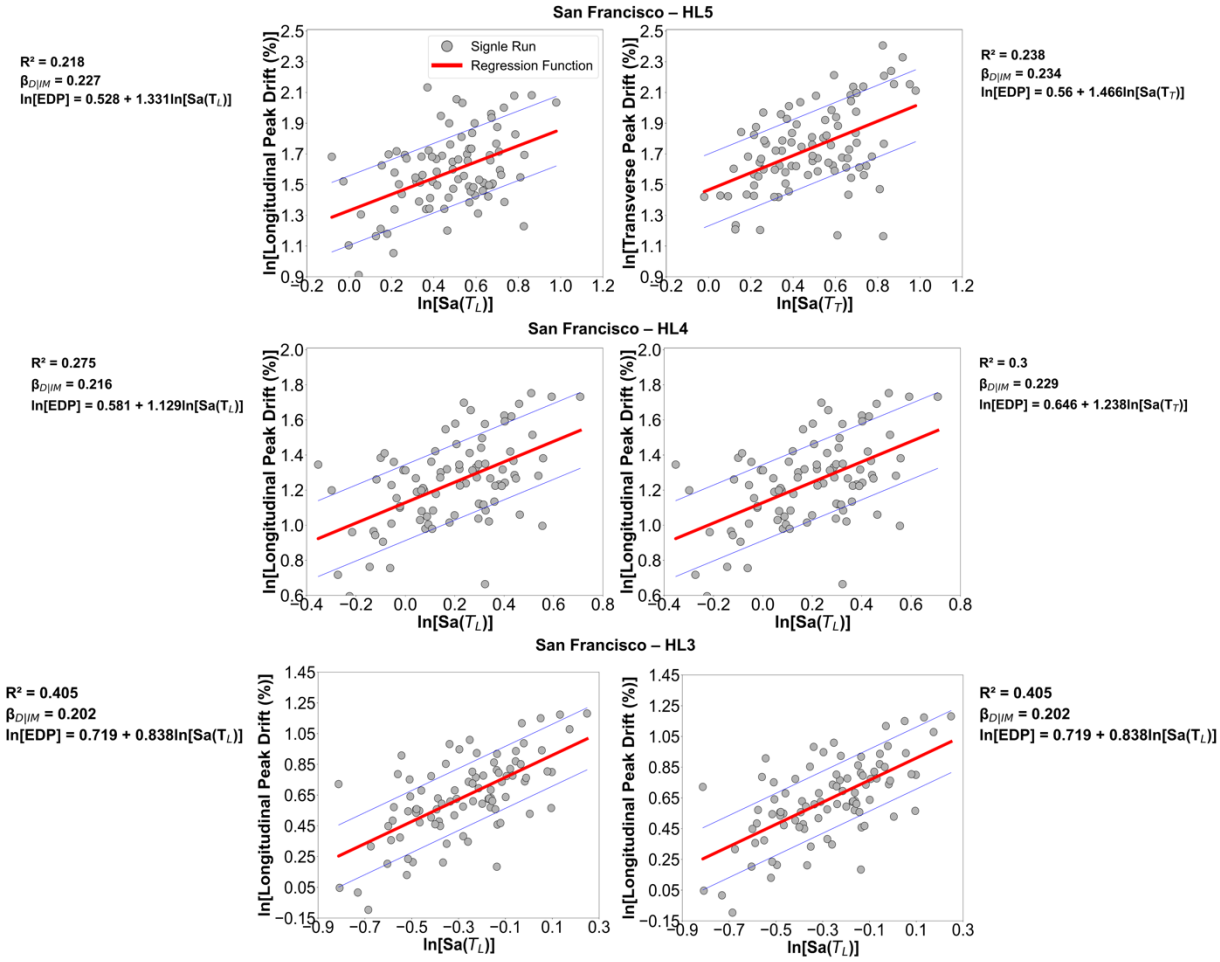


Figure 21. SF: probabilistic seismic demand models.

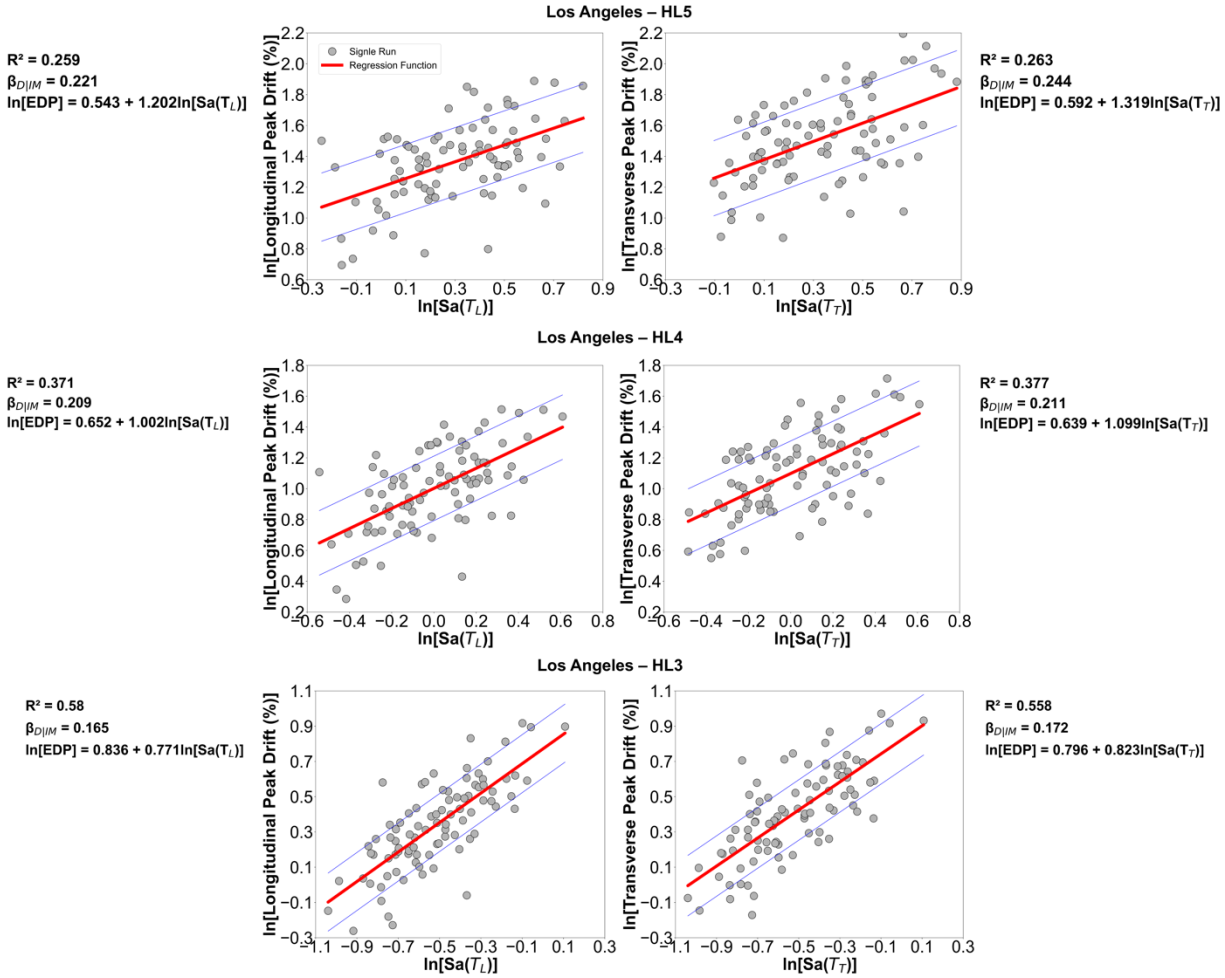


Figure 22. LA: probabilistic seismic demand models.

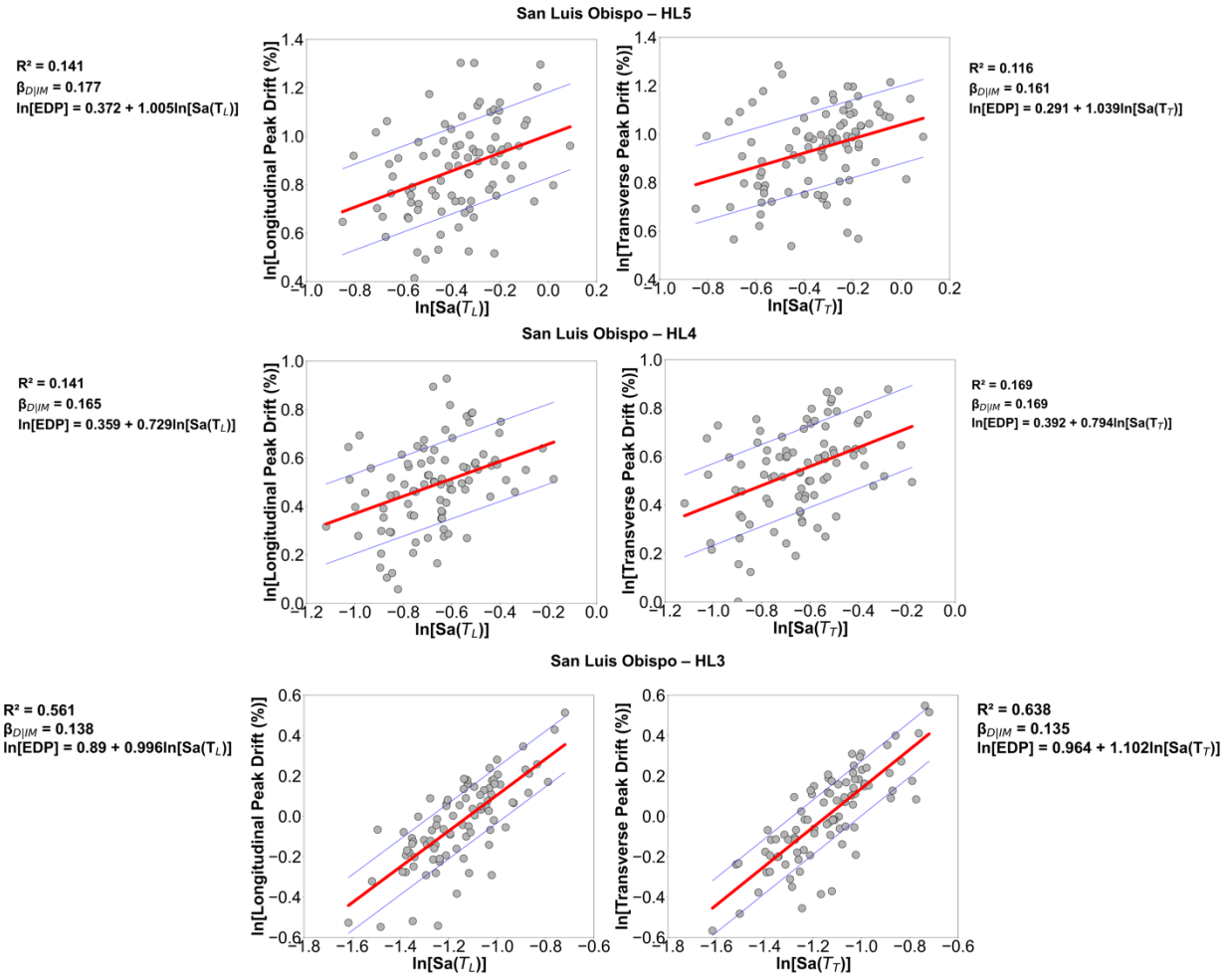


Figure 23. SLO: probabilistic seismic demand models.

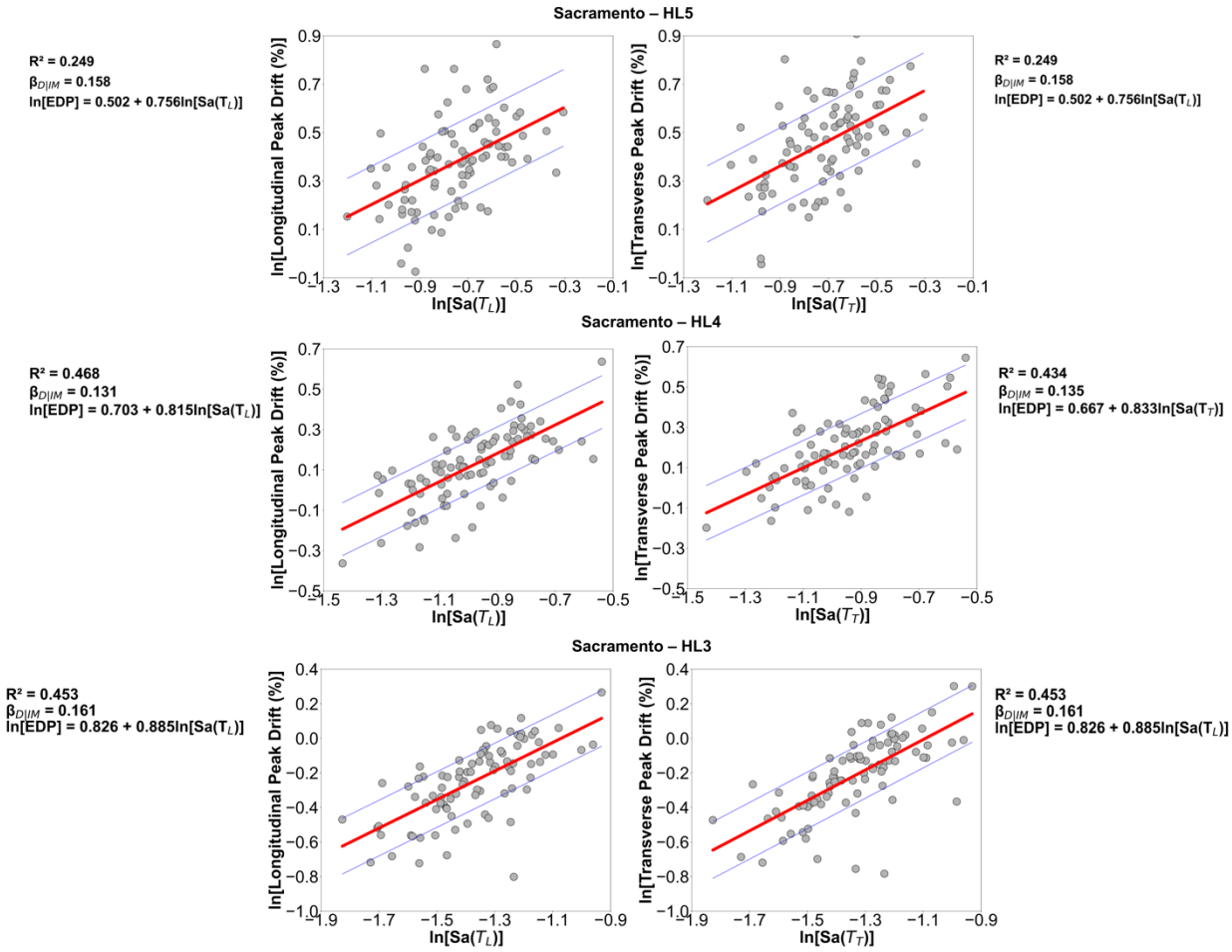


Figure 24. SC: probabilistic seismic demand models.

The fragility functions generated from this set of analyses are shown in Figure 25 and demonstrate that for HL3 the performance of the bridge across the considered locations varies substantially, with a probability of exceeding DS-3 that decreases from 20% for SF to zero percent for SLO. For HL4, however, significant differences arise across the considered locations. Specifically, the probability of exceeding DS-4 is seen to decrease from about 50% for SF to zero percent for SLO and SC. For the highest hazard level, HL5, the probability of exceeding DS-4 drops from 90% for SF to zero for SLO and SC. As expected, this points to the fact that if a baseline bridge meeting the current AASHTO minimum design requirements is adopted across locations with different levels of seismicity, inconsistent performances would be obtained, with Life Safety

(DS-5) attained with an exceedance probability of about 60% for SF, 30% for LA and zero for SLO and SAC.

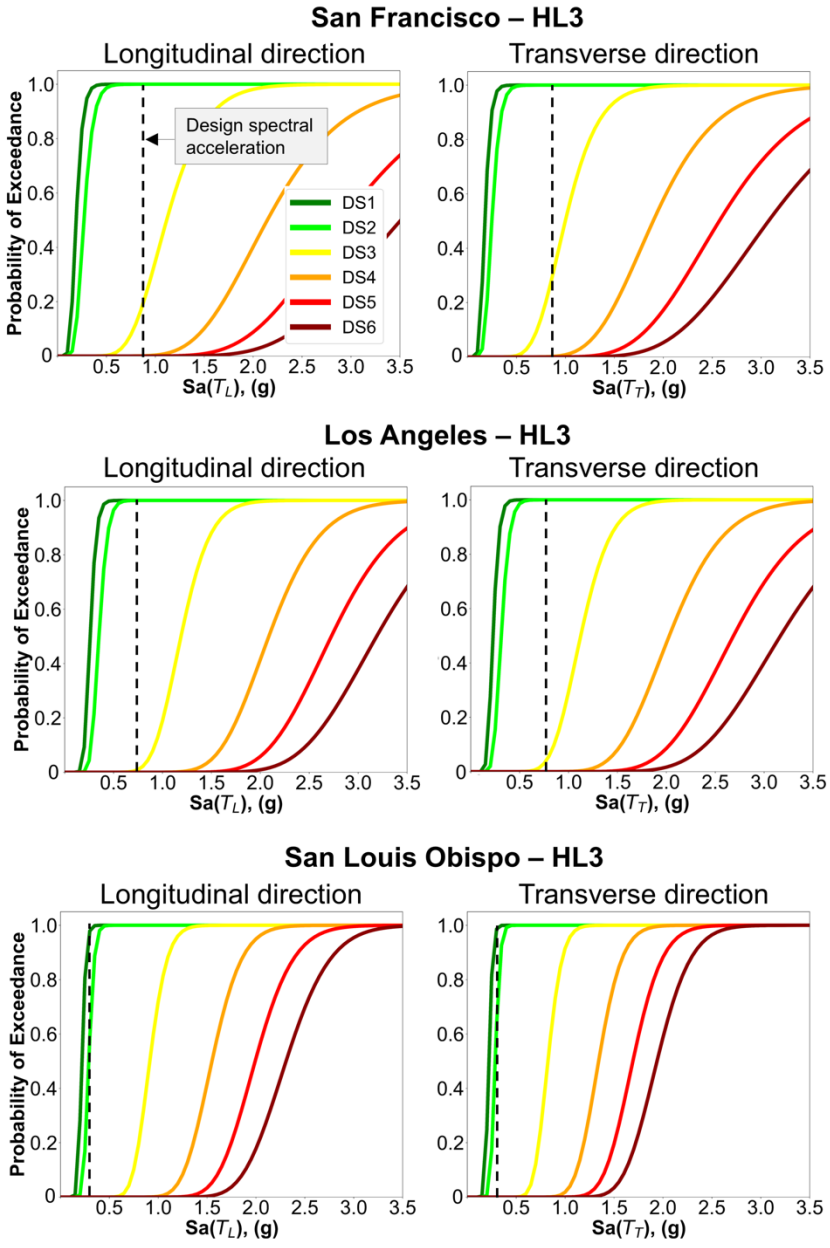

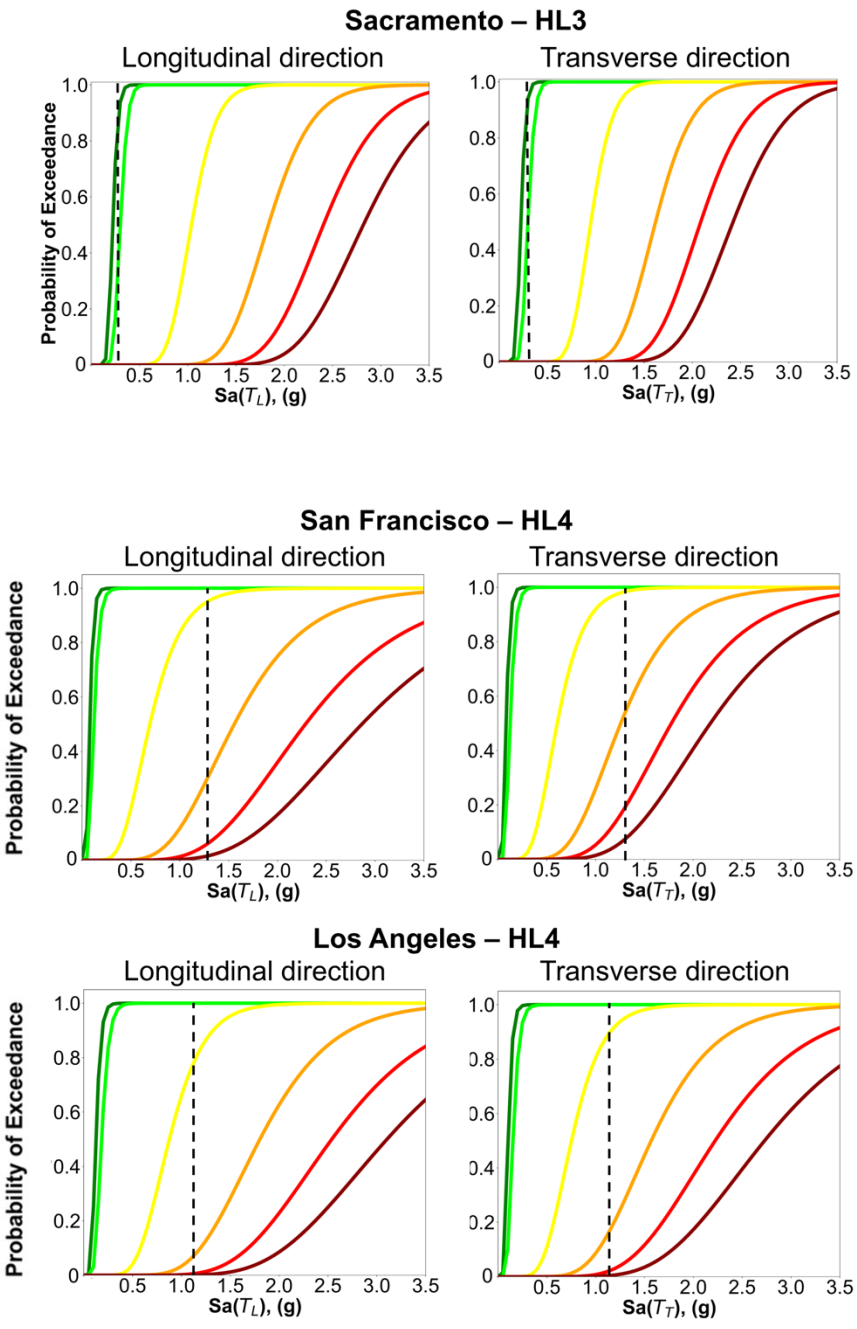
Sacramento – HL3
Longitudinal direction
Transverse direction
Probability of Exceedance
1.0
0.8
0.6
0.4
0.2
0
0.5 1.0 1.5 2.0 2.5 3.0 3.5
Sa($T_L$), (g)
Sa($T_T$), (g)
San Francisco – HL4
Longitudinal direction
Transverse direction
Probability of Exceedance
Sa($T_L$), (g)
Sa($T_T$), (g)
Los Angeles – HL4
Longitudinal direction
Transverse direction
Probability of Exceedance
Sa($T_L$), (g)
Sa($T_T$), (g)

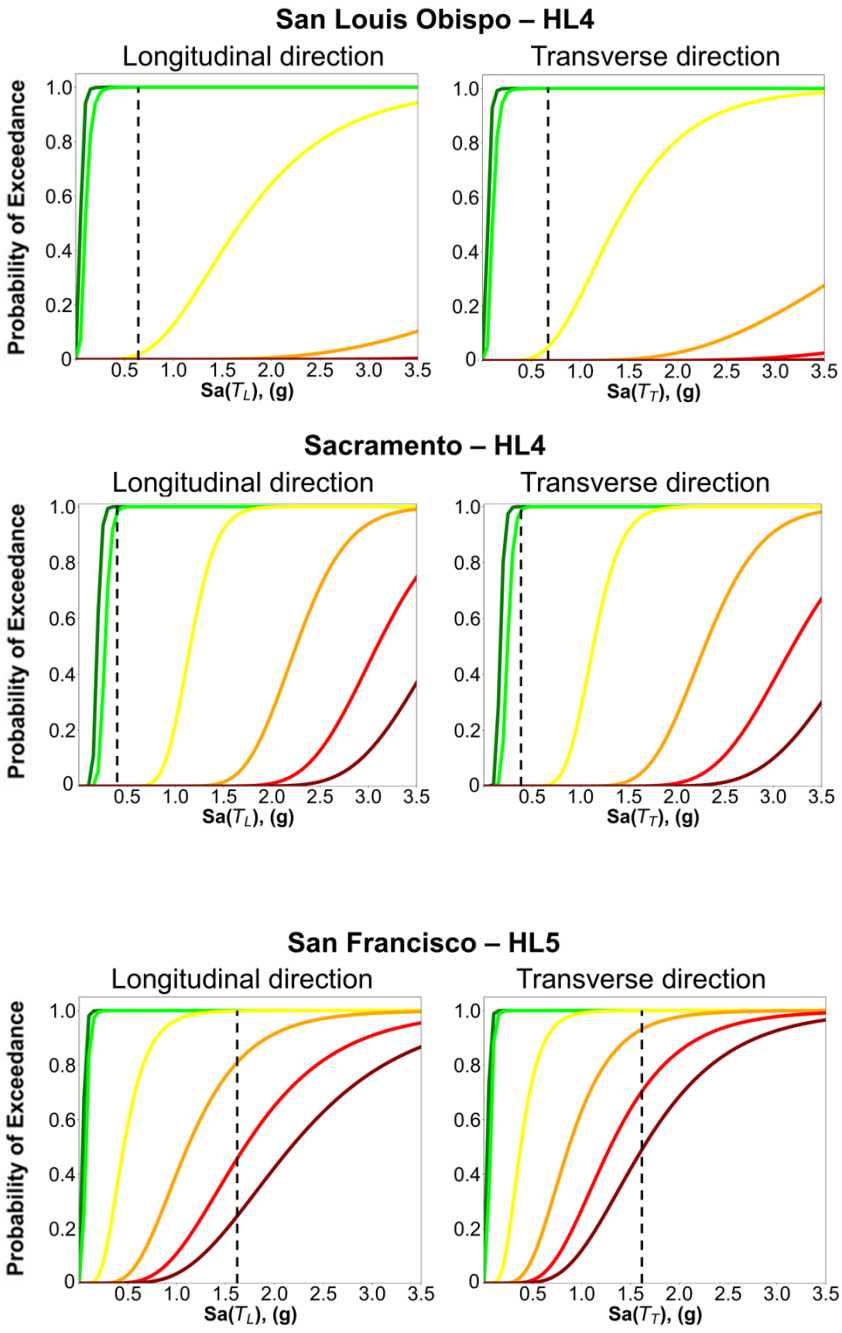
San Louis Obispo – HL4
Longitudinal direction
Transverse direction
Probability of Exceedance
1.0
0.8
0.6
0.4
0.2
0
0.5 1.0 1.5 2.0 2.5 3.0 3.5
Sa($T_L$), (g)
Sa($T_T$), (g)
Sacramento – HL4
Longitudinal direction
Transverse direction
Probability of Exceedance
Sa($T_L$), (g)
Sa($T_T$), (g)
San Francisco – HL5
Longitudinal direction
Transverse direction
Probability of Exceedance
Sa($T_L$), (g)
Sa($T_T$), (g)

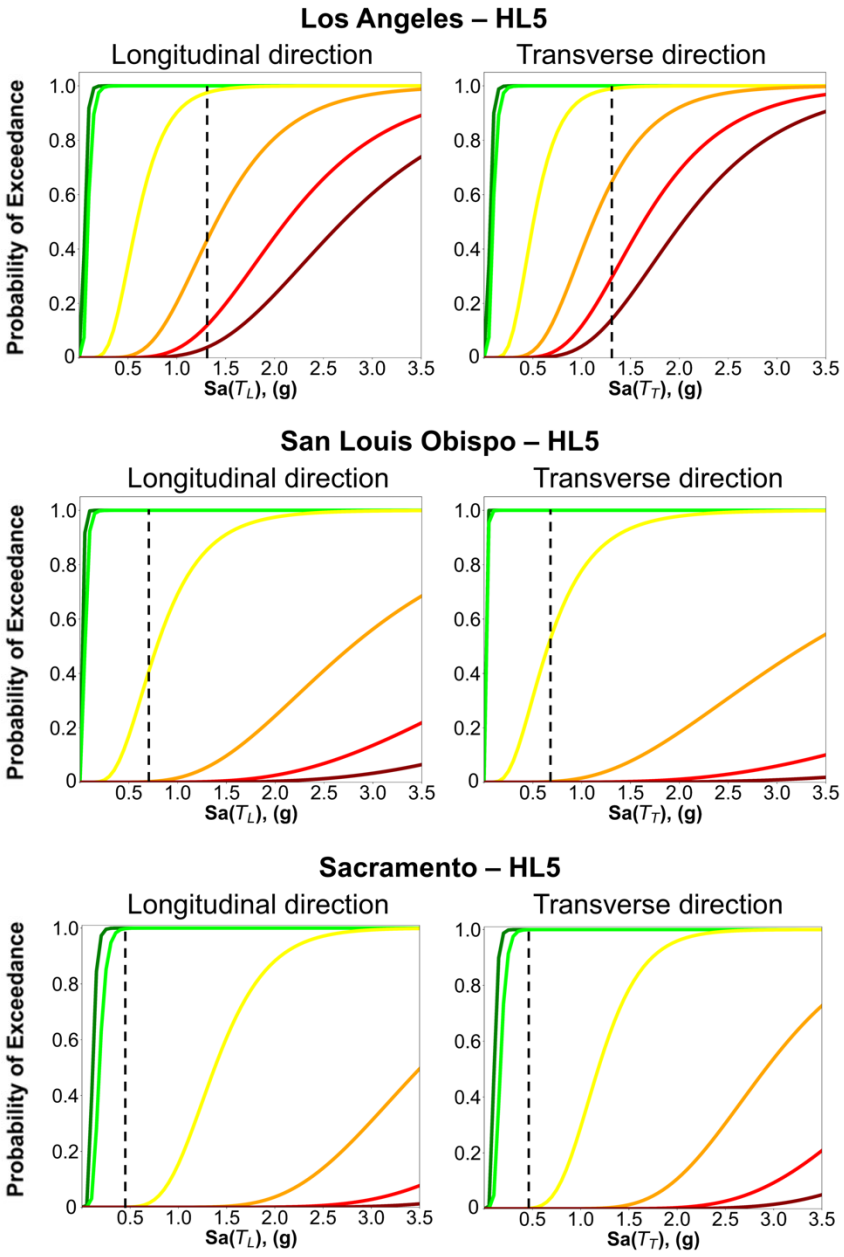


Figure 25. Fragility functions across all considered locations (San Francisco, Los Angeles, San Louis Obispo, and Sacramento), and hazard levels (HL3 = 200-year return period, HL4 = 500-year return period, and HL5 = 1000-year return period)

The results from the fragility analysis are then used to assess the seismic risk of temporary bridges for three different life spans, namely 5, 10, and 15 years. The total risk calculation is performed

following the improved risk model proposed by Yoon et al. (2022). The hazard curves at the latitude and longitude of the locations of interest are obtained from the U.S. Geological Survey web application (https://earthquake.usgs.gov/hazards/interactive/). Linear interpolation between the hazard curves for 0.75 and 1 sec is used to derive the annual rate of exceedance for the spectral periods of the considered bridge, that is 0.83 sec (SF and LA) and 0.96 sec (SLO and SC). The probabilities of exceeding $DS_i$ at the design spectral acceleration (i.e., UHS acceleration at the fundamental period of the bridge) for the three considered return periods (200, 500, and 975 years) are used to derive a new fragility function representing the probability of exceeding the selected $DS_i$ across a range of return periods. The annual rate of occurrence is then multiplied by the probability of exceeding $DS_i$ sampled at the same $S_a$, and all products summed up to obtain the annual rate exceeding $DS_i$. Finally, the probability of exceeding $DS_i$ within a sough life span is calculated with the classical formulation $P(DS_i) = 1 - exp^{-jv(DS_i)}$, where $j$ represents the life span of interest, and $v(DS_i)$ is the annual rate exceeding $DS_i$. Appendix C reports the detailed calculations carried out for Los Angeles and DS-2.

Table 6 reports the results of the risk calculation for all DSs and considered life spans. It should be noted that for selected locations and DSs the fragility functions are not defined because the probabilities of exceeding a certain DS are either all 100% or 0% for the considered return periods and consequently the risk is not calculated. This is an inherent limitation of the total risk model that would require the consideration of a larger number of return periods to represent the risk across all damage states. This is particularly critical for the locations of lower seismicity, where longer return periods should be considered to capture the attainment of more severe damage states, as reflected in Table 6.

Overall, results demonstrate that DS-3 is attained only in SF with a probability varying from 0.91% for a life span of 5 years to 2.72% for a life span of 15 years. Across all other locations, the bridges have a probability of exceeding DS-1 and DS-2 (minor damage) ranging from 3.26% to 8.55% for a life span of 5 years and from 9.46% to 23.52% for a life span of 15 years.

Table 6. Seismic risk for the temporary bridges with the minimum design (MD) column: probability (in percent) that a damage state is exceeded in the life span of the bridge.

| Location | Life span | DS-1 | DS-2 | DS-3 |
|---|---|---|---|---|
| **San Francisco** | 5-y | 8.37 | 6.00 | 0.91 |
| | 10-y | 16.04 | 11.64 | 1.82 |
| | 15-y | 23.07 | 16.94 | 2.72 |
| **Los Angeles** | 5-y | 8.55 | 4.95 | --* |
| | 10-y | 16.37 | 9.66 | -- |
| | 15-y | 23.52 | 14.14 | -- |
| **San Louis Obispo** | 5-y | 6.34 | 4.24 | -- |
| | 10-y | 12.27 | 8.30 | -- |
| | 15-y | 17.83 | 12.18 | -- |
| **Sacramento** | 5-y | 5.28 | 3.26 | -- |
| | 10-y | 10.28 | 6.41 | -- |
| | 15-y | 15.01 | 9.46 | -- |

*-- indicates undefined fragility

Finally, an explicit comparison of the seismic risk for the HCD bridges designed for 100 and 200-year return period was carried out. To this aim, fragilities corresponding to 100, 500, and 975-yeas return periods were developed and used for the HL-2 bridge (i.e., 100-return period design), while the fragilities corresponding to 200, 500, and 975 years return periods were employed for the HL-3 bridge (i.e., 200-year return period design).

Table 7 and Table 8 show the risk calculated for the HL2 and HL3 designs, respectively, and life spans of 5, 10, and 15 years.

Overall, results show that the risk is slightly affected by the change in the design return period from 100 to 200 years. For example, if DS-3 is targeted as the sought performance and a life span of 15 years is considered, the risk for a temporary bridge in SF is seen to change from 4.14% for the HL2 design, to 3.75% for the HL3 design (underlines values in the table across all locations), thereby confirming the adequacy of the current recommendation of 100 years as the target return period when minimum design requirements are relaxed. Further information on this set of analyses can be found in Kashizadeh et al. (2025).

**Table 7**. Seismic risk for HL2-design expressed in terms of probability (%) of exceeding each DS for each considered life span.

| | | HL2 design | | | | | |
|---|---|---|---|---|---|---|---|
| **Location** | **Life span** | **DS-1** | **DS-2** | **DS-3** | **DS-4** | **DS-5** | **DS-6** |
| **San Francisco** | 5-y | --* | 9.90 | 1.40 | 0.71 | 0.47 | 0.36 |
| | 10-y | -- | 18.82 | 2.78 | 1.42 | 0.94 | 0.72 |
| | 15-y | -- | 26.86 | 4.14 | 2.12 | 1.41 | 1.08 |
| **Los Angeles** | 5-y | -- | 5.40 | 1.36 | 0.38 | -- | 0.32 |
| | 10-y | -- | 10.50 | 2.71 | 0.76 | -- | 0.65 |
| | 15-y | -- | 15.33 | 4.03 | 1.13 | -- | 0.97 |
| **San Luis Obispo** | 5-y | 6.80 | 3.89 | 0.85 | 0.47 | 0.26 | -- |
| | 10-y | 13.13 | 7.62 | 1.69 | 0.94 | 0.52 | -- |
| | 15-y | 19.03 | 11.21 | 2.53 | 1.40 | 0.78 | -- |
| **Sacramento** | 5-y | 5.13 | 3.13 | 0.40 | -- | -- | -- |
| | 10-y | 10.00 | 6.17 | 0.80 | -- | -- | -- |
| | 15-y | 14.61 | 9.11 | 1.20 | -- | -- | -- |

*-- indicates undefined fragility

**Table 8**. Seismic risk for HL3-design expressed in terms of probability (%) of exceeding each DS for each considered life span.

| | | HL3 design | | | | | |
|---|---|---|---|---|---|---|---|
| **Location** | **Life span** | **DS-1** | **DS-2** | **DS-3** | **DS-4** | **DS-5** | **DS-6** |
| **San Francisco** | 5-y | --* | -- | 1.26 | 0.62 | 0.41 | 0.32 |
| | 10-y | -- | -- | 2.51 | 1.24 | 0.82 | 0.63 |
| | 15-y | -- | -- | 3.75 | 1.86 | 1.23 | 0.94 |
| **Los Angeles** | 5-y | -- | -- | 1.01 | 0.45 | 0.32 | 0.29 |
| | 10-y | -- | -- | 2.01 | 0.90 | 0.65 | 0.58 |
| | 15-y | -- | -- | 3.00 | 1.35 | 0.97 | 0.87 |

| | | | | | | | |
|---|---|---|---|---|---|---|---|
| **San Luis Obispo** | 5-y | -- | 6.39 | 0.78 | 0.44 | 0.25 | -- |
| | 10-y | -- | 12.38 | 1.55 | 0.87 | 0.51 | -- |
| | 15-y | -- | 17.98 | 2.32 | 1.31 | 0.76 | -- |
| **Sacramento** | 5-y | -- | 3.37 | 0.38 | -- | -- | -- |
| | 10-y | -- | 6.63 | 0.77 | -- | -- | -- |
| | 15-y | -- | 9.78 | 1.15 | -- | -- | -- |

*-- indicates undefined fragility

# 14. Conclusions

This study investigated the seismic performance of temporary bridges designed to meet the strength and ductility criteria in the SDC (2019) and without consideration of the AASHTO (2020) minimum reinforcement requirements, for different hazard levels (10%, 5% and 2.5% in 5 years) and locations in California (San Francisco, Los Angeles, San Louis Obispo, and Sacramento). Temporary bridges with cast-in-place RC columns and a lightweight steel superstructure (ACROW) were used as a case study. Three-dimensional nonlinear models of the bridges were developed in OpenSees (McKenna, 2011) to perform nonlinear time-history analyses and derive fragility functions based on the damage states proposed by Vosooghi and Saiidi (2010) and currently adopted by Caltrans. Results demonstrated that a hazard-based design can ensure satisfactory performance (with damage limited to minor concrete cover spalling to large concrete cover spalling and extensive flexural cracks), even when the design minimum requirements for ordinary bridges are not met.

A baseline bridge model meeting the AASHTO (2020) and Caltrans (2019) minimum reinforcement requirements was then used to identify the level of hazard resulting in Life Safety performance level, herein defined as the initiation of concrete core damage and longitudinal bar bucking. Results across the considered locations and hazard levels (2.5%, 1%, and 0.5% in 5 years) demonstrate that this approach leads to hazard-inconsistent and uneconomical designs. The

seismic risk analysis performed across all locations indicate a probability of attaining DS-3 varying from 0.91% for a lifespan of 5 years to 2.72% for a lifespan of 15 years.

Evidence from this study also demonstrated that the methods currently proposed in the literature to obtain reduced spectral amplitudes can lead to overestimates of the spectral accelerations up to a factor of ~2.4 when using AASHTO-compliant design spectra, see Figure 26.

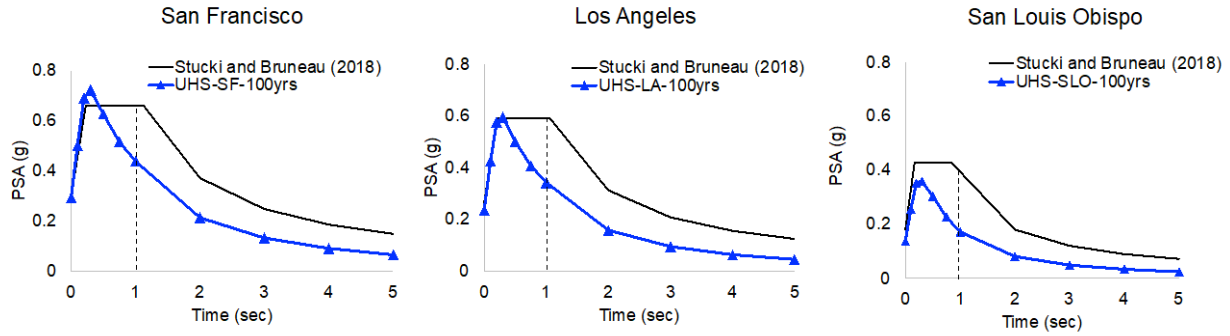


Figure 26. Comparison of the design spectra obtained from the method proposed by Stucki and Bruneau (2018) and the UHS for a return period of 100 years at all four considered locations.

However, it was also established that if HL3 (200-year return period) is targeted as the design return period for temporary bridges, the performance of the 'minimum design' bridge across the considered locations is satisfactory, with a probability of exceeding DS-3 (associated with extensive flexural cracks and relatively large concrete cover spalling) decreasing from 20% for San Francisco to zero percent for Sacramento.

This research advocates the use of hazard-consistent, performance-based design approaches for temporary bridges wherein certain minimum requirements set forth in AASHTO and Caltrans can be relaxed. In this regard, future work should investigate the development of minimum design requirements specific to bridges employing lightweight superstructures and with a service life of

5 years, for which the concrete creep phenomenon controlling current minimum reinforcement ratios is expected to be mitigated.

# 15. References

AASHTO. 2020. AASHTO LRFD bridge design specifications, U.S. customary units. 9th ed. Washington, DC: AASHTO.

AASHTO. 2015. AASHTO guide specifications for LRFD seismic bridge design with 2012, 2014, and 2015 interim revisions. 2nd ed. Washington, DC: AASHTO.

ACI 209-R86, "Prediction of Creep, shrinkage, and Temperature Effects in Concrete Structures," ACI, Detroit, Michigan, 1986.

ACI Committee 318, "Building Code Requirements for Structural Concrete (ACI 318-19) and Commentary (ACI 318R-19)," American Concrete Institute, Farmington Hills, MI, 2019.

ACROW Corporation. 2016. ACROW Panel Bridging Technical Handbook. 700XS Modula Bridge System. Fifth Edition.

Caltrans. 2019. Seismic Design Criteria 2.0. State of California.

Caltrans. 2011. Memo to Designers: Site Seismicity for Temporary Bridges and Stage Construction. Section 20-2. State of California.

Caltrans. 2022. Dr. Fine Bridge Replacement Project

Computers & Structures. 2022. CSiBridge v.25.1.0. Bridge Analysys, Design, and Rating, Software. Berkeley, California, USA.

Hayden, C. P., Bray, J. D., & Abrahamson, N. A. (2014). Selection of near-fault pulse motions. Journal of Geotechnical and Geoenvironmental Engineering, 140(7), 04014030.

Henry, L., & Mahin, S. A. (1999). Study of buckling of longitudinal bars in reinforced concrete bridge columns. Report to the California department of transportation.

Kashizadeh, S., Petrone, F., Kunnath. 2025. “Performance-Based Design and Hazard-Based Risk of Temporary Bridges with Light-Weight Superstructure in California”. *ASCE Journal of Bridge Engineering* (submitted)

Kim CS, Gong Y. Numerical investigation of creep and shrinkage effects on minimum reinforcement of concentrically and eccentrically loaded RC columns. Engineering Structures. 2018 Nov 1;174:509-25.

Lehman, D. E., & Moehle, J. P. (2000, January). Performance-based seismic design of reinforced concrete bridge columns. In Twelfth World Earthquake Engineering Conference (pp. 215-223).

Mander, J. B., M. J. N. Priestley, and R. Park. 1984. Seismic design of bridge piers. Research Rep. 84-2. Christchurch, New Zealand: Dept. of Civil Engineering, Univ. of Canterbury.

McKenna, F. 2011. “Opensees: A framework for earthquake engineering simulation.” Comput. Sci. Eng. 13 (4): 58–66. https://doi.org/10.1109 /MCSE.2011.66.

SDR Engineering Consultants, I. (2005). "Prefabricated Steel Bridge Systems." Federal Highway Administration, Washington, DC.

Scott, M. H., & Fenves, G. L. (2006). Plastic hinge integration methods for force-based beam–column elements. Journal of Structural Engineering, 132(2), 244-252.

Stucki, C., & Bruneau, M. (2018). Reduction of seismic acceleration parameters for temporary bridge design. Journal of Bridge Engineering, 23(10), 04018081.

United States Geological Survey (USGS). 2018. USGS Earthquake Hazard Toolbox. https://earthquake.usgs.gov/nshmp/

Vosooghi, A., and M. Saiidi. 2012.“Experimental fragility curves for seismic response of reinforced concrete bridge columns.” ACI Struct. J.109 (6): 825–834.

Yassin, M. H. M. 1994. “Nonlinear analysis of prestressed concrete structures under monotonic and cycling loads.” Ph.D. thesis, Dept. of Civil and Environmental Engineering, Univ. of California Berkeley.

Yoon, Y.H., Ataya, S., Mahan, M., Malek, A., Abrahamson, N., Zokaie, T., Ong, R. and Ahmed, A., 2022. Total risk model and loss analysis of probabilistic damage control application in seismic design of highway bridges. Journal of Bridge Engineering, 27(5), p.04022020.

Ziehl PH, Cloyd JE, Kreger ME. Evaluation of minimum longitudinal reinforcement requirements for reinforced concrete columns. Center for Transportation Research, Bureau of Engineering Research, University of Texas at Austin; 1998.

Zong, Z., S. Kunnath, and G. Monti. 2014.“Material model incorporating buckling of reinforcing bars in RC columns.” J. Struct. Eng.140 (1):04013032.https://doi.org/10.1061/(ASCE)ST.1943-541X.0000808.© ASCE04023017-13J. Bridge Eng.

# 16. APPENDIX A

This appendix reports the results of the hazard disaggregation and ground-motion selection for San Francisco and Los Angeles at HL3.

**San Francisco – HL3**

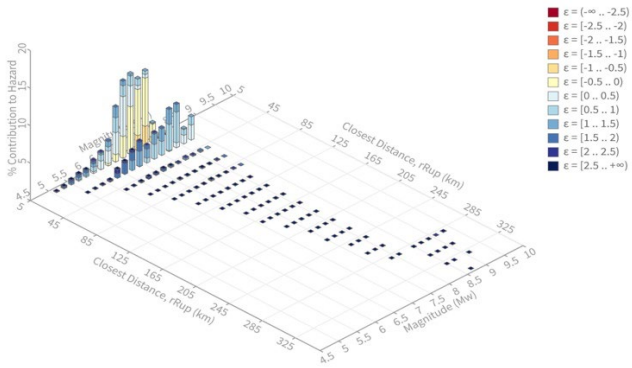


| Source | Closest distance (km) | M | $\varepsilon_0$ | % |
|---|---|---|---|---|
| Hayward (No) [1] | 5.56 | 7.17 | -0.19 | 18.87 |
| San Andreas (Peninsula) [11] | 25.73 | 7.88 | 0.71 | 7.13 |
| Hayward (So) [7] | 10.73 | 6.8 | 0.54 | 2.27 |
| Calaveras (No) [0] | 20.47 | 7.06 | 1 | 2.09 |
| Hayward (No) [2] | 5.85 | 6.86 | 0.04 | 1.95 |
| Hayward (So) [6] | 16.84 | 6.74 | 1.08 | 1.38 |
| Mount Diablo Thrust [3] | 24.24 | 7.06 | 1.09 | 1.02 |

Figure A1. Hazard deaggregation results for San Francisco, HL3 (USGS, 2018).

Table A1. List of earthquakes for 0 and 90 degrees (RSN = record sequence number; SF = scale factor).

| # | RSN | Earthquake Name | Year | Station Name | M | Rrup (km) | VS30 (m/sec) | SF |
|---|---|---|---|---|---|---|---|---|
| **1** | 1063 | "Northridge-01" | 1994 | "Rinaldi Receiving Sta" | 6.69 | 6.5 | 282.25 | 0.624 |
| **2** | 185 | "Imperial Valley-06" | 1979 | "Holtville Post Office" | 6.53 | 7.5 | 202.89 | 2.228 |

| | | | | | | | | |
|---|---|---|---|---|---|---|---|---|
| **3** | 179 | "Imperial Valley-06" | 1979 | "El Centro Array #4" | 6.53 | 7.05 | 208.91 | 1.451 |
| **4** | 1491 | "Chi-Chi_ Taiwan" | 1999 | "TCU051" | 7.62 | 7.64 | 350.06 | 2.395 |
| **5** | 8066 | "Christchurch_ New Zealand" | 2011 | "Christchurch Hospital" | 6.2 | 4.85 | 194 | 0.960 |
| **6** | 181 | "Imperial Valley-06" | 1979 | "El Centro Array #6" | 6.53 | 1.35 | 203.22 | 1.362 |
| **7** | 723 | "Superstition Hills-02" | 1987 | "Parachute Test Site" | 6.54 | 0.95 | 348.69 | 0.970 |
| **8** | 6911 | "Darfield_ New Zealand" | 2010 | "HORC" | 7 | 7.29 | 326.01 | 0.996 |
| **9** | 6906 | "Darfield_ New Zealand" | 2010 | "GDLC" | 7 | 1.22 | 344.02 | 0.695 |
| **10** | 158 | "Imperial Valley-06" | 1979 | "Aeropuerto Mexicali" | 6.53 | 0.34 | 259.86 | 2.134 |
| **11** | 821 | "Erzican_ Turkey" | 1992 | "Erzincan" | 6.69 | 4.38 | 352.05 | 1.027 |
| **12** | 1176 | "Kocaeli_ Turkey" | 1999 | "Yarimca" | 7.51 | 4.83 | 297 | 1.454 |
| **13** | 159 | "Imperial Valley-06" | 1979 | "Agrarias" | 6.53 | 0.65 | 242.05 | 1.844 |
| **14** | 8161 | "El Mayor-Cucapah_ Mexico" | 2010 | "El Centro Array #12" | 7.2 | 11.26 | 196.88 | 1.250 |
| **15** | 1141 | "Dinar_ Turkey" | 1995 | "Dinar" | 6.4 | 3.36 | 219.75 | 1.544 |
| **16** | 1495 | "Chi-Chi_ Taiwan" | 1999 | "TCU055" | 7.62 | 6.34 | 359.13 | 1.889 |
| **17** | 171 | "Imperial Valley-06" | 1979 | "El Centro - Meloland Geot. Array" | 6.53 | 0.07 | 264.57 | 1.379 |
| **18** | 8118 | "Christchurch_ New Zealand" | 2011 | "Papanui High School " | 6.2 | 9.06 | 263.2 | 1.560 |
| **19** | 1044 | "Northridge-01" | 1994 | "Newhall - Fire Sta" | 6.69 | 5.92 | 269.14 | 0.705 |
| **20** | 728 | "Superstition Hills-02" | 1987 | "Westmorland Fire Sta" | 6.54 | 13.03 | 193.67 | 2.077 |
| **21** | 170 | "Imperial Valley-06" | 1979 | "EC County Center FF" | 6.53 | 7.31 | 192.05 | 1.616 |

| | | | | | | | | |
|---|---|---|---|---|---|---|---|---|
| **22** | 6927 | "Darfield_ New Zealand" | 2010 | "LINC" | 7 | 7.11 | 263.2 | 1.328 |
| **23** | 1042 | "Northridge-01" | 1994 | "N Hollywood - Coldwater Can" | 6.69 | 12.51 | 326.47 | 2.297 |
| **24** | 183 | "Imperial Valley-06" | 1979 | "El Centro Array #8" | 6.53 | 3.86 | 206.08 | 1.496 |
| **25** | 5825 | "El Mayor-Cucapah_ Mexico" | 2010 | "CERRO PRIETO GEOTHERMAL" | 7.2 | 10.92 | 242.05 | 1.600 |
| **26** | 8134 | "Christchurch_ New Zealand" | 2011 | "Styx Mill Transfer Station " | 6.2 | 11.25 | 247.5 | 2.411 |
| **27** | 8130 | "Christchurch_ New Zealand" | 2011 | "Shirley Library" | 6.2 | 5.6 | 207 | 1.071 |
| **28** | 1048 | "Northridge-01" | 1994 | "Northridge - 17645 Saticoy St" | 6.69 | 12.09 | 280.86 | 1.110 |
| **29** | 6975 | "Darfield_ New Zealand" | 2010 | "TPLC" | 7 | 6.11 | 249.28 | 2.758 |
| **30** | 1119 | "Kobe_ Japan" | 1995 | "Takarazuka" | 6.9 | 0.27 | 312 | 0.675 |

List of earthquakes for 45 degrees (RSN = record sequence number; SF = scale factor).

| # | RSN | Earthquake Name | Year | Station Name | M | Rrup (km) | Vs30 (m/sec) | SF |
|---|---|---|---|---|---|---|---|---|
| **1** | 161 | "Imperial Valley-06" | 1979 | "Brawley Airport" | 6.53 | 10.42 | 208.71 | 2.694 |
| **2** | 6911 | "Darfield_ New Zealand" | 2010 | "HORC" | 7 | 7.29 | 326.01 | 1.017 |
| **3** | 8066 | "Christchurch_ New Zealand" | 2011 | "Christchurch Hospital" | 6.2 | 4.85 | 194 | 1.027 |
| **4** | 179 | "Imperial Valley-06" | 1979 | "El Centro Array #4" | 6.53 | 7.05 | 208.91 | 1.410 |
| **5** | 181 | "Imperial Valley-06" | 1979 | "El Centro Array #6" | 6.53 | 1.35 | 203.22 | 1.448 |
| **6** | 1491 | "Chi-Chi_ Taiwan" | 1999 | "TCU051" | 7.62 | 7.64 | 350.06 | 2.258 |

| | | | | | | | | |
|---|---|---|---|---|---|---|---|---|
| **7** | 8118 | "Christchurch_ New Zealand" | 2011 | "Papanui High School " | 6.2 | 9.06 | 263.2 | 1.538 |
| **8** | 821 | "Erzican_ Turkey" | 1992 | "Erzincan" | 6.69 | 4.38 | 352.05 | 1.088 |
| **9** | 1063 | "Northridge-01" | 1994 | "Rinaldi Receiving Sta" | 6.69 | 6.5 | 282.25 | 0.617 |
| **10** | 8161 | "El Mayor-Cucapah_ Mexico" | 2010 | "El Centro Array #12" | 7.2 | 11.26 | 196.88 | 1.260 |
| **11** | 185 | "Imperial Valley-06" | 1979 | "Holtville Post Office" | 6.53 | 7.5 | 202.89 | 2.333 |
| **12** | 8064 | "Christchurch_ New Zealand" | 2011 | "Christchurch Cathedral College" | 6.2 | 3.26 | 198 | 0.838 |
| **13** | 183 | "Imperial Valley-06" | 1979 | "El Centro Array #8" | 6.53 | 3.86 | 206.08 | 1.600 |
| **14** | 170 | "Imperial Valley-06" | 1979 | "EC County Center FF" | 6.53 | 7.31 | 192.05 | 1.815 |
| **15** | 1176 | "Kocaeli_ Turkey" | 1999 | "Yarimca" | 7.51 | 4.83 | 297 | 1.450 |
| **16** | 4894 | "Chuetsu-oki_ Japan" | 2007 | "Kashiwazaki NPP_ Unit 1: ground surface" | 6.8 | 10.97 | 329 | 0.467 |
| **17** | 5825 | "El Mayor-Cucapah_ Mexico" | 2010 | "CERRO PRIETO GEOTHERMAL" | 7.2 | 10.92 | 242.05 | 1.587 |
| **18** | 1141 | "Dinar_ Turkey" | 1995 | "Dinar" | 6.4 | 3.36 | 219.75 | 1.414 |
| **19** | 723 | "Superstition Hills-02" | 1987 | "Parachute Test Site" | 6.54 | 0.95 | 348.69 | 0.916 |
| **20** | 8063 | "Christchurch_ New Zealand" | 2011 | "Christchurch Botanical Gardens" | 6.2 | 5.55 | 187 | 1.090 |
| **21** | 184 | "Imperial Valley-06" | 1979 | "El Centro Differential Array" | 6.53 | 5.09 | 202.26 | 1.270 |

| | | | | | | | | |
|---|---|---|---|---|---|---|---|---|
| **22** | 159 | "Imperial Valley-06" | 1979 | "Agrarias" | 6.53 | 0.65 | 242.05 | 2.032 |
| **23** | 6927 | "Darfield_ New Zealand" | 2010 | "LINC" | 7 | 7.11 | 263.2 | 1.283 |
| **24** | 158 | "Imperial Valley-06" | 1979 | "Aeropuerto Mexicali" | 6.53 | 0.34 | 259.86 | 1.932 |
| **25** | 5264 | "Chuetsu-oki_ Japan" | 2007 | "NIG018" | 6.8 | 10.78 | 198.26 | 1.016 |
| **26** | 728 | "Superstition Hills-02" | 1987 | "Westmorland Fire Sta" | 6.54 | 13.03 | 193.67 | 1.947 |
| **27** | 6962 | "Darfield_ New Zealand" | 2010 | "ROLC" | 7 | 1.54 | 295.74 | 1.386 |
| **28** | 8134 | "Christchurch_ New Zealand" | 2011 | "Styx Mill Transfer Station " | 6.2 | 11.25 | 247.5 | 2.532 |
| **29** | 6906 | "Darfield_ New Zealand" | 2010 | "GDLC" | 7 | 1.22 | 344.02 | 0.705 |
| **30** | 6 | "Imperial Valley-02" | 1940 | "El Centro Array #9" | 6.95 | 6.09 | 213.44 | 1.888 |

**Los Angeles – HL3**

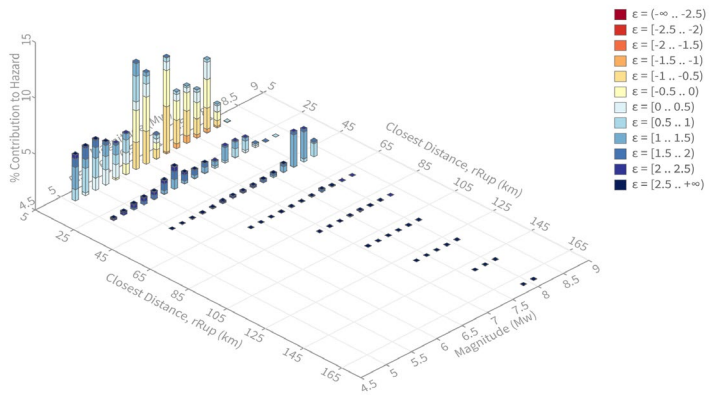


| Source | Closest distance (km) | M | ε0 | % |
|---|---|---|---|---|
| Elysian Park (Upper) [0] | 4.36 | 6.46 | -0.49 | 7.57 |
| San Andreas (Mojave S) [9] | 50.66 | 8 | 1.24 | 3.92 |
| Elysian Park (Upper) [1] | 4.46 | 7.11 | -0.7 | 3.17 |
| Compton [2] | 16.07 | 7.37 | -0.45 | 2.35 |
| Raymond [2] | 6.92 | 7 | -0.22 | 2.14 |
| Whittier alt 1 [7] | 12.62 | 6.73 | 0.51 | 1.98 |
| Puente Hills [3] | 8.17 | 7.09 | -0.75 | 1.62 |

Figure A2. Hazard deaggregation results for Los Angeles, HL3 (USGS, 2018).

Table A2. List of earthquakes for 0 and 90 degrees (RSN = record sequence number; SF = scale factor).

| # | RSN | Earthquake Name | Year | Station Name | M | Rrup (km) | Vs30 (m/sec) | SF |
|---|---|---|---|---|---|---|---|---|
| **1** | 185 | "Imperial Valley-06" | 1979 | "Holtville Post Office" | 6.53 | 7.5 | 202.89 | 1.77 |
| **2** | 8066 | "Christchurch_ New Zealand" | 2011 | "Christchurch Hospital" | 6.2 | 4.85 | 194 | 0.76 |
| **3** | 179 | "Imperial Valley-06" | 1979 | "El Centro Array #4" | 6.53 | 7.05 | 208.91 | 1.15 |
| **4** | 181 | "Imperial Valley-06" | 1979 | "El Centro Array #6" | 6.53 | 1.35 | 203.22 | 1.08 |
| **5** | 158 | "Imperial Valley-06" | 1979 | "Aeropuerto Mexicali" | 6.53 | 0.34 | 259.86 | 1.69 |

| | | | | | | | | |
|---|---|---|---|---|---|---|---|---|
| **6** | 723 | "Superstition Hills-02" | 1987 | "Parachute Test Site" | 6.54 | 0.95 | 348.69 | 0.77 |
| **7** | 6911 | "Darfield_ New Zealand" | 2010 | "HORC" | 7 | 7.29 | 326.01 | 0.79 |
| **8** | 6906 | "Darfield_ New Zealand" | 2010 | "GDLC" | 7 | 1.22 | 344.02 | 0.55 |
| **9** | 159 | "Imperial Valley-06" | 1979 | "Agrarias" | 6.53 | 0.65 | 242.05 | 1.46 |
| **10** | 8118 | "Christchurch_ New Zealand" | 2011 | "Papanui High School " | 6.2 | 9.06 | 263.2 | 1.24 |
| **11** | 147 | "Coyote Lake" | 1979 | "Gilroy Array #2" | 5.74 | 9.02 | 270.84 | 2.78 |
| **12** | 1141 | "Dinar_ Turkey" | 1995 | "Dinar" | 6.4 | 3.36 | 219.75 | 1.23 |
| **13** | 821 | "Erzican_ Turkey" | 1992 | "Erzincan" | 6.69 | 4.38 | 352.05 | 0.81 |
| **14** | 8161 | "El Mayor-Cucapah_ Mexico" | 2010 | "El Centro Array #12" | 7.2 | 11.26 | 196.88 | 0.99 |
| **15** | 1044 | "Northridge-01" | 1994 | "Newhall - Fire Sta" | 6.69 | 5.92 | 269.14 | 0.56 |
| **16** | 728 | "Superstition Hills-02" | 1987 | "Westmorland Fire Sta" | 6.54 | 13.03 | 193.67 | 1.65 |
| **17** | 183 | "Imperial Valley-06" | 1979 | "El Centro Array #8" | 6.53 | 3.86 | 206.08 | 1.19 |
| **18** | 1042 | "Northridge-01" | 1994 | "N Hollywood - Coldwater Can" | 6.69 | 12.51 | 326.47 | 1.82 |
| **19** | 171 | "Imperial Valley-06" | 1979 | "El Centro - Meloland Geot. Array" | 6.53 | 0.07 | 264.57 | 1.09 |
| **20** | 6927 | "Darfield_ New Zealand" | 2010 | "LINC" | 7 | 7.11 | 263.2 | 1.05 |
| **21** | 161 | "Imperial Valley-06" | 1979 | "Brawley Airport" | 6.53 | 10.42 | 208.71 | 2.44 |
| **22** | 5619 | "Iwate_ Japan" | 2008 | "IWT011" | 6.9 | 8.44 | 279.36 | 2.83 |
| **23** | 8134 | "Christchurch_ New Zealand" | 2011 | "Styx Mill Transfer Station " | 6.2 | 11.25 | 247.5 | 1.91 |
| **24** | 5825 | "El Mayor-Cucapah_ Mexico" | 2010 | "CERRO PRIETO GEOTHERMAL" | 7.2 | 10.92 | 242.05 | 1.27 |
| **25** | 170 | "Imperial Valley-06" | 1979 | "EC County Center FF" | 6.53 | 7.31 | 192.05 | 1.28 |
| **26** | 1048 | "Northridge-01" | 1994 | "Northridge - 17645 Saticoy St" | 6.69 | 12.09 | 280.86 | 0.88 |
| **27** | 1119 | "Kobe_ Japan" | 1995 | "Takarazuka" | 6.9 | 0.27 | 312 | 0.54 |

| | | | | | | | | |
|---|---|---|---|---|---|---|---|---|
| **28** | 4117 | "Parkfield-02_ CA" | 2004 | "Parkfield - Fault Zone 15" | 6 | 2.67 | 307.59 | 2.01 |
| **29** | 184 | "Imperial Valley-06" | 1979 | "El Centro Differential Array" | 6.53 | 5.09 | 202.26 | 1.12 |
| **30** | 6975 | "Darfield_ New Zealand" | 2010 | "TPLC" | 7 | 6.11 | 249.28 | 2.19 |

List of earthquakes for 45 degrees (RSN = record sequence number; SF = scale factor).

| # | RSN | Earthquake Name | Year | Station Name | M | Rrup (km) | VS30 (m/sec) | Scale Factor |
|---|---|---|---|---|---|---|---|---|
| **1** | 161 | "Imperial Valley-06" | 1979 | "Brawley Airport" | 6.53 | 10.42 | 208.71 | 2.14 |
| **2** | 8066 | "Christchurch_ New Zealand" | 2011 | "Christchurch Hospital" | 6.2 | 4.85 | 194 | 0.81 |
| **3** | 6911 | "Darfield_ New Zealand" | 2010 | "HORC" | 7 | 7.29 | 326.01 | 0.81 |
| **4** | 181 | "Imperial Valley-06" | 1979 | "El Centro Array #6" | 6.53 | 1.35 | 203.22 | 1.15 |
| **5** | 185 | "Imperial Valley-06" | 1979 | "Holtville Post Office" | 6.53 | 7.5 | 202.89 | 1.85 |
| **6** | 179 | "Imperial Valley-06" | 1979 | "El Centro Array #4" | 6.53 | 7.05 | 208.91 | 1.12 |
| **7** | 8118 | "Christchurch_ New Zealand" | 2011 | "Papanui High School " | 6.2 | 9.06 | 263.2 | 1.22 |
| **8** | 8161 | "El Mayor-Cucapah_ Mexico" | 2010 | "El Centro Array #12" | 7.2 | 11.26 | 196.88 | 1.00 |
| **9** | 147 | "Coyote Lake" | 1979 | "Gilroy Array #2" | 5.74 | 9.02 | 270.84 | 2.36 |
| **10** | 8064 | "Christchurch_ New Zealand" | 2011 | "Christchurch Cathedral College" | 6.2 | 3.26 | 198 | 0.66 |
| **11** | 184 | "Imperial Valley-06" | 1979 | "El Centro Differential Array" | 6.53 | 5.09 | 202.26 | 1.01 |
| **12** | 6927 | "Darfield_ New Zealand" | 2010 | "LINC" | 7 | 7.11 | 263.2 | 1.02 |
| **13** | 159 | "Imperial Valley-06" | 1979 | "Agrarias" | 6.53 | 0.65 | 242.05 | 1.61 |
| **14** | 5825 | "El Mayor-Cucapah_ Mexico" | 2010 | "CERRO PRIETO GEOTHERMAL" | 7.2 | 10.92 | 242.05 | 1.26 |
| **15** | 183 | "Imperial Valley-06" | 1979 | "El Centro Array #8" | 6.53 | 3.86 | 206.08 | 1.27 |

| | | | | | | | | |
|---|---|---|---|---|---|---|---|---|
| **16** | 821 | "Erzican_ Turkey" | 1992 | "Erzincan" | 6.69 | 4.38 | 352.05 | 0.86 |
| **17** | 8134 | "Christchurch_ New Zealand" | 2011 | "Styx Mill Transfer Station " | 6.2 | 11.25 | 247.5 | 2.01 |
| **18** | 8063 | "Christchurch_ New Zealand" | 2011 | "Christchurch Botanical Gardens" | 6.2 | 5.55 | 187 | 0.86 |
| **19** | 170 | "Imperial Valley-06" | 1979 | "EC County Center FF" | 6.53 | 7.31 | 192.05 | 1.44 |
| **20** | 1141 | "Dinar_ Turkey" | 1995 | "Dinar" | 6.4 | 3.36 | 219.75 | 1.12 |
| **21** | 6 | "Imperial Valley-02" | 1940 | "El Centro Array #9" | 6.95 | 6.09 | 213.44 | 1.50 |
| **22** | 502 | "Mt. Lewis" | 1986 | "Halls Valley" | 5.6 | 13.54 | 281.61 | 2.91 |
| **23** | 1119 | "Kobe_ Japan" | 1995 | "Takarazuka" | 6.9 | 0.27 | 312 | 0.55 |
| **24** | 529 | "N. Palm Springs" | 1986 | "North Palm Springs" | 6.06 | 4.04 | 344.67 | 1.07 |
| **25** | 8606 | "El Mayor-Cucapah_ Mexico" | 2010 | "Westside Elementary School" | 7.2 | 11.44 | 242 | 1.33 |
| **26** | 6886 | "Darfield_ New Zealand" | 2010 | "Canterbury Aero Club" | 7 | 14.48 | 280.26 | 2.95 |
| **27** | 158 | "Imperial Valley-06" | 1979 | "Aeropuerto Mexicali" | 6.53 | 0.34 | 259.86 | 1.53 |
| **28** | 728 | "Superstition Hills-02" | 1987 | "Westmorland Fire Sta" | 6.54 | 13.03 | 193.67 | 1.54 |
| **29** | 766 | "Loma Prieta" | 1989 | "Gilroy Array #2" | 6.93 | 11.07 | 270.84 | 1.18 |
| **30** | 1042 | "Northridge-01" | 1994 | "N Hollywood - Coldwater Can" | 6.69 | 12.51 | 326.47 | 1.79 |

# 17. APPENDIX B

This appendix reports the statistics of the ductility indicator ($\mu_D$) for the MD column obtained across all locations (SF, LA, SLO, and SC) and hazard levels (HL3-200 years, HL4-500 years, and HL5-975 years). The ductility indicator is calculated as $\mu_D = {\Delta_{max}}/{\Delta_y}$, where $\Delta_{max}$ is the maximum drift recorded in each NLTH analysis and $\Delta_y$ is the drift corresponding to the yielding point (i.e., DS-2)

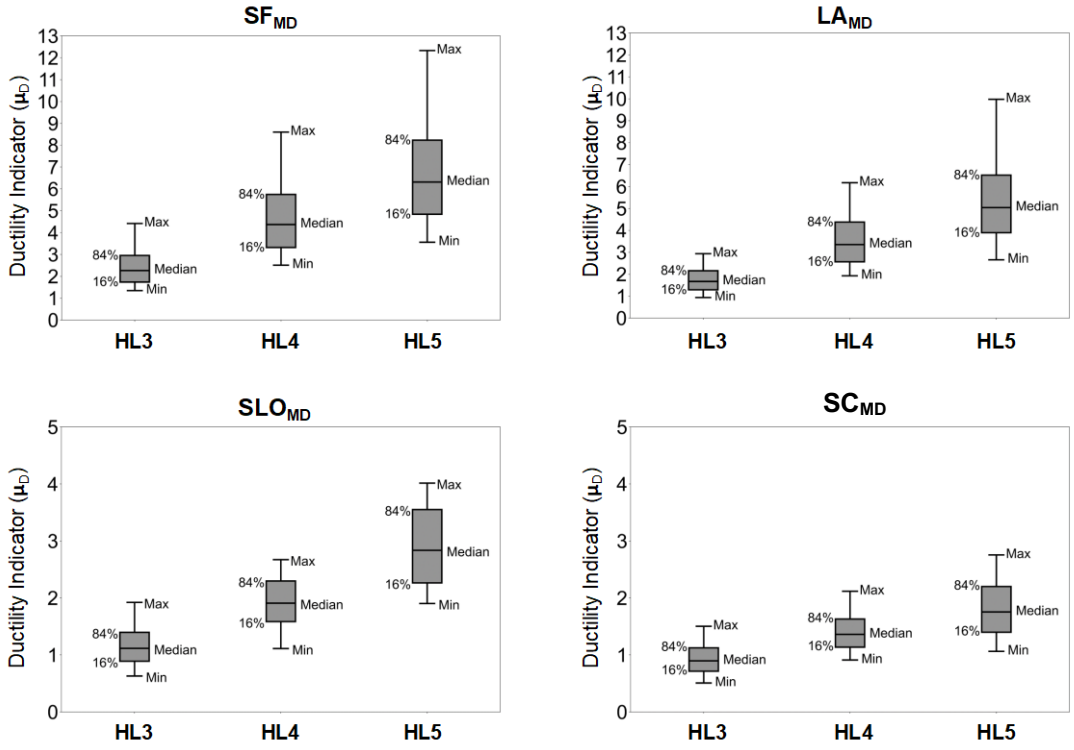


Figure B1. Ductility indicator for the minimum design (MD) column for HL3, HL4 and HL5 and across all four locations (San Francisco, Los Angeles, San Luis Obispo, and Sacramento)

# 18. APPENDIX C

This appendix reports the step-by-step calculation of the total risk performed following the method by Yoon et al. (2022). Only the case of Los Angeles (LA) and DS-2 is illustrated as an example, but the same methodology was used for all locations and damage states considered in this research.

The method relies on the principles of probabilistic seismic hazard analysis (PSHA) and starts with the computation of the mean annual frequency of exceedance ($\upsilon$) of the intensity measure ($IM$) at a threshold ($z$), that is:

$$\upsilon(IM > z) = \sum_{i=1}^{n} P(IM > z|S_i)\lambda(S_i) \quad \text{(C-1)}$$

Where $\sum^{n}_{i=1}$ is the summation over all considered seismic sources $S_i$, with $i = 1,2,3..n$ , $P(IM > z|S_i)$ denotes the conditional probability that $IM$ exceeds the threshold value ($z$), given the occurrence of an earthquake from the seismic source $S_i$, and $\lambda(S_i)$ is the annual rate of occurrence (frequency) of earthquakes at source $S_i$.

By replacing $IM$ with the damage state of interest $DS_i$ and $S_i$ with the ground motion with return period $T$ ($GM_{T\ year}$), Eq. C-1 can be re-written as:

$$\upsilon(DS_i) = \sum_{S_a=1}^{n} P(DS_i|GM_{T\ year})\lambda(GM_{T\ year}) \quad \text{(C-2)}$$

Where $\upsilon(DS_i)$ represents the annual rate of exceeding $DS_i$, $\sum^{n}_{Sa=1}$ is the summation over all considered spectral accelerations $S_a$ indexed from 1 to $n$, $P(DS_i|GM_{T\ year})$ is the conditional

probability that $DS_i$ exceeds the threshold value (note that the notation $DS_i > DS_{i,th}$, where $th$ stands for threshold, has been simplified to have $DS_i$ only) within the return period $T$, and $\lambda(GM_{T\ year})$ is the annual occurrence rate of $GM_{T\ year}$.

Making the classical assumption that the earthquake occurrence follows a Poisson process, the probability of exceeding $DS_i$ within a target bridge lifespan of $j$ years, that is $P(DS_i)$, is calculated as:

$$P(DS_i) = 1 - exp^{-j\upsilon(DS_i)} \quad \text{(C-3)}$$

A continuum function defining the relationship between $P(DS_i|GM_{T\ year})$ and $\lambda\left(GM_{T\ year}\right)$ in Eq. C-2 is herein defined through $S_a$. Curve fitting is then performed to find the best cumulative density function (CDF) for a lognormal distribution closest to the three points corresponding to three values of the return period $GM_{T\ year}$ such that the $P(DS_i|GM_{T\ year})$ can be predicted using the CDF.

This procedure is illustrated step-by-step for LA and DS-2:

1. The spectral accelerations from the uniform hazard spectra (UHS) at the fundamental period of the bridge are determined. The fundamental period of the bridges in LA is 0.83 sec. The spectral accelerations for three designs (i.e., HL1 = 50yr, HL2 = 100yr and HL3 = 200yr) are $S_{a\text{-}50yr}$ = 0.24g, $S_{a\text{-}100yr}$ = 0.39g and $S_{a\text{-}200yr}$ = 0.60g, as illustrated in Figure C-1.

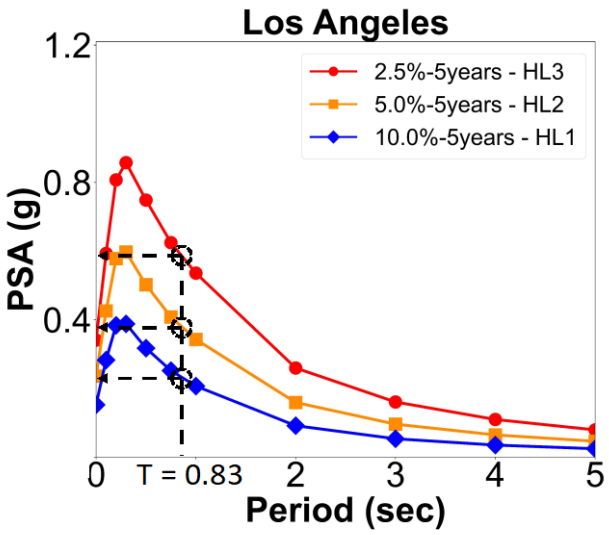


Figure C-1. UHS for 50-year, 100-year, and 200-year return periods with the spectral accelerations at the fundamental period of the bridge highlighted with black dots.

2. For DS-2, the probability of exceedance is obtained from the fragility functions at the spectral accelerations identified in Step 1. Using the fragility functions in Figure C-2, $P(DS2|GM_{50\,year}) = 0.01$, $P(DS2|GM_{100\,year}) = 0.645$ and $P(DS2|GM_{200\,year}) = 0.998$ are obtained.

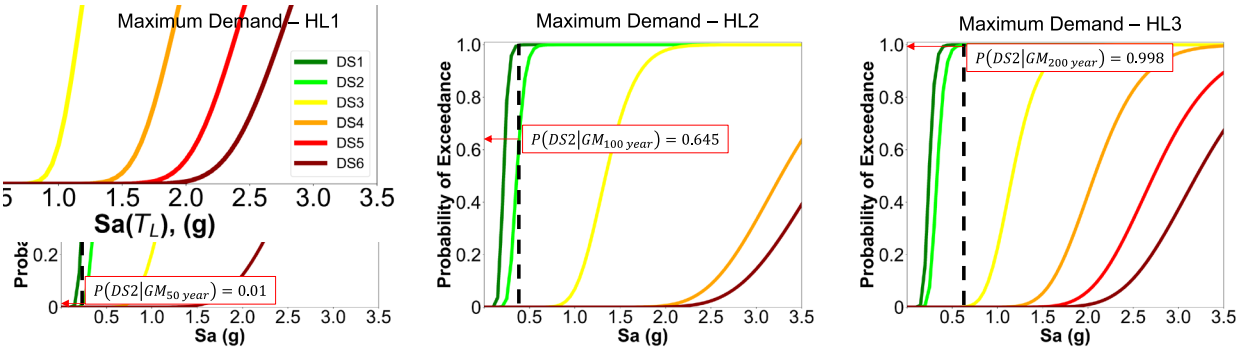


Figure C-2. Fragility functions for LA at the three considered hazard levels.

For convenience, the probabilities of exceedance are summarized in Table C-1.

Table C-1. Derived fragility values for damage state 2 (DS-2) in 3 levels of hazard.

| $P(DS_2 \mid EQ_{50\ yr})$ | $P(DS_2 \mid EQ_{100\ yr})$ | $P(DS_2 \mid EQ_{200\ yr})$ |
|---|---|---|
| 0.010 | 0.645 | 0.998 |

3. The USGS unified hazard tool is used to obtain the hazard curve for the location of interest (Unified Hazard Tool). For the case study bridge, linear interpolation between T = 0.75 sec and T = 1.0 sec is used to derive the curve for T=0.83 sec. The hazard curves for LA are shown below, with the ones used to perform the interpolation highlighted in bold.

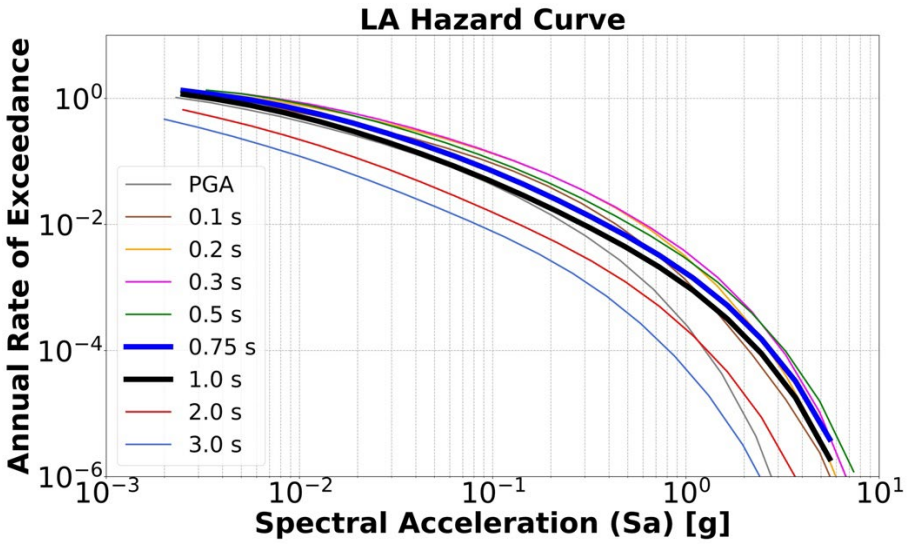


Figure C-3. Hazard curves for LA

4. The probability of exceeding DS-2 derived in Step 2 for different return periods are plotted against the corresponding spectral accelerations ($S_{a\text{-}50y}$, $S_{a\text{-}100y}$ and $S_{a\text{-}200y}$), yielding the red dots in Figure C-4. Curve fitting is performed using least-squares regression to obtain the

cumulative density function (CDF) that best matches the three data points. Interpolation of the three points is performed using functions from the *scipy.stats* module in *Python*. The optimized lognormal mean and standard deviation are $\mu_{\ln Sa} = -1.01$ and $\sigma_{\ln Sa} = 0.18$.

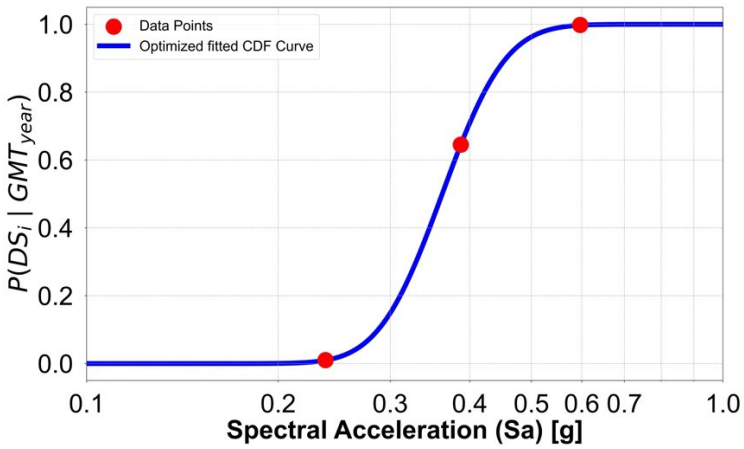


Figure C-4. Cumulative density function using $S_a$ for $P(DS_i|GM_{T\,year})$

5. An Excel spreadsheet is used to create a table of interpolated $S_a$ values along with their corresponding annual exceedance rates from Step 3, as shown in column [1] of Table C-2. Following the suggestion in Yoon et al. 2019, an increment of 0.0025g is used for $S_a$.

Table C-2. Tabulated data of Sa and annual rate of exceedance.

| | [1] | [2] | [3] | |
|---|---|---|---|---|
| # Sa(g) | Annual rate of exceedance | Annual rate of occurrence | $P(DS_2\|GM_{T\,Yr})$ | [2]x[3] |
| 0.0025 | 1.279 | | 0% | |
| 0.005 | 0.945796 | 0.333204 | 0% | 3.1399E-126 |
| 0.0075 | 0.75254 | 0.193256 | 0% | 3.2219E-104 |
| 0.01 | 0.618722 | 0.133818 | 0% | 6.3082E-90 |
| 0.0125 | 0.526539 | 0.092183 | 0% | 1.21714E-79 |
| 0.015 | 0.456268 | 0.070271 | 0% | 1.02201E-71 |
| 0.0175 | 0.400663 | 0.055605 | 0% | 2.29438E-65 |
| 0.02 | 0.356045 | 0.044618 | 0% | 3.96476E-60 |

| | | | | |
|---|---|---|---|---|
| 0.0225 | 0.319624 | 0.036421 | 0% | 1.03895E-55 |
| 0.025 | 0.289768 | 0.029856 | 0% | 6.37648E-52 |
| 0.0275 | 0.264919 | 0.024849 | 0% | 1.26466E-48 |
| 0.03 | 0.243576 | 0.021343 | 0% | 1.03077E-45 |
| 0.0325 | 0.224926 | 0.01865 | 0% | 4.01994E-43 |
| ⋮ | ⋮ | ⋮ | ⋮ | ⋮ |
| 1 | 0.001513 | 8.00E-06 | 100% | 8.00E-06 |
| 1.0025 | 0.001505 | 8.00E-06 | 100% | 8.00E-06 |
| 1.005 | 0.001497 | 8.00E-06 | 100% | 8.00E-06 |
| 1.0075 | 0.001489 | 8.00E-06 | 100% | 8.00E-06 |
| ⋮ | ⋮ | ⋮ | ⋮ | ⋮ |

**Σ [2]x[3] = 0.01016/yr**

6. The annual occurrence is determined by calculating the difference between adjacent annual exceedance rates from Table C-2 in Step 5, as reported in Column [2] of Table C-2.
7. With $\mu_{\ln Sa}$ and $\sigma_{\ln Sa}$ calculated in Step 4, the Excel function NORM.DIST(LN("$S_a$"), $\mu_{\ln Sa}$, $\sigma_{\ln Sa}$, TRUE) is used to compute the probability of exceeding DS-2 for each tabulated $S_a$ value. The resulting values for $P\left(DS2\middle|GM_{T\ year}\right)$ are reported in Column [3] of Table C-2.
8. The probability of exceeding DS-2 computed in Step 7 is multiplied by the annual occurrence in Step 6. The summation of all products across all spectral accelerations will give the annual rate of exceeding, as shown in Eq. C-2.

   For example, for $S_a$ = 1g, $P\left(DS_2\middle|GM_{T\ year}\right) \times \lambda\left(GM_{T\ year}\right) = 8.0E-6 \times 1.0 = 8E-6$.

   The annual rate of exceeding $\upsilon(DS_2)$, which is $\Sigma$[2]×[3], is equal to 0.01016/year.

   Finally, the probability of exceeding DS2 for life spans j = 5, 10, 15 years is calculated with Eq. C-3. In this example for 5-year lifespan, $P(\text{DS2}) = 1 - exp^{-5\times0.01016} = 4.95\%$.